Modeling and Experimentation of Throated Downdraft Gasifier Using Mango Seed Hull and Peanut Shell as a Feedstock for Syngas Production

Behailu Ibrahim Ali

A Thesis Submitted to the Department of Mechanical Engineering,
School of Mechanical, Chemical and Materials Engineering

Presented in Partial Fulfilment of the Requirement for the Degree of Master of Science in Thermal Engineering

Office of Graduate Studies
Adama Science and Technology University

June, 2023
Adama, Ethiopia

Modeling and Experimentation of Throated Downdraft Gasifier Using Mango Seed Hull and Peanut Shell as a Feedstock for Syngas Production

Behailu Ibrahim Ali

Advisor

Dr. Dawit Gudeta

(Associate Professor)

A Thesis Submitted to the Department of Mechanical Engineering,
School of Mechanical, Chemical and Materials Engineering

Presented in Partial Fulfilment of the Requirement for the Degree of Master of Science in Thermal Engineering

Office of Graduate Studies
Adama Science and Technology University

June, 2023
Adama, Ethiopia

DECLARATION

I hereby declare that this Master Thesis entitled "*Modeling and Experimentation of Throated Downdraft Gasifier Using Mango Seed Hull and Peanut Shell as a Feedstock for Syngas Production*" is my original work. That is, it has not been submitted for the award of any academic degree, diploma, or certificate in any other university. All sources of materials that are used for this thesis have been duly acknowledged through citation.

Behailu Ibrahim Ali	_____	_____
Name of student	Signature	Date

RECOMMENDATION

I, the advisor of this thesis, hereby certify that I have read the revised version of the thesis entitled "*Modeling and Experimentation of Throated Downdraft Gasifier Using Mango Seed Hull and Peanut Shell as a Feedstock for Syngas Production*" prepared under my guidance by Behailu Ibrahim Ali, submitted in partial fulfillment of the requirements for the degree of Master's of Science in Thermal Engineering. Therefore, I recommend the submission of revised version of the thesis to the department following the applicable procedures.

Dr. Dawit Gudeta	_____	_____
Advisor	Signature	Date

APPROVAL PAGE

I, the advisor of the thesis entitled "*Modeling and Experimentation of Throated Downdraft Gasifier Using Mango Seed Hull and Peanut Shell as a Feedstock for Syngas Production*" and developed by Behailu Ibrahim Ali, hereby certify that the recommendation and suggestions made by the board of examiners are appropriately incorporated into the final version of the thesis.

Dr. Dawit Gudeta	_____	_____
Advisor	Signature	Date

We, the undersigned, members of the Board of Examiners of the thesis by Behailu Ibrahim Ali have read and evaluated the thesis entitled "*Modeling and Experimentation of Throated Downdraft Gasifier Using Mango Seed Hull and Peanut Shell as a Feedstock for Syngas Production*" and examined the candidate during open defense. This is, therefore, to certify that the thesis is accepted for partial fulfillment of the requirement of the degree of Master of Science in Thermal Engineering.

_____	_____	_____
Chairperson	Signature	Date
_____	_____	_____
Internal Examiner	Signature	Date
_____	_____	_____
External Examiner	Signature	Date

Final approval and acceptance of the thesis is contingent upon submission of its final copy to the Office of Postgraduate Studies (OPGS) through the Department Graduate Council (DGC) and School Graduate Committee (SGC).

_____	_____	_____
Department Head	Signature	Date
_____	_____	_____
School Dean	Signature	Date
_____	_____	_____
Office of Postgraduate Studies, Dean	Signature	Date

ACKNOWLEDGEMENT

First and foremost, I want to express my deepest thankfulness to God Almighty, who created and sustains the earth, the skies, and everything in between. Additionally, I want to take this chance to express my sincere gratitude and recognition for my advisor Dr. Dawit Gudeta for his astounding support, insightful advice, never-ending generosity, lively conversations, and capable leadership from the start to the present, all of which contributed to the success of the current study.

Additionally, I would like to extend my sincere gratitude to my instructors, Dr. Addisu Bekele and Dr. Gezahegne Habtamu, for their invaluable inspiration, helpful criticism, and encouragement throughout my academic career. Finally, I would like to express my gratitude to all of my beloved parents, friends, and colleagues for their support in making this thesis more worthwhile and for their contributions to my study.

ABSTRACT

Downdraft gasifiers are often used to produce syngas with very little tar and impurities. However, their product gas quality and performance are highly affected by the nature of biomass used in the system. Because it requires a lot of time and is impractical to evaluate the performance of a gasification system using all the available biomass kinds under numerous parameters, fast and quick simulation approaches with well-developed mathematical models are required for the efficient and economical utilization of energy resources. A theoretical analysis was carried out under various circumstances after studying the scientific literature on this subject. To evaluate the system performance of a typical biomass gasifier, a stoichiometric equilibrium model was created. Mango seed hull and peanut shell, two biomass wastes that were readily available locally, were used for the analyses. The impact of several parameters, including moisture content, equivalence ratio, and gasification temperature on the gasification system, was studied. The methodology used to achieve this study was based on the predetermined objectives. Along with the model evaluation, an experimental investigation was carried out to evaluate the system performance of a throated downdraft biomass gasifier based on variables which were not included in the model, such as temperature variation over time in the gasifier, gas flame intensity, the quantity of condensate particles, and amount of char left over, for additional performance investigation. The exploitation of biomass in size-reduced and densified form, as well as two air supply systems employing atmospheric and pressured air, were studied experimentally in gasifiers. It was demonstrated that the theoretical analysis and the experimental results were in good agreement. According to the model result, the system using mango seed hull has a lower exergy efficiency of 61.42 % than a system using peanut shell, which had an exergy efficiency of 64.69 %. For the experimental case, it was discovered that gasification with atmospheric air was effective and economical. The temperature distribution along the gasifier has been impacted by the size of the biomass. In order to produce syngas gas with good flame characteristics using biomass gasification, both feedstocks are found to be suitable biomass feedstocks. The producer gas generated with mango seed hull has a composition of 30.29 % H_2, 18.18 % CO, and 1.28 % CH_4 and the calorific value was determined to be 6.02 MJ/m^3. Similarly, the producer gas generated with 9 mm peanut shell pellets contained 27.41% H_2, 20.39% CO, and 1.291% CH_4 and the calorific value was found to be 5.47 MJ/m^3.

Keywords: *Gasification, Downdraft, Syngas, Biomass, Feedstock*

CONTENTS

LIST OF TABLES

TABLE **PAGE**

LIST OF FIGURES

FIGURE **PAGE**

LIST OF ACRONYMS AND ABBREVIATIONS

ACRONYMS

Symbols	Description	Symbols	Description
ANN	Artificial Neural Networks	LHV	Lower Heating Value
CFD	Computational Fluid Dynamics	MC	Moisture Content
CCE	Carbon conversion efficiency	MSH	Mango Seed Hull
CGE	Cold Gas Efficiency	PG	Producer Gas
DME	Dimethyl Ether	PS	Peanut Shell
ER	Equivalence Ratio	RMSE	Root Mean Square Error
FBG	Fluidized Bed Gasifier	SBR	Steam to Biomass Ratio
GEM	Gibbs Energy Minimization	SV	Superficial Velocity
GT	Gasification Temperature	TEM	Thermodynamics Equilibrium Model
HHV	Higher Heating Value	TGD	Throat to Gasifier Diameter

GREEK LETTERS

Symbols	Description	Units [IS]
α	Carbon conversion factor or relative amount of carbon in the producer gas present as a compound	$-$
β	a factor dependent on the mass fraction of C, H, N, and O in the feedstock	$-$
ε_{ch}	Specific chemical exergy	$J/kmol$
ε_{ph}	Specific physical exergy	$J/kmol$
η	Efficiency	%
η_{exe}	Exergy efficiency	%
ν	Stoichiometric number	$-$

LATIN LETTERS

Symbols	Description	Units [IS]
%C, %H, %O, %N, %S	Mass fraction of carbon, hydrogen, oxygen, nitrogen, and sulfur of a fuel on dry basis, respectively	$wt\%$
a, b, c	Molar ratio of elemental species hydrogen, oxygen, and nitrogen by carbon of a fuel on dry ash-free basis, respectively	–
A	Area	m^2
cp	Isobaric heat capacity	$J/mol\,K$
D	Diameter	m
E	Energy	J
Exe	Exergy	J
G	Gibbs free energy	J
g	Specific Gibbs free energy	$J/kmol$
Δg	Gibbs free energy variation	$J/kmol$
GCV	Gross calorific value	J/kg
H	Enthalpy	J
h	Specific enthalpy	$J/kmol$
Δh	Specific enthalpy variation	$J/kmol$
k	Thermodynamic equilibrium constant	
M	Molecular mass	$kg/kmol$
m	Molar quantity of water	–
N	Number of data	–
NCV	Net calorific value	J/kg
n	Number of moles	–
R	Universal gas constant	$J/mol\,K$
S	Entropy	J
Δs	Specific entropy variation	$J/kmol$
Vm	Molar volume of ideal gas at normal conditions of pressure and temperature	$m^3/kmol$
w	Oxygen per mole of feedstock	–
x	Mole fraction	–

SUBSCRIPTS

Symbols	Description	Symbols	Description
0	referred to standard state	*gas*	referred to produced gas
air	referred to air supplied	*in*	referred to inlet of process
act	referred to actual	*mod*	referred to value predicted by the model
biomass/fuel	referred to biomass fed	*out*	referred to outlet of process
ch	referred to chemical	*ph*	referred to physical
daf	referred to dry ash free basis	*redu*	referred to reduction
db	referred to dry basis	*sto*	referred to stoichiometric
exp	referred to value obtained by experiment	*th*	referred to throat
f	referred to the property of formation at standard state	*wb*	referred to wet basis
frus	referred to frustum		

CHAPTER ONE
INTRODUCTION

1.1. Background of the study

Biomass is one of the most promising, widespread, and heavily subsidized renewable energy sources. It is capable of increasing energy security in areas without access to large fossil fuel reserves, proliferating the supply of liquid fuels for transportation, and lessening net carbon emissions per unit of energy supplied (Field et al., 2008). In tropical nations and in places where agriculture is the mainstay of the economy, a particularly large amount of biomass is available in the form of waste. To meet the projected rise in energy consumption, this should be prioritized for energy generation (Roy et al., 2013). Waste and biomass account for up to 92.2% of the total primary energy supply in Ethiopia, with oil at 5.7 % and hydropower at 1.6 % coming in second and third respectively (IEA, 2019; Tiruye et al., 2021). While nearly 90% of urban residents utilize electricity for lighting, almost all homes in rural areas rely on traditional fuels for cooking, and the traditional method of using biomass, such as open burning in a system of three stone stoves, satisfies the requirement (Tiruye et al., 2021). However, since open burning is toxic and less efficient with high fuel consumption, an alternative way which is a thermochemical procedure called gasification can be used to transform the biomass into a synthetic gas that can be burned (Barman et al., 2012; Centeno et al., 2012; Martínez et al., 2012). Gasification is seen to be the most ideal alternative for producing energy from biomass because it is an easy and affordable process to produce thermal energy or distributed electricity generation (Patra & Sheth, 2015).

Due to their simple construction and operation, as well as the fact that the product gas contains less tar, downdraft gasifiers are particularly appealing. Downdraft gasifiers are fixed bed types of gasifiers, that are often used to produce a gas with very little tar and impurities using different biomass feedstocks (Panwar et al., 2012). However, this effort is mostly affected by the nature of the biomass feedstocks. Therefore, the choice of gasification system and design is greatly influenced by the thermochemical properties of the biomass (Patra & Sheth, 2015). Numerous studies have been carried out to address this problem. The impurities in the gas can be minimized using appropriate biomass pretreatment to improve the system performance. By employing a model and experiments based on the characterization of pretreated biomass feedstocks, the current study aimed to bridge the research gap by examining the performance of the gasification system.

1.2. Working principle of downdraft gasifier

Downdraft gasifiers are fixed bed gasifiers designed for highly volatile fuels like wood or other biomass gasification (Bridgwater, 1995; Hamad et al., 2017). Drying, pyrolysis, oxidation, and reduction zones are the four distinct zones of the this gasifier (Patra & Sheth, 2015). The gasifying agent (air, oxygen, or steam) is supplied into the combustion zone above the stationary grate, and the producer gas exits the gasifier from the bottom of the gasifier beneath the fixed grate, as shown in Figure 1.1. The product gas and biomass are flowing downward through a drying zone, a pyrolysis zone, a combustion zone, and a reduction zone. Moisture from the biomass is evaporated and the solid fuel is dried in the drying zone. The dry solid fuel is heated further as it moves down, where it decomposes into char and gases in the pyrolysis zone. When a gasification agent is injected slightly, partial burning of char and some combustible gases takes place, providing the necessary heat to maintain the desired gasification temperature. Then the gases and char reach the reduction zone, resulting in the formation of the producer gas. Finally, for further cleaning, the producer gas goes through downstream elements such as a cyclone separator and a filter (Molino et al., 2018; Patra & Sheth, 2015).

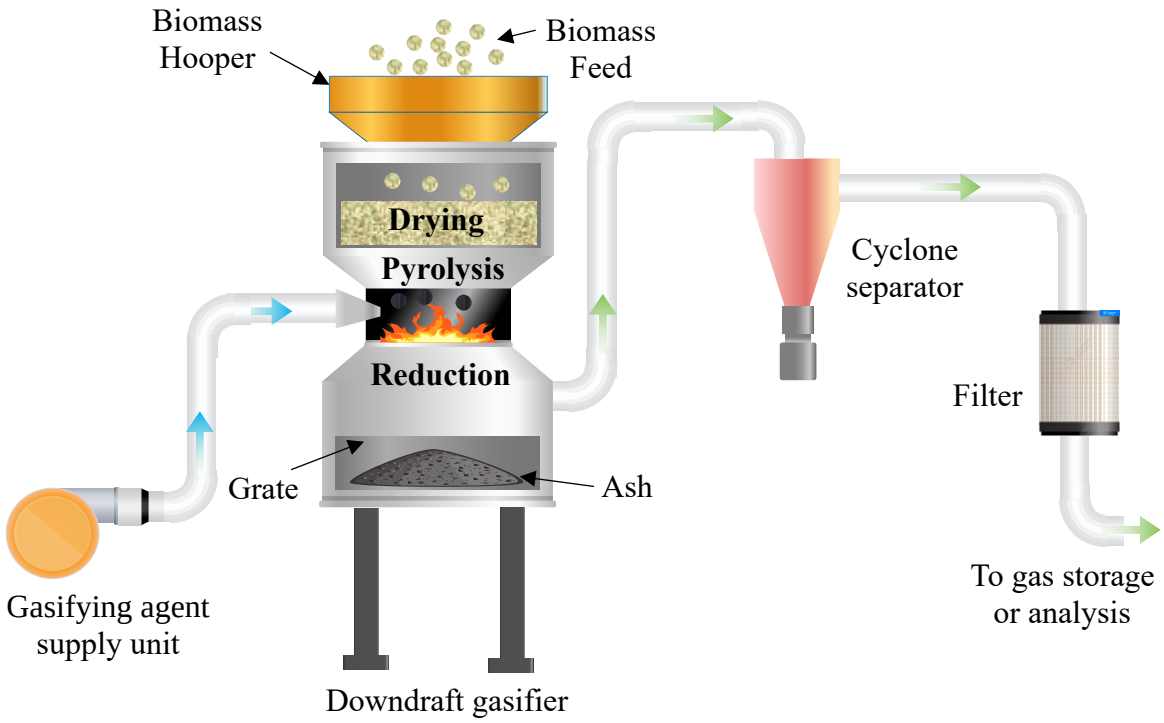

Figure 1.1. Schematic diagram of downdraft gasifier: Adapted from (Inayat et al., 2016; La Villetta et al., 2017; Silva et al., 2019)

1.3. Statement of the problem

Downdraft gasifiers are often used to produce syngas with very little tar and impurities, but this effort is mostly affected by the nature of the biomass feedstocks. However, the impurities in the gas can be minimized using appropriate biomass pretreatment to improve the system performance (Jha et al., 2022). Since it has a higher cost of fuel generation, requires a lot of time, and is impractical to evaluate the performance of a gasification system using all the available biomasses, fast and quick simulation approaches with well-developed mathematical models are also required for the efficient and economical utilization of energy resources. The current study aims to investigate the performance of the gasification system by using a model and experiments based on the characterization of pretreated biomass feedstocks.

1.4. Objectives of the study

1.4.1. General objective

The general objective of this study is to investigate the performance of a throated downdraft biomass gasifier for syngas production using a numerical and experimental approach.

1.4.2. Specific objectives

The specific objectives of this study were to

- Model and simulate the gasification system numerically.
- Develop the desired gasifier's prototype and conduct an experimental test.
- Investigate how biomass feedstocks variation affects the performance of the gasifier
- Analyze the effects of different parameters on the performance of the gasifier.
- Examine the gas quality that is produced from biomass feedstock samples.
- Validate the experimental and numerical results by comparison.

1.5. Significance of the study

The current work was advantageous since it produced an alternate gas that may be used in a burner, boiler, or generator. Additionally, there were several benefits, including good gas quality, time and money saved on fuel acquisition, decreased biomass consumption, and less strain on forestry and energy resources. The results of this study were relevant to waste management, fuel production, environmental cleanliness, and human health. The research entails the application of gasification as a fuel generation technique, mainly in rural areas.

1.6. Scope and limitations

Design, analysis, and validation of numerical and experimental results of a downdraft gasifier with throat were the objectives ambit of this work. The performance reliance on biomass type and quantity, syngas quality, tar content, ER, and MC were all addressed. This work did not comprise the testing of syngas for engines and stoves, only the producer gas quality, composition, and other properties were investigated using appropriate techniques and equipment.

1.7. Organization of the study

The contents of the thesis report are briefly summarized as follows. Chapter two provided a quick overview of the biomass gasification literature. The methods and materials used to accomplish the objectives are the subject of chapter three. The theoretical analysis and design calculations of the gasification system are covered in detail within chapter four. In chapter five, the development of the experimental setup and its analysis were discussed. Various results are included in chapter six along with their discussions. Finally, conclusions obtained from the findings are addressed, along with recommendations for further research.

CHAPTER TWO

LITERATURE REVIEW

2.1. Introduction

In this chapter, numerous literature reviews that are pertinent to various forms of biomass gasification are included. Additionally, biomass conversion technologies, the current state of biomass gasification, various gasification technologies, the viability of using different feedstocks in a gasifier, and modeling approaches for gasification systems are covered. Moreover, the chapter concludes with a synopsis of the literature and provides the relevant research gap as a basis for this study.

2.2. Biomass and conversion technologies

All biologically produced material is referred to as biomass, which also serves as the designation for all living things on earth (Babu, 2008; Sheth & Babu, 2009). Figure 2.1 illustrates that apart from industrial, human, or animal waste processes, wood from natural forests, agricultural and forestry waste, and other plant sources are used to create biomass energy (Sheth & Babu, 2009).

Through the process of photosynthesis, biomass converts carbon dioxide and solar energy into chemical energy in the form of carbohydrates. Since the carbon dioxide that was taken during photosynthesis is liberated after its burning, using biomass as fuel is a carbon-neutral process (Kumar et al., 2009).

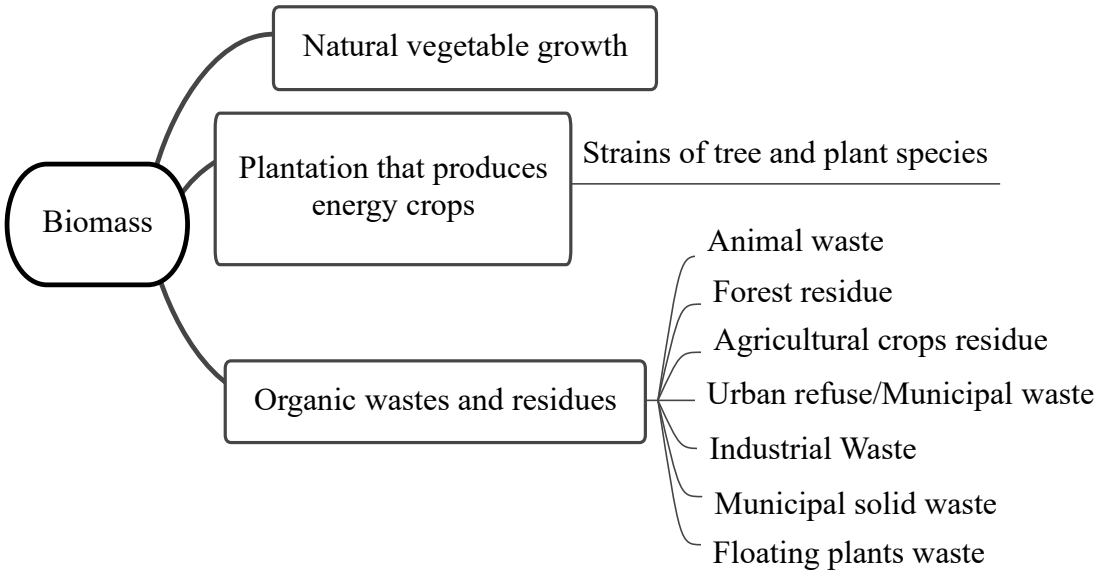

Figure 2.1. Classifications of biomass: Adapted from (Panwar et al., 2012; Sheth & Babu, 2009)

2.2.1. Conversion technologies

The conversion of biomass into gas or liquid has recently attracted a lot of attention and it is motivated primarily by three factors which are renewability, sociopolitical, and environmental benefits (Basu, 2010).

As can be seen form Figure 2.2, biochemical conversion and thermochemical conversion are the two main techniques used to transform biomass energy into biofuels and biopower (Kumar et al., 2009).

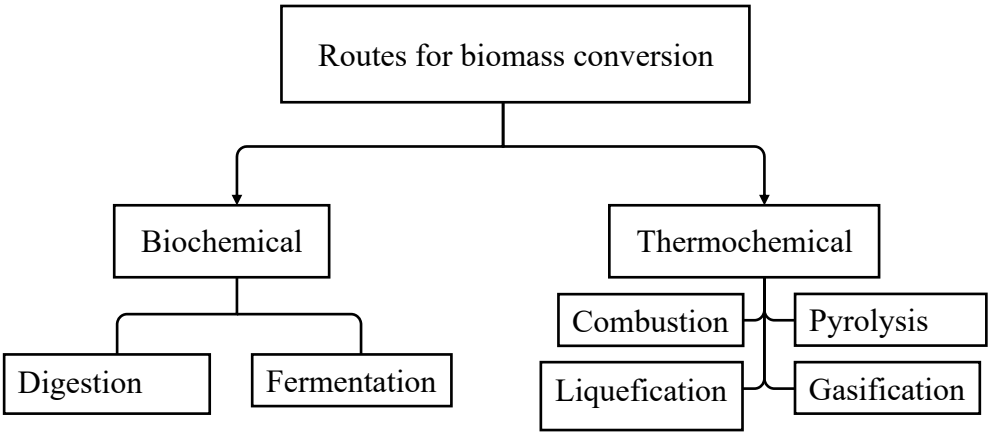

Figure 2.2. Two paths for conversion of biomass: Adapted from (Basu, 2010; Prasertcharoensuk et al., 2018)

2.2.1.1. Biochemical process

It encompasses procedures that involve natural breakdown, which can be induced artificially, by the activity of enzymes or bacteria, such as the creation of bioethanol through enzymatic hydrolysis, fermentation, or anaerobic digestion (McKendry, 2002a; Osman et al., 2021). The primary barrier to successful biochemical conversion is biomass recalcitrance, which is characterized as a plant's innate resistance to enzymatic and microbial breakdown (Himmel et al., 2007). The physical makeup and chemical constituent of the plant are what cause biomass recalcitrance. Application of pretreatments that change the physical structure and chemical nature of biomass and improve the accessibility of cellulose and also hemicelluloses to enzymatic digestion can help overcome biomass recalcitrance (Dupuis et al., 2021).

I. Digestion (anaerobic and aerobic)

Methane, carbon dioxide, and solid residue are the primary byproducts of anaerobic digestion. Instead of using outside air, bacteria draw their oxygen from the biomass itself. Composting, also known as aerobic digestion, is a metabolic breakdown of biomass that occurs with oxygen present. It uses a variety of microorganisms to produce carbon dioxide, heat, and a solid digestate by gaining access to oxygen in the air (Basu, 2010).

II. Fermentation

During fermentation, acids or enzymes are used to turn a portion of the biomass into sugars. Afterward, yeast is used to transform the sugar into ethanol or other compounds. The lignin is not changed; instead, it is left either for burning or for thermochemical chemical conversion. The end result of fermentation is liquid, unlike anaerobic digestion (Basu, 2010).

2.2.1.2. Thermochemical conversion

I. Combustion

The most direct method of a fuel's thermochemical reaction with oxygen, combustion produces CO_2, alkaline ash particles, water vapor, heat, tar, and smoke as a byproduct of the reaction. The ash content, moisture content, incomplete combustion, and heat dissipation are a few internal characteristics that affect how effectively biomass material burns. The heat produced by the combustion process can be employed as a source for further conversion processes that result in the production of electrical energy, which again depends on a few other elements (Sivabalan et al., 2021).

II. Pyrolysis

Biofuels are created by the irreversible thermochemical degradation of the organic material found in biomass. In order to produce bio-oil, charcoal, and non-condensable gases (H_2, CH_4, CO, and CO_2), biomass is thermally cracked at higher temperatures between 300 and 700 °C without oxygen. There are three types of pyrolysis technologies: slow, moderate, and quick. Fast heating rates and short vapor residence periods cause the volatile hydrocarbon vapors to condense quickly into bio-oil, whereas slow pyrolysis produces more biochar as a result of delayed carbonization of biomass as a result of slow heating rates and prolonged vapor residence times (Jha et al., 2022; Zaimes et al., 2015).

III. Gasification

It involves intricate interactions, pressure changes, and processes for the transfer of heat and mass. By using this process, solid fuels (such as coal or biomass) are transformed into goods that can be utilized to create chemicals with added value or burned to produce heat for heating and generating electricity. In order to turn carbonaceous materials into gaseous fuels, gasification needs oxidants or gasifying agents like oxygen, air, and steam (Ong et al., 2019).

IV. Liquefaction

When biomass is thermochemically converted into liquid fuels in a high-temperature, pressured environment the polymer structure disintegrates into liquid components in less than 60 minutes. Hot compressed water is utilized as a catalyst for the reactant to produce a reaction similar to pyrolysis. The liquefaction process has several advantages over pyrolysis,

including lower operating temperature, higher energy efficiency, and tar output (Gollakota et al., 2018; Ong et al., 2019).

2.2.1.3. Products of biomass conversion

Three primary fuels could be derived from biomass (Basu, 2010):

- Liquid fuels such as biodiesel, ethanol, methanol, pyrolysis oil, and vegetable oil.
- Gaseous fuels such as biogas (CH_4, CO_2), syngas (CO, H_2), producer gas (CO, H_2, CH_4, CO_2, N_2), substitute natural gas (CH_4).
- Solid fuels such as biocoke, torrefied biomass, biochar, and charcoal.

2.3. Theory of gasification

2.3.1. Process zones and reaction chemistry

Various overlapping subprocesses make up biomass gasification including drying, pyrolysis, and partial oxidation (Sikarwar et al., 2016). Every conceivable gasification route is shown in Figure 2.3.

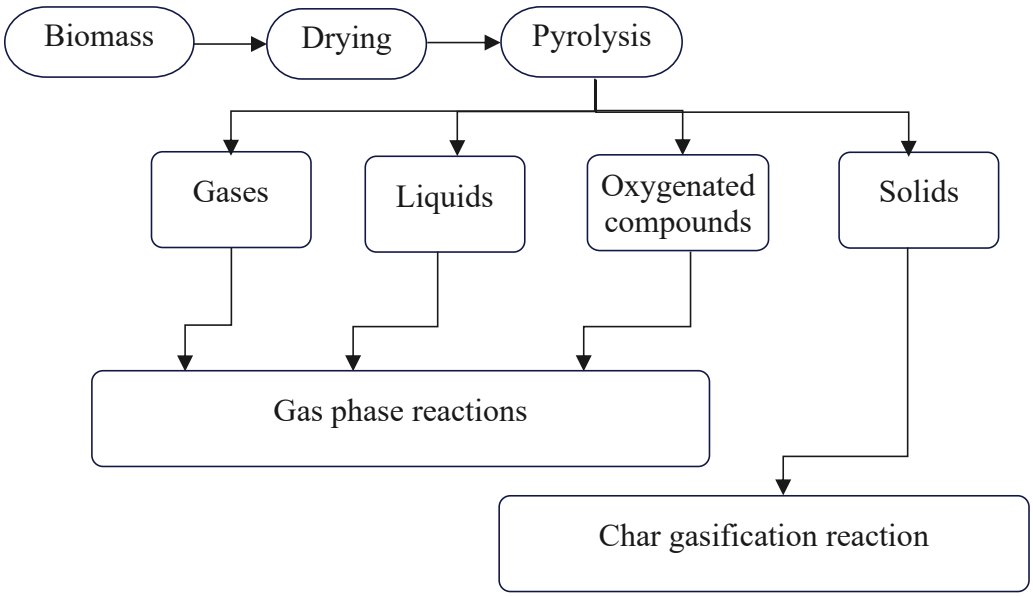

Figure 2.3. Viable gasification route: Adapted from (Basu, 2010; Sikarwar et al., 2016)

Gases from the pyrolysis process include CO, H_2, CH_4, and H_2O, similarly the process yields various liquids including tar, oil, and naphtha. Oxygenated chemicals include phenols and acid, and char is the final solid byproduct. Furthermore, cracking, reforming, combustion, and water gas shift processes are examples of gas phase reactions. Combustion, gasification, and water gas shift processes are all a part of char gasification reactions (Sikarwar et al., 2016).

Equation 2.1 can be utilized to represent the overall reaction in an air and/or steam gasifier. This reaction involves numerous reactions and routes (Kumar et al., 2009).

$$CH_aO_b(biomass) + O_2(21\,\%\,of\ air) + H_2O\ (steam) = C(char) + H_2 + CO + CO_2 + CH_4 + H_2O(unreacted\ steam) + tar \quad (2.1)$$

The significant outcome of gasifying both renewable and non-renewable sources, such as coal and lignocellulosic biomass, is syngas. Nitrogen, oxygen, carbon dioxide, and a small number of light hydrocarbons are also present, along with CO, H_2, and CH_4 (Havilah et al., 2022). One of the main outcomes of biomass gasification is syngas, a mixture of CO and H_2. It is a crucial source of fuels and chemicals that are safe for the environment. Additionally, it makes good fuel for the creation of electricity (Alzate et al., 2018).

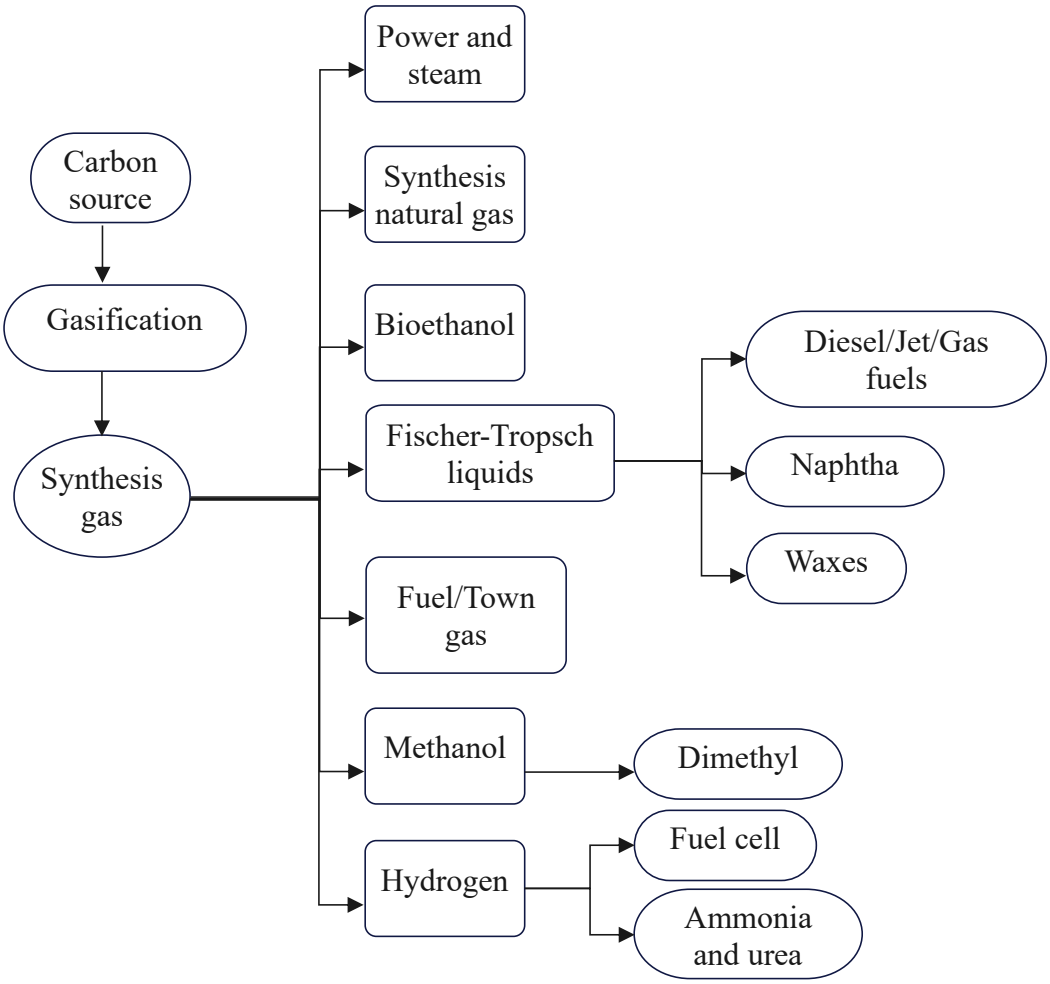

Figure 2.4. Applications of synthesis gas: Adapted from (Havilah et al., 2022)

As depicted in Figure 2.4, fuels like gasoline and diesel can be produced using the Fischer Tropsch (FT) method (Wilhelm et al., 2001). Syngas is easily turned into methanol or DME, which can then be converted into either gasoline when present with zeolites or methyl tertiary

butyl ethylene (MTBE) when present with isobutylene. It can also be converted into hydrogen using a process known as the water gas shift reaction, which has a wide range of uses, including fuel cells. SNG (synthetic natural gas, CH_4) is another important application for syngas. Applications for synthesized gas include integrated gasification combined cycles (IGCC) and the production of medium- British Thermal Units (BTU) gas used as turbine fuel (Sikarwar et al., 2016).

2.3.2. Gasifying medium

The kind of gasifying agent used has a big impact on syngas composition and biomass reactivity, which determines how efficient the process is. As shown in Table 2.1, air, oxygen, steam, carbon dioxide, or their combinations can be used in the gasification process to produce the desired syngas quality for downstream applications.

Table 2.1. Advantages and disadvantages of various gasifying agents (Basu, 2018; Shahbeig et al., 2022)

Gasifying agent	Advantages	Disadvantages
Air	✓ Easy operation ✓ A simple method of heating ✓ Moderate tar and char content ✓ Mature technology ✓ Low formation of soot	✓ Lower levels of CO and H_2 ✓ Lower syngas calorific value ✓ and efficiency. ✓ Increased expenses for gas cleaning and separation ✓ Increased nitrogenous component levels in syngas
Oxygen	✓ Relatively mature technology ✓ Enhancing H_2 and CO to produce high-quality syngas ✓ Low levels of tar and char production ✓ Reduced reaction temperature ✓ Small dilution of nitrogen	✓ Possible risks related to its container ✓ Higher operational and capital expenses ✓ Increasing process complexity
Steam	✓ Higher efficiency ✓ H_2 and CO concentrations in syngas are higher.	✓ Higher energy consumption ✓ Possibility of increased tar formation

	✓ Improved carbon conversion capability ✓ Higher syngas calorific value	
Carbon dioxide	✓ Negative emissions of CO_2 ✓ More efficient gasification ✓ Higher syngas energy content	✓ Increased char production ✓ Longer reaction time

Due to its straightforward heating mechanism, ease of operation, and, most importantly, its affordability based on the comparison in Table 2.1, the air is chosen as a gasifying medium in this study.

2.3.3. Types of biomass gasifier

Based on reactor design, gasification systems can be categorized as a fixed bed, fluidized bed, and entrained flow gasifier. (Anukam et al., 2016; Gómez-Barea & Leckner, 2010).

2.3.3.1. Fixed bed gasifiers

The gasifying media and gas are either moved up or down via the fixed-bed gasifier's bed of solid fuel particles, or they enter the reactor from one side and exit on the same horizontal level from the other side (Puig-Arnavat et al., 2010). They can further be classified as updraft, downdraft, and cross-draft fixed bed gasifiers (Mishra & Upadhyay, 2021; Ren et al., 2019).

As depicted in Figure 2.5, there are three different kinds of fixed bed gasifiers.

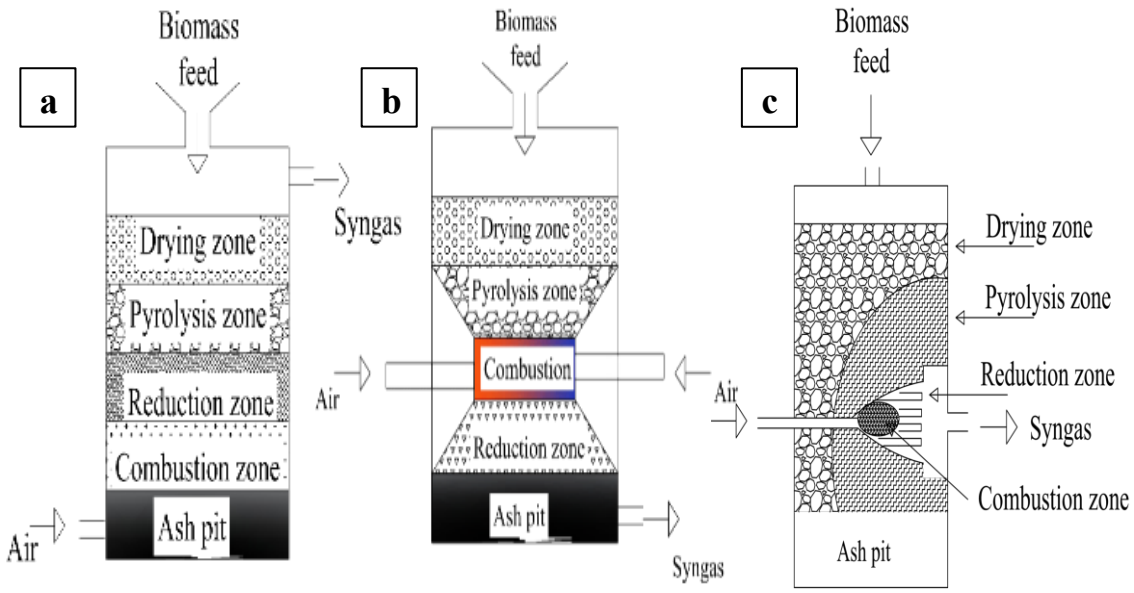

Figure 2.5. Schematic diagram of fixed bed gasifiers (a) updraft, (b) downdraft, (c) cross draft: Adapted from (Mishra & Upadhyay, 2021; Rajvanshi, 1986; Ren et al., 2019)

I. Updraft gasifiers

The feedstock undergoing gasification in an updraft gasifier is fed from the top and flows downhill while being transformed into syngas, or flows in the opposite direction of the product gas's flow. For this reason, this type of gasifier is sometimes referred to as a counter-current type of gasifier (Anukam et al., 2016). As can be seen in Figure 2.5a, when the biomass is introduced from the top, it is dried, devolatilized, and gasified as well as oxidized by the hot, low-oxygen gas as it rises upward and transfers heat to the other zones (La Villetta et al., 2017). It is not advisable to use the PG from this gasifier for engines because it contains more tar. Thermal applications have proven to be its best use. The product gas can be utilized for motor power generation if it runs on fuel like charcoal after being cleaned and cooled (Panwar et al., 2012).

II. Downdraft gasifiers

Figure 2.5b demonstrates, that through a packed bed that is plummeting and is supported over a throat-like restriction, where the majority of gasification reactions take place, the downdraft gasifier incorporates a simultaneous flow of gases and solids. The turbulence and high temperature in the region surrounding the neck, where the reaction products are intimately combined, promote tar cracking (Bridgwater, 1995; Hamad et al., 2017). This particular style of gasifier was probed to be the most effective at transforming highly volatile fuel such as wood or biomass, into low-tar gas, making it the best design for producing electricity (Panwar et al., 2012). They can further be classified as Imbert (throated) and Stratified (throat less or open top) downdraft gasifiers (Chopra & Jain, 2007).

III. Cross-flow gasifier

In a cross-flow gasifier, the air enters from the side, while the biomass fed at the top of the unit travels downhill as illustrated in Figure 2.5c. At roughly the same level that the biomass is supplied, product gas exits through the other side. Around the air entrance, a hot combustion zone develops, while inside the vessel, pyrolysis and drying zones develop (Patra & Sheth, 2015).

2.3.3.2. Fluidized bed gasifiers (FBG)

To keep the solid particles suspended, the gasifying agent is blown through the bed of particles at a fast enough rate (La Villetta et al., 2017; Puig-Arnavat et al., 2010). At the bottom of the reactor, fuel particles are introduced, swiftly mixed with the material that will form the bed, and almost immediately heated to the temperature of the bed. This process causes the fuel to pyrolyze very quickly, resulting in a component mix with a sizable

proportion of gaseous elements (Puig-Arnavat et al., 2010). The schematic diagram for two of mostly used FBGs is depicted in Figure 2.6.

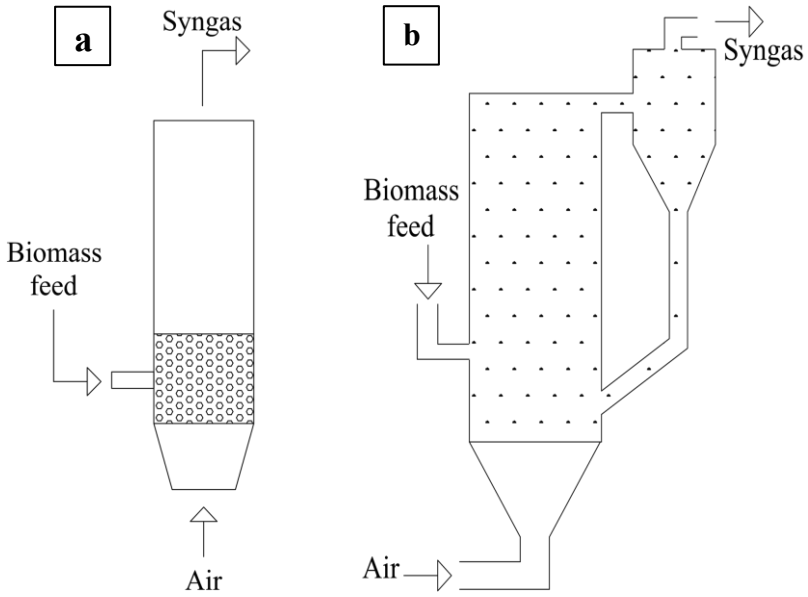

Figure 2.6. Schematic diagram of FBG (a) bubbling FBG (b) circulating FBG: Adapted from (Loha et al., 2014; Molino et al., 2018; Sikarwar & Zhao, 2017)

I. Bubbling fluidized bed

Figure 2.6a depicts a vessel with a grate at the bottom through which air is introduced to make up the gasifier. The fine-grained material moving bed, which receives the prepared biomass feed, is located above the grate (Couto et al., 2013). The frictional force between the particles and the gas eventually balances the weight of the solids as the gasifying agent is forced through the inert particles. When gas moves through a medium at this gas velocity or minimum fluidization velocity, it bubbles and channels through the medium, such as the particles continue to exist in the reactor and seem to be in a boiling state. The biomass that is fed to the bed tends to be broken up by the fluidized particles, which also enable efficient heat transfer throughout the reactor (Ciferno & Marano, 2002).

II. Circulating fluidized bed

Gas velocities higher than the minimum fluidization point are used in circulating fluidized bed gasifiers, which entrains particles into the gas stream (Ciferno & Marano, 2002). As depicted in Figure 2.6b, when the gas leaves the reactor's top, the entrained particles are sorted in a cyclone before being sent back into the reactor (Couto et al., 2013). Due to the large heat capacity of the bed material, substantial heat transfer rates are achievable; however, temperature gradients develop in the direction of solid flow (Ciferno & Marano, 2002).

III. Twin bed

With the use of these reactors, a syngas can be produced that has a larger calorific power than what can be produced by a single gasifier. They are made up of two reactors: the first is a pyrolyzing reactor and is heated by inert material which is hot and dwells in a second reactor or by sand. By burning the char from the first reactor, the second gets heat (Ruiz et al., 2013).

2.3.3.3. Entrained flow gasifiers

As depicted in Figure 2.7, air, oxygen, and/or steam, is delivered into the system concurrently with fine particles. So, as the solid particles move through the gasifier in a thick cloud, the oxidant and steam surround or entrain them (La Villetta et al., 2017). The syngas throughput of this particular gasifier is high. The high working temperature which is above 1000 ^{0}C and pressure ranging from 19.96 to 70.01 bars, however, necessitate gas cooling before use, which might lower the system's total thermal efficiency if the heat recovered during cooling is not recycled (Zhang et al., 2010).

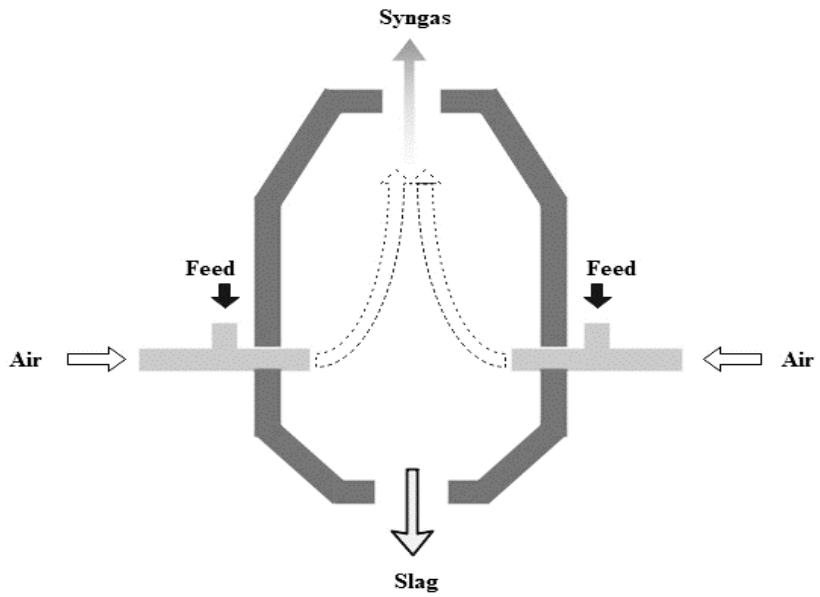

Figure 2.7. Schematic configuration of entrained flow gasifier: Adapted from (Kushwah et al., 2022; Zhang et al., 2010)

2.4. Advantages and disadvantages of different gasifiers

Gasifiers can be used for various application based on the required system output, but still, each and every kind of gasification system have its own merits and demerits. The primary benefits and drawbacks of fixed bed, fluidized bed, and entrained flow gasifiers with their operating temperature range are presented in Table 2.2.

Table 2.2. Advantages and disadvantages of different gasifiers (Begum et al., 2013; Chen et al., 2013; Higman, 2008; Molino et al., 2018; Shahbeig et al., 2022; Van der Drift et al., 2004)

No.	Type	Operating temperature range	Advantages	Disadvantages
1	Updraft	$700 - 900$ ℃	✓ Simple construction ✓ Excellent thermal efficiency ✓ Able to work with a variety of materials and sizes ✓ Optimal contact between the oxidizing agent and the solid ✓ Capable of handling highly hygroscopic materials	✓ High amount of tar in the syngas ✓ Processing and loading flexibility are limited ✓ The tar has an energy content of more than 20%. ✓ Low CO and H_2 production
2	Downdraft	$700 - 1200$ ℃	✓ Very little tar is produced ✓ High level of carbon conversion ✓ Simple construction ✓ Reliable technology ✓ Insignificant amounts of ash and dust are entrapped. ✓ Superior residence time	✓ Low-moisture materials are required. ✓ An identical size is needed for input (pellets < 100 mm) ✓ Minimal heat transfer coefficient ✓ Processing and loading flexibility are limited
3	Cross draft	Up to 1300 ℃	✓ Able to work with a variety of biomass feedstock materials	✓ The overall energy efficiency is low ✓ Difficult operation

			✓ High level of carbon conversion ✓ Excellent thermal efficiency ✓ Simple configuration	✓ High amount of tar in the syngas
4	Bubbling fluidized bed	$800 - 900\ ℃$	✓ Tar content in the syngas is minimal. ✓ The ability to endure high thermal loads ✓ Gas and solid contact at high mixing levels ✓ High carbon conversion	✓ Carbon loss in the ashes ✓ Dust and ashes being dragged ✓ Dimensional limitations ✓ High maintenance and investment costs
5	Circulating fluidized bed	$900 - 1200\ ℃$	✓ Able to handle flexible loads ✓ Good ability to scale-up ✓ Less residence time ✓ High level of carbon conversion	✓ Carbon loss in the ashes ✓ High start-up and investment costs. ✓ The technology is complex and difficult to manage. ✓ Limited solid to gas interaction
6	Entrained flow	Up to $1500\ ℃$	✓ Short reactor residence time ✓ Great fuel versatility ✓ Very little tar content. ✓ High level of carbon conversion ✓ Great control over process parameters ✓ Uniform temperature	✓ System components have a short lifespan ✓ High requirements for oxidants ✓ High maintenance and investment costs ✓ Cold gas efficiency is low.

2.5. Selection criteria for the gasifier

As shown in Table 2.3, for the selection of the gasifier, seven factors are taken into account including cost of manufacturing, simplicity of operation, tar content, cold gas efficiency, feedstock versatility, LHV, and application flexibility of syngas. Entrained flow gasifiers were not included in the selection process since they are expensive and not viable for lower outputs. The gasifiers were compared to one another on each criterion, which was weighted out of five.

Table 2.3. Gasifier selection criteria (Basu, 2010; Chopra & Jain, 2007; Guangul et al., 2012; Hsi et al., 2008; La Villetta et al., 2017)

Gasifier type	**Cost**	**Ease of operation**	**Tar content**	**Cold gas efficiency**	**LHV**	**Feedstock versatility (Moisture and size)**	**Application versatility of syngas**
Updraft	E	E	P	E	G	E	P
Downdraft	V.G	V.G	E	G	G	V.G	E
Cross draft	E	E	V.G	P	P	G	G
Fluidized bed	P	P	G	G	E	P	E
Assigned score values							
P-Poor = 1, F-Fair = 2, G-Good = 3, V.G-Very Good = 4, E-Excellent = 5							

Based on the comparison conducted downdraft gasifier is selected for this study because Table 2.3 demonstrates that a downdraft gasifier has a satisfactory result when it comes to decently meeting the selection criteria.

In small-scale applications with thermal capacities under 1MW, downdraft gasifiers have been extensively employed for biomass gasification (Basu, 2010; Susastriawan et al., 2019). Due to their simple construction and operation, as well as the fact that the PG contains less tar, downdraft gasifiers are particularly appealing (Panwar et al., 2012). Because gas produced with little or no tar is acceptable as fuel for internal combustion engines. Additionally, using PG is more environmentally affable than burning biomass directly (Hernández et al., 2010; Susastriawan et al., 2019).

2.6. Downdraft gasifiers

As depicted in Figure 2.8, downdraft gasifiers are comparable to updraft gasifiers, with the exception that the zones are arranged in reverse order, allowing pyrolysis products to pass through the high-temperature oxidation zone before further decomposing into combustion products (Anukam et al., 2016).

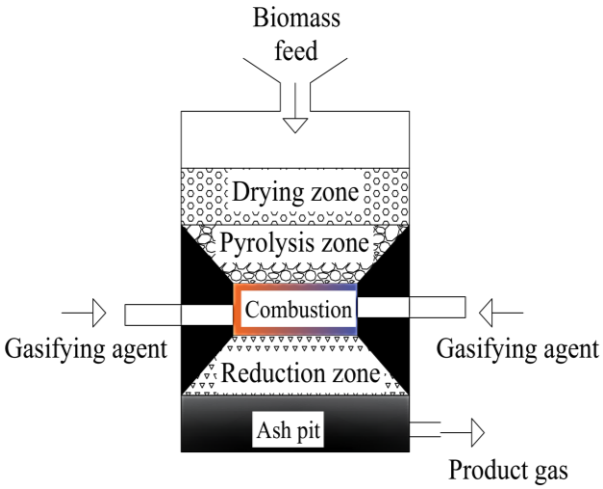

Figure 2.8. Schematic diagram of downdraft gasifier: Adapted from (Mishra & Upadhyay, 2021; Rajvanshi, 1986; Ren et al., 2019).

Drying, pyrolysis, oxidation, and reduction zones are the four distinct areas of the downdraft gasifier as shown in Figure 2.8 (Patra & Sheth, 2015).

I. Drying or dehydration zone

The downdraft gasifier at the top is fed with biomass and utilizing the heat produced by the partial combustion of some of the fuel wood in the combustion zone, the moisture in the wet biomass is reduced, accompanied by the formation of water vapor in the drying zone as it can be seen in chemical reaction [R1] (Chawdhury & Mahkamov, 2011; Diyoke et al., 2018).

$$Moist\ feedstock + Heat \rightarrow Dry\ feedstock + H_2O \qquad [R1]$$

As it descends, the water vapor joins another vapor that already exists in the oxidation zone. The remainder becomes moisture in the gas and part of it is reduced to hydrogen (Chawdhury & Mahkamov, 2011).

II. Pyrolysis zone or devolatilization

In essence, this is the thermal breakdown of biomass in the absence of air or oxygen (Buragohain et al., 2010). Due to the numerous chemical and physical changes that occur quickly and concurrently during devolatilization, this process is very complex (Kaushal et al., 2010). The dried biomass feedstock pyrolyzes when it is heated to more than 250 ^{o}C (Chawdhury & Mahkamov, 2011).

This region is where the big molecules cellulose, hemicellulose, and lignin are broken down into carbon (char) and medium-sized molecules, also known as volatiles which can be seen from chemical reaction [R2] (Mishra & Upadhyay, 2021).

$$Dry\ feedstock + Heat \rightarrow Char + Volatiles \qquad [R2]$$

The devolatilization product subsequently combines with the gasifying medium which can be air, oxygen, or steam to create CO, CO_2, H_2, and lighter hydrocarbons (Kaushal et al., 2010).

III. Combustion or oxidation zone

Technically, the most straightforward and direct method for processing biomass degradation is the combustion process (Mishra & Upadhyay, 2021). Some of the flammable volatiles and char from the pyrolysis zone interact with the scarce oxygen in this zone, causing combustion reactions. The exothermic nature of the reaction causes a fast increase in temperature to over 1200 ^{o}C (Chawdhury & Mahkamov, 2011; Diyoke et al., 2018). The final products created in this zone are CO, CO_2, H_2, and H_2O, and the heat released is utilized in both the pyrolysis process and partially drying the constituents (Mishra & Upadhyay, 2021).

The chemical reactions [R3] and [R4] are the main reactions in this zone (Chawdhury & Mahkamov, 2011).

$$C + O_2 \rightarrow CO_2 \qquad \Delta H = -393\ MJ/kg\ mol \qquad [R3]$$

$$2H_2 + O_2 \rightarrow 2H_2O \qquad \Delta H = -242\ MJ/kg\ mol \qquad [R4]$$

IV. Reduction zone

The reduction zone is so named because it decreases the tar particles present in the generated gas by heating them to a high temperature of around 1000 ^{o}C (Mishra & Upadhyay, 2021). The chemical energy of the syngas is formed in this situation by converting the sensible heat of the gases and charcoal (Chawdhury & Mahkamov, 2011). Numerous reduction processes take place in the temperature range of 800-1000 ^{o}C in the absence or sub-stoichiometric presence of oxygen (Buragohain et al., 2010). A complicated series of heterogeneous gas-solid interactions are taking place in this zone, where the leftover char or carbon from the oxidization zone is gasified with CO_2, H_2, and H_2O, and also most of these reactions are endothermic (Das & Hoque, 2014; Kathi, 2016). The chemical phenomenon from [R5] to [R8] are the main reactions throughout this stage (Buragohain et al., 2010):

$$Water - gas\ reaction: C + H_2O \rightarrow CO + H_2 - 131.4\ kJ/gmol \qquad [R5]$$

$$Boudouard\ reaction: C + CO_2 \rightleftharpoons 2CO - 172.6\ kJ/gmol \qquad [R6]$$

$$Shift\ reaction: CO_2 + H_2 \rightleftharpoons CO + H_2O - 42\ kJ/gmol \qquad [R7]$$

$$Methane\ reaction: C + 2H_2 \rightleftharpoons CH_4 + 75\ kJ/gmol \qquad [R8]$$

2.7. Factors affecting the performance of gasification process

The gasification process for all types of gasifiers is affected by many factors. An overview is provided below for a few variables that affect how effectively the gasification process operates including, biomass type and size, biomass feeding rate, ash content, equivalence ratio (ER), moisture content (MC), residence time, superficial velocity (SV), gasifying agent.

2.7.1. Biomass type

The gasification process is significantly influenced by the type of biomass used. The biomass's carbon content, volatile matter content, and HHV have an effect on carbon monoxide, on gas concentrations that are combustible, on the final gas's calorific value, and also on gas and energy yields (González-Vázquez et al., 2018).

2.7.2. Biomass size

In order to uphold an acceptable pressure drop within the reactor without the development of preferential channels, and preserve a specific consumption rate, solid particles that are to be gasified must be of sufficient size (La Villetta et al., 2017). Smaller particles have a tendency to clog the available air voids, causing a large pressure drop that causes the gasifier to shut down and also larger particles have the potential to create bridges that prohibit the feed from going down. For that reason, typical feed particle sizes are between 20 and 80 mm (McKendry, 2002b).

2.7.3. Biomass feeding rate

Starve-feeding causes less gas yield, but overfeeding biomass can result in clogging and decreased conversion efficiency. Therefore, for the gasification system to achieve maximum energy efficiency, the ideal biomass flow rate is desired. The gasifier's design and the characteristics of the biomass are the main determinants of the optimal biomass flow rate (Kumar et al., 2009).

2.7.4. Ash content

High mineral content can prevent gasification from occurring. The problem of clinkering or slagging in the hearth and consequent feed obstructions are caused by the oxidation temperature, which is frequently higher than the melting point of the biomass ash. For ash contents exceeding 5%, clinker is an issue, especially if the ash is strong in alkali oxides and salts, following feed which results in eutectic mixtures with low melting points (McKendry, 2002b).

2.7.5. Equivalence ratio (ER)

It can be determined as the ratio of actual air needed to fuel to the stoichiometric amount of air required to fuel, which indicates the extent of partial combustion (Kumar et al., 2009; Martínez et al., 2012; Mishra & Upadhyay, 2021). No oxidant is present in the system when ER is equal to zero, while ER of one indicates stoichiometric combustion. Combustion takes place under fuel-lean conditions when ER exceeds one. Lastly, fuel-rich combustion occurs when ER is lower than one (La Villetta et al., 2017).

2.7.6. Moisture content (MC)

The amount of moisture in the fuel is critical to the gasification process because it determines how much energy is needed for the reactions that result in steam gasification and water evaporation (Ruiz et al., 2013). Fuel having MC beyond 30% is difficult to ignite and has a lower calorific value since it must first be evaporated before combustion or gasification can actually occur. The hydrocarbons emitted from the pyrolysis zone do not completely fracture because excessive MC lowers the temperature (McKendry, 2002b) reached in the oxidation zone.

2.7.7. Residence time

It is the average time in which the feedstock particles reside within the gasifier, that should be sufficient to guarantee that the reactions in the gasification process occur properly, resulting in the required syngas (Ruiz et al., 2013).

2.7.8. Superficial velocity (SV)

The ratio of the syngas generation rate under ideal conditions to the gasifier's narrowest cross-sectional area is called superficial velocity. The syngas energy content, fuel consumption rate, and rates of char and tar production are all related to SV (La Villetta et al., 2017). Low SV values cause the pyrolysis process to proceed rather slowly, producing large amounts of unburned tars and substantial char yields. Contrarily, a larger value of SV result in a very quick pyrolysis process, and the generation of less char and extremely hot gases within a flame zone. (Martínez et al., 2012).

2.7.9. Gasifying agent

Air, which is plentiful and simple to use, is the most popular gasifying agent. Temperature and ER have a big impact on how well air-based gasification works. The amount of heating value in the dry syngas produced specifically increases with the temperature of the air introduced into the gasifier (La Villetta et al., 2017; Maitlo et al., 2022). The produced gas is considerably diluted since air contains up to 79 percent nitrogen, which raises the expense

of gas separation treatment. As a result, air gasification has significant drawbacks. A low calorific value of 3.50 to 7.80 MJ/m^3 is also a characteristic of the gaseous byproducts of air gasification. As a result, the use of air as a gasifying medium is typically only for producing low-temperature heat and electricity (Maitlo et al., 2022). Because nitrogen is removed during oxygen gasification, the LHV is increased, and this process also offers a high level of carbon storage. Due to the necessity for heat, steam, and oxygen combinations are typically used in steam gasification, which produces high-quality syngas with a high hydrogen concentration and high LHV (La Villetta et al., 2017).

2.8. Gasification mathematical models

The modeling and analysis of biomass gasification processes have been the subject of several studies (Ferreira et al., 2019; Jia et al., 2018; Paiva et al., 2021; Prasertcharoensuk et al., 2018). And to properly understand the thermochemical processes involved in gasification, gasification models are developed. These models also assess the impact of the operational parameters. Gasification operating parameters that affect the process include the gasifying agent, equivalency ratio, temperature, residence time, and pressure. Models that have been used in studies of the gasification process include thermodynamic equilibrium, computational fluid dynamics (CFD), artificial neural networks (ANN), and kinetics, (Baruah & Baruah, 2014; Marcantonio et al., 2020; Musse et al., 2020; Safarian et al., 2019; Silva et al., 2019). A gasifier's performance may not be predicted with great accuracy by mathematical modeling. Nevertheless, it can provide qualitative information and guidance regarding the impact of design and also feedstock operation factors (Basu, 2010). In order to explain the gasification process, mathematical models are useful tools. A model can accurately predict an operation with a permissible degree of error (de Souza-Santos, 2010)

2.8.1. Kinetic models

To analyze the progression of the reaction in the reactor, kinetic models are utilized, enabling the product composition to be varied throughout the gasifier while taking geometry and fluid dynamics into consideration (La Villetta et al., 2017). Though they come with a high computing cost, kinetic-based models deliver precise and thorough findings (Puig-Arnavat et al., 2010). The two parts of kinetic modeling are reactor hydrodynamics and reaction kinetics. A gasifier's gas production and final product composition are determined by kinetic models over a finite period of time. The model takes into account variables including reaction rate, particle residence period, and reactor hydrodynamics (Basu, 2010).

An archaic work, Singh *et al.* (2014) integrated theoretical and experimental research on a 50-kW downdraft biomass gasifier using a variety of biomass materials, that are typically

found in the villages on which the investigation was concentrated, including wood, coconut shells, rubber seed kernels, and coir pith. The temperature and composition of the PG were predicted using a two-zone kinetic equilibrium model technique. The work reconnoitered how the ER affected the reaction temperature, PG quality, and gasifier conversion efficiency. The viability of employing different biomass energy sources in an Imbert-type downdraft gasifier has been thoroughly investigated analytically and experimentally.

To mimic the constant and transient states of the gasification process, a downdraft gasifier mathematical model has been developed by Jia *et al.* (2018). The model was based on unidimensional reaction kinetics in the reduction zone and the lumped capacitance approach, as well as chemical equilibrium in the pyrolysis and oxidation zones. Inquiries had been done on how the ER (0.37-0.45), the SBR (0-4), and the mass flow rate of biomass (18-25 kg/h) affect the steady and transient features of the gasifier.

To model downdraft biomass gasification, Smith *et al.* (2019) suggested a kinetics model which was based on detailed kinetics of gasification. The model's accuracy was compared directly to experimental data from two downdraft gasifiers that were published in the literature, and it was shown to be superior to the frequently utilized GEM model. Eight biomass samples were taken for this study. Furthermore, the impacts of the biomass MC, ER, gasification temperature, and biomass composition on the production of syngas and tar were then studied.

2.8.2. ANN models

The processing components of an artificial neural network are part of a computational model that produces an output and receives inputs in accordance with predetermined activation functions (La Villetta et al., 2017). Typically, this modeling strategy comprises partial first-principles models that outline the properties of the simulated process. They use a multilayer feedforward neural network (MFNN), which acts as an estimate of unmeasured process parameters that are challenging to model from the ground up (Safarian et al., 2020).

Baruah et al. (2017) created an ANN-based model to predict how biomass is gasified in fixed-bed downdraft gasifiers. Furthermore, to estimate the product gas composition in terms of concentration of four important gas species CH_4, CO, CO_2, and H_2, ANN-based models were developed. The C, H, O, ash, moisture, and temperature of the reduction zone were the input parameters employed in the models. One input, one hidden, and one output layer made up the model. Moreover, to train the ANNs, reported experimental data were used.

Safarian et al. (2020) developed an ANN model that was combined with a thermodynamic equilibrium technique for a downdraft biomass gasification integrated power production

unit. The study's goal was to make predictions about the systems' net output power under different operating circumstances and air pressure using a variety of biomass feedstocks. Proximate and elemental analysis compositions and operating characteristics like gasifier temperature and air-to-fuel ratio served as the models' input parameters. One input, one hidden, and one output layer made up the model. The ANN was trained using 1032 simulated data points from 86 distinct types of biomasses under various operating settings.

2.8.3. CFD models

CFD modeling has shown to be a potent tool for the creation of innovative concepts and technology. In addition to fluid flow behavior, CFD algorithms also forecast heat and mass transport, chemical reactions such as volatilization and combustion, phase transitions such as vaporization during drying and melting during slagging, and mechanical motion. Results from the CFD model can, in many circumstances, predict accurate quantitative information as well as qualitative information when compared to experimental data. The intricacy of the thermochemical process and the biomass feedstock, however, continues to provide a substantial difficulty for CFD modeling for biomass thermochemical conversion (Pandey et al., 2021; Shaikh & Sinhal, 2018).

Using the simulated outcomes of a CFD model, (Jayathilake & Rudra, 2017) inspected the peculiarities of Birchwood gasification. The experimental findings from the University of Agder's moving bed downdraft gasifier were used to create and test the CFD model. Several factors were studied, including the syngas' production, composition, cold gas efficiency (CGE), and LHV. By changing the biomass particle size, the behavior of the aforementioned parameters was investigated. biomass samples were 9.18 mm and 11.5 mm in diameter. Furthermore, within the ER range of 0.2 to 0.5, all the process parameters were studied.

Prasertcharoensuk *et al.* (2018) used CFD modeling and ANSYS FLUENT to design and numerically optimize a 20 cm diameter throated downdraft gasifier. The work thoroughly examined and attested using experimental data on how the gasifier's temperature profile and the characteristics of the gas were affected by the throat diameter as well as the placement of the air input nozzles above the throat. The synthesized gas composition as well as temperature distribution throughout the throated downdraft gasifier were anticipated and validated over different ratios of throat to gasifier diameter (TGD) ranging from 0.25 to 0.50 and the placements of the air input nozzles at 8, 10, and 12 cm above the gasifier throat.

Ngamsidhiphongsa *et al*. (2020) evaluated the performance of an Imbert downdraft biomass gasifier using a two-dimensional CFD model. The work investigated how producer gas compositions were distributed spatially within the gasifier. On the basis of the relationship

between the throat and gasifier diameters and the height of the air nozzle from the throat, the important design parameter of throat diameter and its impacts on gasifier performance were predicted. The CGE and tar content were calculated.

2.8.4. TEM

Although thermodynamic equilibrium cannot be achieved during the gasification process, the findings of a thermodynamic model show the potential greater performance in an ideal system at any given feedstock. The foundation of TEM is gasification reactions occurring inside the gasifier, with the idea that the system can eventually attain an equilibrium state (Silva et al., 2019). A comparison of several modeling approaches is shown in Table 2.4.

Table 2.4. Comparison of various modeling techniques (Kushwah et al., 2022; Mikulandrić et al., 2014)

Mathematical model	Advantages	Disadvantages
Kinetic	✓ Provides in-depth details about how processes work ✓ Greater realism in the process description ✓ Beneficial for improving gasifier design	✓ Not all potential process reactions are taken into account ✓ It is dependent on how the gasifier is designed ✓ Various kinetic constants and reaction coefficients in the models
ANN	✓ No requirement for in-depth process expertise	✓ Many idealized presumptions are taken into account ✓ A significant amount of experimental data is required.
CFD	✓ It utilizes numerical methods, different algorithms, and ideas from fluid mechanics to address fluid flow problems. ✓ In a steady-state or transient scenario, it can predict the reactant flow patterns along with heat and mass transfer.	✓ It requires a lot of processing power and frequently necessitates the use of specialized software, which is typically quite expensive. ✓ High requirement for in-depth process expertise

TEM	✓ Quickly converges and is simple to implement ✓ Valuable in predicting gasifier characteristics under various operating factors ✓ Independent of the type and design of the gasifier or any particular operating conditions	✓ Only briefly describe the stationary gasification operation ✓ Thermodynamic equilibrium is not possible in an actual process

Because they rely on the reaction mechanisms of different chemical reactions that take place in the gasifier, kinetic models (Massoudi Farid et al., 2016) are considered to be fairly sophisticated models. Likewise, CFD models (Luo et al., 2019) are also quite complex models since they comprise sub-models for oxidation, vaporization, and pyrolysis in addition to a wide range of physical phenomena (such as particle shape and fluid flow characteristics, etc.) that are necessary for the simulation.

Compared to more intricate kinetic and CFD models, TEM is straightforward and can be solved with less computation time. Equilibrium conditions in the gasifier may not be reached when dealing with experiments, however, these TEMs provide an estimate of the producer gas' composition at its output. Stoichiometric and non-stoichiometric models are the two methods used in equilibrium modeling (Ayub et al., 2020b; Gambarotta et al., 2018). Calculating the corresponding equilibrium constants is necessary to solve stoichiometric models, which are built on the premise that some chemical reactions reach equilibrium. Furthermore, other than the additional mentioned advantages which are shown in Table 2.4, TEM is mainly independent of the type and design of the gasifier or any particular operating conditions which makes it suitable for this study.

Thus, in this work, the individual fraction of syngas will be anticipated using a thermodynamic equilibrium technique that includes stoichiometric models, and the performance of a downdraft gasifier will then be investigated using numerical methods. Both the LHV and composition of the syngas will be determined by specifying the elemental compositions and the MC of the chosen biomass, as well as utilizing the Engineering Equation Solver (EES) tool.

2.9. Modeling and performance evaluation

Numerous researchers are drawn to developing the downdraft gasifier because of their benefits (Hernández et al., 2010; Susastriawan et al., 2019). Due to this, profuse research projects and developments have been carried out on numerical and experimental performance analysis of throated downdraft gasifiers utilizing locally available biomass as a fuel.

Upadhyay *et al.* (2019) discussed modeling and experimental research on a downdraft gasifier with various ERs. The performance of the downdraft gasifier was examined with seven different ER ranging from 0.24 to 0.386. The feedstock for a 10-kW atmospheric pressure downdraft gasifier was made up of lignite and sawdust briquettes. LHV, gas yield, tar, particulate matter, and cold gas efficiency were identified along with fuel and air consumption. To calculate the PG compositions and LHV, a thermo-equilibrium model was implemented.

In order to accurately replicate the operating behavior of a downdraft gasifier, Paiva *et al.* (2021) used the chemical process modeling and simulation program known as UniSim Design to model and simulate biomass gasification processes. To forecast the composition of the produced syngas, the analysis was conducted for two residual biomasses, hardwood chips, and almond shells. Furthermore, the minimization of Gibbs' free energy was used for the simulation of gasification. The ER, steam to biomass ratio (SBR), and GT were the three key operating parameters taken into account. In order to maximize these three variables in the process with the selection of the optimal operating parameters, a sensitivity analysis was performed in the simulations to examine the effects of these parameters on the composition of syngas, the flow of syngas, and heating value.

Awais *et al.* (2021) designed, constructed, and evaluated a 24-kW downdraft biomass gasifier fed by sugarcane bagasse and coconut shells. The CE-400 elemental analyzer was used to perform elemental analysis on biomass feedstock. The work also, assessed how the ER affected the composition, yield gasification efficiency, heating value, and tar content of syngas. Furthermore, the results of the experiment demonstrated that in addition to other factors such as feedstock, MC, and ER, uniform air distribution in the gasifier reactor significantly influenced the PG composition by raising the internal temperature of the reactor.

A downdraft biomass gasifier was designed and built by Sharma *et al.* (2020) to investigate the gasification properties of Lantana camara biomass. The diameter of the reaction chamber, the specific biomass feed rate, the char reaction time, and the characteristics of the

biomass fuel were all standard parameters used in the design and construction of the gasifier. The gasifier's performance was assessed using ERs, heating value, gas composition, zone temperatures, gas yield, gasifier efficiency, and carbon conversion efficiency. In addition, air was used as an oxidizing agent in the gasification experiments.

In order to evaluate, forecast, and optimize the efficiency of the downdraft gasification process, a mathematical model centered on the minimization of Gibbs' free energy for the system was employed by Kashyap *et al.* (2019), keeping track of the gasifying agent's reactant flow rates and understanding the properties of biomass. To determine the constituents of the syngas produced by gasifying Lantana camera, which is utilized as a feedstock, the model was also further expanded. Moreover, the data presented by other writers in the literature were used to validate the model.

Rabea *et al*. (2021) studied the performance and dynamic behavior of an Imbert downdraft gasifier integrated with an internal gasifying agent heating system. A batch of cotton stalks served as the feedstock for the gasifier, while air was used as the gasifying agent. In order to achieve ER between 0.305 and 0.195, the air flow rate was varied from 60 to 200 l/min. The LHV, carbon conversion efficiency, gasification efficiency, and gas production were all taken into consideration when assessing the process. As the air supply rate was increased during the batch-mode operation, the rate at which biomass was used also rose, which in turn caused the computed ER to shift in the other direction. The dependence on the H_2O supplied by both the drying and pyrolysis zones causes the hydrogen-based ingredients in the generated gas to drastically decreased with time.

Arnaldo *et al*. (2019) investigated the use of palm kernel shells (PKS) made by the Colombian palm oil mill industry as fuel for an industrial downdraft fixed bed gasifier (Ankur Scientific WGB-20) built to burn wood chips. To achieve the best gasifier performance, measured as the ratio of production gas chemical energy to biomass feeding energy, operational parameters including ash removal time, hopper shaking time, and airflow were changed. Behavior indicators were examined as a function of ER because these characteristics have an impact on ER. Additionally, it was shown that whilst removal time is not important, the shaking duration and airflow significantly affected the HHV and process effectiveness.

Singla *et al*. (2020) investigated the Imbert type gasifier's performance by employing rice straw briquettes as fuel while researching how airflow rate affects fuel consumption and combustion zone temperature. The ratio of air flow rate to temperature within the oxidation zone was linear. The varying air flow rates had a considerable impact on the fuel

consumption rate. The feedstock consumption rate significantly increased as the airflow rate increased from 0.0022 to 0.0042 m^3/s. Furthermore, a test was conducted to see how long it would take to boil 20 liters of water, and the results revealed that higher air flow rates took the longest.

Khonde *et al*. (2021) estimated the composition of the product gas from biomass gasification using the MS Excel Solver tool and the Gibbs free energy minimization approach, which only considers the influence of temperature on reaction equilibrium conditions. Operating temperature, ultimate analysis of a biomass sample, and thermodynamic coefficients for each gas component and element were the inputs needed for the simulation. When partial carbon conversion was taken into account, the model's predictions for all of the gaseous products closely matched those found in the literature.

Ayub *et al.* (2020a) introduced non-stoichiometric equilibrium models to the design equations that had been changed and improved with correction factors so that model predictions would be more accurate when the Gibbs free energy was minimized. For each syngas component in the product, correction factors were added to the Gibbs function to change these models. Utilizing the optimization toolkit in MATLAB, the equilibrium models were optimized based on experimental data from the literature. It was demonstrated that the updated non-stoichiometric models were more accurate than the original ones.

Gambarotta *et al*. (2018) provided a non-stoichiometric equilibrium model to be employed in simulation models of complex energy systems to simulate the gasification process of downdraft gasifiers. Five elements make up the feedstock, while 15 chemical species were taken into account for the syngas, and the chemical equilibrium was established by reducing the Gibbs free energy. The LHV of the syngas and the relative quantities of the gasification products were estimated.

Shin *et al*. (2022) conducted a theoretical analysis of the biomass gasifier-based biochar manufacturing process. The impact of biochar production rate on producer gas properties, such as gas composition, LHV, and cold gas efficiency, was demonstrated using a thermodynamic model established on chemical equilibrium analysis. In order to simulate gasifiers that produce biochar, three gasifier models were rebuilt using the chemical equilibrium model, and seven different types of biomasses were taken into account as feedstock. In order to provide more straightforward prediction correlations, correlations for LHV_{PG} and CGE were also developed based on the thermodynamic simulation.

Madadian *et al*. (2020) investigated how the ER affected the reaction temperature and product gas during the breakdown of woody biomass inside a downdraft gasifier using a

thermodynamic model developed in MATLAB and CANTERA. By minimizing the Gibbs free energy required to calculate the equilibrium constants, the producer gas's composition was estimated. The ultimate equilibrium state was discovered using the Newton-Raphson algorithm. Furthermore, at the ideal ER of 0.31, CGE and HHV were maximized. It was discovered that the enthalpy of oxidation and the Gibbs free energy shift through the reactor's primary components were both negative.

Bijesh *et al.* (2021) formed a modified stoichiometric thermodynamic equilibrium model that uses sewage sludge as the gasification feedstock. By employing the Newton-Raphson method to solve the equations on the MATLAB platform, the generated model looked into the impacts of operating parameters. Sulfur was included, which is typically found in significant amounts in sewage sludge. The model was used to forecast how temperature and ER would affect the mole fraction of the syngas constituents. With an increase in temperature, it was discovered that the product gas yield, gas efficiencies which are CGE and CCE, and LHV of product gases all increased.

An erstwhile research, Dutta *et al.* (2014) employed CHN analysis to examine five readily available biomasses in the area: dimaru *(Ficus lepidosa wall)*, shisham *(Delbergia sissoo)*, neem *(Melia azedarach)*, bamboo *(Banbusea tulda)* and gulmohar *(Delonix regia)*. A downdraft gasification process with a thermal capacity of 10 kW was modeled in terms of PG composition using the results of the elemental characterization. Based on equilibrium constants and reasonable assumptions, a thermodynamic equilibrium modeling for a throated downdraft gasifier had been proposed. By using gas chromatography analysis, the PG compositions made from these five woody biomasses had been identified. At a GT of 850 °C, the gas compositions of the aforementioned biofuels were examined with various MCs from 0 to 30%.

2.10. Literature summary

As per the literature reviewed, the modeling and experimentation of throated downdraft gasifiers have been done to assess the performance of the gasification system under numerous parameters. The kinetic model, TEM, and CFD were the major modeling techniques that were implemented to simulate the gasification system by predicting the composition and temperature of PG. Furthermore, with various biomass samples, the performance evaluation for the gasifier was done by considering input parameters mainly, biomass size, MC, ER, steam to biomass ratio, gasification temperature, TGD ratio, and placement of air input nozzle. The observed and estimated effects of these main input

parameters on yield, composition, exit temperature, CGE, and LHV of syngas, and also on the gasification temperature were validated through related literature.

As it is shown in Table 2.5, some of the literature reviewed are listed with their corresponding author, year of publication, biomass samples used, mathematical modeling techniques utilized, main input performance parameters, and also the outcomes.

Table 2.5. Summary of literature review

No.	Author (year)	Feedstock samples	Modeling technique	Main input parameters	Outcomes
1	Upadhyay *et al.* (2019)	Lignite and sawdust briquettes	TEM	ER	Increment of GT and decrement in a concentration of CO_2 and H_2 in the PG as ER raises.
2	Paiva *et al.* (2021)	Hardwood chips, and almond shell.	TEM	ER, SBR, and GT	When ER and SBR increased, the heating value of syngas dropped, but as GT augmented, it intensified for both biomass samples. Given that it encouraged the creation of H_2, the ER was a crucial process variable.
3	Jayathilake and Rudra (2017)	Birchwood	CFD	Biomass size and ER	As ER increased up to 0.35 and as biomass size decreased, the majority of the observed and estimated parameters including yield,

					CGE, and LHV of syngas, had shown an upward trend.
4	Prasertchar-oensuk *et al.* (2018)	Wood	CFD and ANSYS FLUENT	TGD ratio and placement of air input nozzle	The concentration of CH_4 was reduced when the TGD ratio was raised up to 0.4. Moreover, CH_4 was found to be reduced by 31% when the air inlet nozzles were raised from 8 to 12 cm well above the throat.
5	Kashyap *et al.* (2019)	Lantana camera	TEM	ER and biomass size	As ER grew from 0.434 to 0.44 and particle size elevated from 3.3 to 5.5 cm, the levels of H_2 and CO_2 in the syngas dropped.
6	Smith *et al.* (2019)	Eight biomass samples	Kinetic model	ER, MC, biomass composition, and GT	The volume percentage of CO fell, however, the volume fractions of H_2 and CO_2 augmented as the MC increased. When ER was increased, the CO % grew until a peak value was reached, and then it fell.

7	Singh *et al.* (2014)	Wood, coconut shells, rubber seed kernels, and coir pith.	Two-zone kinetic equilibrium model	ER	All biomass samples had higher conversion efficiency when the ER was near 0.2.

2.11. Research gap

A thorough analysis of previous work from researchers revealed that numerous studies on the modeling and performance evaluation of downdraft gasifiers with throats employing various biomass feedstocks and parameters had been carried out. It is clear from the above review that there is a wide range of parameters that can be used to evaluate the performance of a gasification system. However, it has been discovered that when it comes to the experimental findings, the majority of assessments of performance for the gasification system rely heavily on the PG composition and LHV. This performance evaluation can be improved by considering additional variables that can also determine the performance of the gasification system. The following research gaps are noted in relation to the literature.

- The literature did not thoroughly address analyses such as the temperature variation over time in the gasifier. Insufficient research has been found about the temperature distribution in throated downdraft gasifiers.
- The majority of the literature did not examine the analysis of the PG flame intensity for different feedstocks. Hardly any attempts have been made to evaluate the impact of biomass type on the characteristics of the PG flame.
- The majority of research did not take into account analysis such as the quantity of condensate particles after gasification.
- The amount of char left over after experimental works have hardly ever been considered a performance evaluation parameter in the literature. Hardly any attempts had been made to investigate how different biomass types affected the quantity of char that remained unconverted.

Hence, in this work, an effort will be made to bridge the aforementioned research gap through an experimental and theoretical examination.

CHAPTER THREE

MATERIALS AND METHODS

3.1. Introduction

In this chapter, the overall design of the study, which includes the materials and measuring equipment used, the methodology used for carrying out the different tasks, and several stages of this research are introduced. Furthermore, the work that was done at each step, as well as the tools, approaches, and models that were implemented, are all covered thoroughly in this section.

3.2. Materials

The gasifier reactor section was subjected to great temperature, thus to withstand the high internal temperatures and prevent welded strips from rusting, it was important to carefully select a material for the cylinder of the reactor, which was in direct contact with the burning fuel. In addition, parts that might come into direct contact with the wet producer gas coming out of the gasifier should be made of materials that have been carefully chosen to avoid rusting. The choice of materials was made based on their rigidity, durability, corrosiveness, and maintainability, as well as their strength, durability, availability, machinability, and malleability for the components to be cold worked to ensure a longer machine life span and affordability of the machine.

Various materials selected for the construction of the gasification system different components are listed in Table 3.1.

Table 3.1. Material selection for the gasifier parts

No.	Component	Material selected
1	Gasifier reactor	Mild steel
2	Gas outlet pipe	Galvanized pipe
3	Cyclone separator	Mild steel
4	Cyclone gas inlet and outlet	Galvanized pipe
5	Gas passage	Galvanized pipe
6	Gasifier stand	Mild steel hollow rectangular bar
7	Air inlet pipe	Galvanized pipe

As a computation tool and to draw different parts of the gasification system, Engineering Equation Solver (EES) and AutoCAD 2018, were used respectively.

Various instruments required for measurements which are taken during and after the gasifier performance evaluation are presented in Table 3.2. Furthermore, the imageries of them are presented in Appendix D.

Table 3.2. Measuring instruments and their application

No.	Instrument	Application
1	Thermocouple	Measures zone temperatures
2	Thermometer	Measures ambient temperature
3	Weighting scale	Measures sample weights
4	Gas analyzer	Measures compositions of the product gas
5	Digital thermometer	Displays measured temperatures
6	Anemometer	Measures air velocity
7	Stop watch	Measures time taken for complete gasification

3.3. Methodology and research design

In order to create a mathematical model and conduct experimental analysis for the proposed gasifier, this study was conducted. Based on predetermined objectives, a methodology was used to carry out this study. In this work, starting with the preparation of biomass samples, numerical and experimental methods were also included. The scientific literature was reviewed, followed by theoretical and experimental analysis, to undertake this work. The numerical approach makes use of the different governing equations. Furthermore, it employs an equilibrium model of a downdraft gasification process to examine how well a downdraft gasifier performs using biomass samples that are readily available locally, specifically: mango seed hull, and peanut shell. A comparison study was presented for the calorific values of the aforementioned biomass samples, and data from the proximate and ultimate analyses is presented. The impact of fuel and process parameters was easily studied because thermodynamic equilibrium calculations are independent of gasifier design. The uppermost attainable yield of desired products from a reacting system was predicted via TEM. Additionally, design work was done on the proposed gasifier. Following that, the designed components were built and put to the test while having various parameters changed. Experimental analysis was conducted and the influence of several parameters including biomass type, biomass size, and gasification temperature on the performance of the gasifier was conducted. Figure 3.1 shows the general development of the study, from the preparation of the proposal to the completion of the thesis, as well as the technique that was suggested and used.

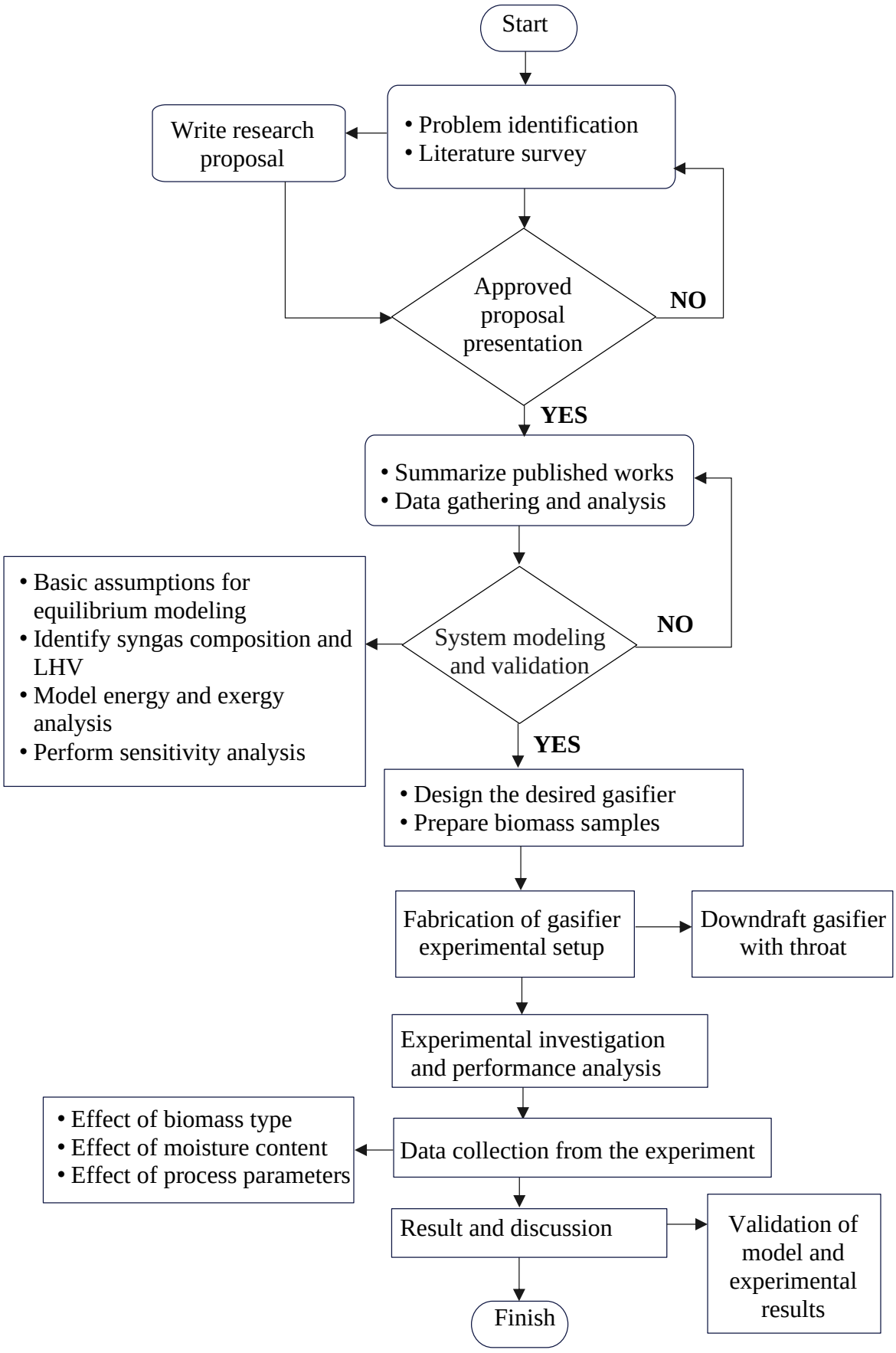

Figure 3.1. Methodological approach flow chart

3.3.1. Literature survey

The first step was to conduct a survey of the literature on biomass gasification and its classification. Through a review of the literature, several methods and approaches for system model and design were covered, along with a discussion of the available gasifiers, gasifier selection criteria, and gasifying medium selection as well as numerical and experimental results. From many research papers and journals, as much information as possible regarding the available downdraft gasifiers, factors influencing the gasifier's performance, and design parameters was gathered.

3.3.2. Data collection method

The study starts by gathering data on biomass with a low ash level that would be appropriate for the anticipated process output, which is syngas with a low tar concentration. In order to understand the properties of the chosen biomasses, the elemental and proximate analysis for the biomass was conducted. The availability of the biomass, as well as other relevant materials and information, were also gathered from experimental analysis, literature review, reliable references, and other available sources.

3.3.2.1. Biomass availability

The information regarding the availability and growing season of the chosen biomass feedstocks was thoroughly examined from prior literature in the area. In terms of geographical coverage, Ethiopia ranks second in the world for the production of mango (*Mangifera indica*). About 16,363.48 hectares of mango production were carried out in the 2019/20 crop year, accounting for 12.49 % of the nation's total fruit production (Abate & Dechassa, 2021). On the other hand, groundnut, often known as peanut (*Arachis hypogaea*), was produced in 2019 in quantities totaling 157 kilotons (Cervini et al., 2022).

3.3.3. Mathematical model

The performance of the gasifier in this study was examined using a mathematical model after the individual fraction of syngas is predicted via a stoichiometric equilibrium technique. By providing the elemental compositions of the selected biomass, with the MC and also other model inputs, Engineering Equation Solver (EES) tool was used to determine the composition of syngas and also the LHV for the input parameters.

3.3.4. Physical concept

Following the development of the required downdraft gasifier, a schematic depiction of the system integration and each component was presented. Using AutoCAD 2018 software, a pictorial depiction of the proposed downdraft gasifier was constructed.

3.3.5. Experimental methods

This investigation comprises an examination of the biomass used as a feedstock as well as an assessment of the prototype's performance in light of numerous factors.

3.3.5.1. Analysis of biomass feedstock

Proximate studies to determine MC, calorific value, volatiles, ash, and fixed carbon content were presented for the biomass samples. Additionally, ultimate analyses to determine the C, H, N, O, and S content were provided.

3.3.5.2. Performance analysis on the prototype of the gasifier

An exhaust gas analyzer was used to determine the components of the PG that were produced from the gasification of biomass samples. The experiment also considered the tar content and PG exit temperature.

3.3.6. Validation

After the mathematical modeling is developed it was validated with available literature Moreover, the experimental investigation is conducted and validation with the mathematical model is done.

CHAPTER FOUR

EQUILIBRIUM MODEL AND GASIFIER DESIGN

4.1. Introduction

In this chapter, the overall development of the equilibrium model for the study, which includes the model formulation, mass balance, energy balance, exergy analysis, and model implementation is introduced. Furthermore, the geometrical dimensions of different parts of the proposed gasifier are designed with proper assumptions and data with a thorough literature survey.

4.2. Model formulation

The following assumptions have been taken into account in the development of the stoichiometric thermodynamic equilibrium model (Ayub et al., 2020b; Bijesh et al., 2021; La Villetta et al., 2017; Sittisun et al., 2019).

- Carbon, hydrogen, oxygen, and nitrogen are the main elements in the biomass feedstock. and the chemical formula of biomass is taken to be $CH_aO_bN_c$.
- Metal and alkali contents in the biomass are neglected;
- The temperature of the reactor is uniform and it is in steady state.
- The system is thought to be adiabatic and there is no heat loss from it;
- In all reactions, ash is considered to be inert.
- A negligible amount of tar is produced from the gasifier;
- Dry (zero relative humidity) air containing 79 % nitrogen and 21 % oxygen by mass enters the chamber.
- Biomass undergoes complete carbon conversion to gaseous products;
- Each and every gas in the established system is regarded as an ideal gas;
- The partial oxidation of the air supply renders the calculated gas oxygen-free and all oxygen is consumed during combustion reaction.
- Air and biomass feedstock enters the gasifier at a temperature of 25℃, and the gasifier's pressure is 101.13 kPa;
- The only gases that are produced are H_2, CO, CH_4, CO_2, N_2, and H_2O.
- The pyrolysis process, which yields gas, tar, and char, is regarded as a one-step reaction.
- N_2 is regarded as inert and not undergoing any chemical reactions.

From the assumption the chemical composition of the biomass is $CH_aO_bN_c$. It is gasified in w moles of air; the overall gasification reaction can be written using equation (4.1) (Ayub et al., 2020b; Dutta et al., 2014; Gambarotta et al., 2018; La Villetta et al., 2017; Silva et al., 2019).

$$CH_aO_bN_c + mH_2O + w(O_2 + 3.76N_2) = (1-\alpha)C + n_{H_2}H_2 + n_{CO}CO + n_{co_2}CO_2 + n_{H_2O}H_2O + n_{CH_4}CH_4 + x_{N_{2,gas}}N_2 \quad (4.1)$$

Where: -

n_{H_2} , n_{CO} , n_{co_2} , n_{H_2O} , n_{CH_4} and $(1-\alpha)$ are moles of the components in the reaction

$x_{N_{2,gas}}$ is the mole of nitrogen in the gas side

a, b, and c are mole ratios ($\frac{H}{C}$, $\frac{O}{C}$, and $\frac{N}{C}$) obtained from the elemental analysis biomass.

m, is the molar quantity of water, and it can be expressed using equation (4.1a)

w, oxygen per mole of feedstock, and it can be expressed using equation (4.1b)

α, is the carbon conversion factor, and it can be expressed using equation (4.1c)

$$m = \frac{MC \times (12 + a + 16b)}{18 \times (1 - MC)} \quad (4.1a)$$

$$w = ER \times (1 + \frac{a}{4} - \frac{b}{2}) \quad (4.1b)$$

$$\alpha = 0.32 + 0.84 \times \left(1 - \exp\left(-\frac{ER}{0.299}\right)\right) \quad (4.1c)$$

4.2.1. Mass balance

Equations from (4.2) to (4.5) can be used to write equations that balance the global reaction's moles of carbon, hydrogen, oxygen, and nitrogen:

For carbon

$$n_{CO} + n_{co_2} + n_{CH_4} = \alpha \quad (4.2)$$

For hydrogen

$$2 \times m + a = 2n_{H_2} + 2n_{H_2O} + 4n_{CH_4} \quad (4.3)$$

For oxygen

$$m + b + 2 \times w = n_{CO} + 2n_{co_2} + n_{H_2O} \quad (4.4)$$

For nitrogen

$$x_{N_{gas}} = \frac{c}{2} + 3.76 \times w \quad (4.5)$$

The fundamental gasification process at 25℃ is described by the simplified chemical formulas in equation (4.6) (Basu, 2010; Dutta et al., 2014).

$Boudouard\ reaction$	$C + CO_2 \rightarrow 2CO + 172\ kJ/mol$	(4.6a)
$Water\ gas\ or\ steam$	$C + H_2O \rightarrow 2CO + H_2 + 131\ kJ/mol$	(4.6b)
$Hydrogasification$	$C + 2H_2 \rightarrow CH_4 - 74.8\ kJ/mol$	(4.6c)
$Oxidation\ reactions$	$C + O_2 \rightarrow CO_2 - 394\ kJ/mol$	(4.6d)
	$C + 0.5O_2 \rightarrow CO_2 - 284\ kJ/mol$	(4.6e)
	$CH_4 + 2O_2 \rightarrow CO_2 + 2H_2O - 803\ kJ/mol$	(4.6f)
	$H_2 + 0.5O_2 \rightarrow H_2O + 242\ kJ/mol$	(4.6g)
$Water\ gas\ shift\ reaction$	$C + H_2O \rightarrow CO_2 + H_2 - 41.2\ kJ/mol$	(4.6h)
$Methanation$	$2CO + 2H_2 \rightarrow CH_4 + CO_2 - 247\ kJ/mol$	(4.6i)
	$CO_2 + 4H_2 \rightarrow CH_4 + CO_2 - 165\ kJ/mol$	(4.6j)
$Steam\ reforming$	$CH_4 + H_2O \rightarrow CO + 3H_2O + 206\ kJ/mol$	(4.6k)
	$CH_4 + 0.5O \rightarrow CO + 2H_2O - 36\ kJ/mol$	(4.6l)

Applying the phase rule, the number of independent reactions must be established for the creation of an equilibrium model. Since equilibrium is considered to be reached when no solid carbon is left in the equilibrium state, then only two reactions, the water gas shift, and the hydrogasification can handle this (Dutta et al., 2014).

For the model used in this study, all gases are considered to be ideal, and all reactions take place at atmospheric pressure in addition to the assumption of thermodynamic equilibrium. As a result, the equilibrium constants for the hydrogasification or methane formation, and water gas shift reaction that depend on temperature are expressed using equation (4.7) and (4.8) respectively (La Villetta et al., 2017; Silva et al., 2019).

$$k_1 = \prod_i (x_i)^{v_i} \left(\frac{P}{P_0}\right)^{\sum_i v_i} = \frac{x_{CH_4}}{\left(x_{H_2}\right)^2} \tag{4.7}$$

$$k_2 = \prod_i (x_i)^{v_i} \left(\frac{P}{P_0}\right)^{\sum_i v_i} = \frac{x_{H_2} x_{CO_2}}{x_{CO} x_{H_2O}} \tag{4.8}$$

Where: -

$x_i = \frac{n_i}{\sum n_i}$, is the mole fraction of the compound i in the ideal gas mixture

v - is the stoichiometric number

$P\ and\ P_0$ are reaction pressure and standard pressure, respectively

The equations for calculating the equilibrium constant and the reaction's Gibbs free energy can be written using equation (4.9) and (4.10) respectively (La Villetta et al., 2017; Silva et al., 2019).

$$\ln K = -\frac{\Delta G_T^{\circ}}{RT} \tag{4.9}$$

$$\Delta G_T^{\circ} = \sum_i v_i \, \Delta g_{f,T,i}^{\circ} \tag{4.10}$$

Where: -

R - is the universal gas constant

ΔG_T° - the standard Gibbs function of reaction,

$\Delta g_{f,T,i}^{\circ}$ - is the standard Gibbs function of formation at a given temperature T of the gas species i, and it can be formulated using equation (4.10a) (Jarungthammachote & Dutta, 2007; La Villetta et al., 2017).

$$\Delta g_{f,T,i}^{\circ} = h_f^{\circ} - aT\ln(T) - bT^2 - \frac{c}{2}T^3 - \frac{d}{3}T^4 + \frac{e}{2T} + f + gT \tag{4.10a}$$

The values of coefficients a, b, c, d, e, f, g and the enthalpy of formation of the gases h_f° are presented in Table E-1 of Appendix E.

4.2.2. Energy balance

The overall energy balance for the gasification of 1 $kmol$ of fuel is written in the form of equation (4.11) (La Villetta et al., 2017; Silva et al., 2019).

$$LHV_{Fuel} + n_{air}\Delta h_{air} = n_{gas}(\Delta h_{gas} + LHV_{gas}) \tag{4.11}$$

Δh_i , is the enthalpy difference in $kJ/kmol$ between any given state and the reference state which is ($T = 298\ K, P = 0.1\ MPa$)

The enthalpy difference between the reference state and the condition at which the air is heated to T_p before entering the gasifier is computed using equation (4.11a).

$$\Delta h_{air} = X_{O_2,air}\int_{T_0}^{T_p} C_{p,O_2}\, dT + X_{N_2,air}\int_{T_0}^{T_p} C_{p,N_2}\, dT \tag{4.11a}$$

When air at the reference condition is used for gasification, the term in equation (4.11a) equals zero. The product gas's gasification state at time T differs in enthalpy from the reference state as formulated in equation (4.11b).

$$\Delta h_{air} = \sum_i x_i(h_T - h_{T_0}) = \sum_i x_i \int_{T_0}^{T_p} C_{p,i}\, dT \tag{4.11b}$$

The third-order polynomial equations are used to determine the specific heat capacity at constant pressure for the ideal gases utilized in this model. They are included in Table E-2 of Appendix E along with the pertinent temperature ranges and the maximum errors.

As it can be seen in equation (4.11c), in the absence of data, the HHV calculation formula which is equation (4.11d), can be used to calculate the LHV of solid fuel in MJ/kg.

$$LHV_{Fuel} = HHV - 9m_h \times h_{fg} \quad (4.11c)$$

$$HHV = 1.1783\,H + 0.3491\,C + 0.1005\,S - 0.1034\,O - 0.0151\,N - 0.0211\,Ash \quad (4.11d)$$

Where: C, H, O, N, S, and Ash are percentages of mass of carbon, hydrogen, oxygen, nitrogen, sulfur, and ash in the dry solid fuel, m_h is the mass fraction of hydrogen in solid fuel and h_{fg} is the enthalpy of vaporization of water.

Using equation (4.11e), it is possible to calculate the lower heating value of the product gas (LHV_{gas}) produced under the same temperature and pressure conditions as the biomass material used, by multiplying the mole fraction (x_i) by the lower heating values (LHV_i) of each gas component (Mhilu, 2012).

$$LHV_{gas} = \sum_i x_i\, LHV_i \quad (4.11e)$$

The LHV of the different compounds of the produced gas is shown in Table 4.1.

Table 4.1. The volumetric LHV of product gas from biomass gasification (Basu, 2010; Waldheim & Nilsson, 2001)

Product gas	$\boldsymbol{LHV}$ $(\boldsymbol{MJ/Nm^3})$
H_2	10.78
CO	12.63
CO_2	-
CH_4	35.88
N_2	-

4.2.3. Exergy efficiencies

The gasifier, whose performance is evaluated using the second law of thermodynamics and the exergy analysis approach to describe the energy exchange processes, is a key factor in the efficiency of biomass conversion. Potential exergy, kinetic exergy, physical exergy, and chemical exergy are the four main components of the total system exergy (ε), and each has a thermomechanical and chemical component (La Villetta et al., 2017; Silva et al., 2019).

The maximum amount of work that a substance is capable of performing when it approaches thermal and mechanical equilibrium with its surroundings is known as thermomechanical

exergy or physical exergy (La Villetta et al., 2017). A system's exergy efficiency can be calculated using only its chemical exergy efficiency. This is done under the assumption that the kinetic and potential energy contributions are negligible and that only the chemical and physical exergies of species exist. As shown in equation (4.12), a process' chemical exergy efficiency is determined by dividing the chemical and physical exergies of the product gas by the total materials input (Mhilu, 2012; Silva et al., 2019).

$$\eta_{exe,ch} = \frac{n_{gas}(\varepsilon_{ch,gas} + \varepsilon_{ph,gas})}{\varepsilon_{ch,biomass}} \quad (4.12)$$

Where:

$\varepsilon_{ch,gas}$ is the chemical exergy of the product gas,

$\varepsilon_{ch,biomass}$ is the chemical exergy of the biomass material,

$\varepsilon_{ph,gas}$ is the physical exergy of the product gas.

n_{gas} is the molar amount of product gas

4.2.3.1. Chemical exergy of the product gas

Equation (4.12a) can be used to represent the chemical exergy of the various components of the product gas (Mhilu, 2012; Silva et al., 2019).

$$\varepsilon_{ch,gas} = \sum_i x_i \varepsilon_{ch,i} + R_0 T_0 \sum_i x_i \, ln\,(x_i) \quad (4.12a)$$

Where:

x_i is the mole fraction of individual gas components i,

$\varepsilon_{ch,i}$ is chemical exergy of individual gas components i,

R_0 is the universal gas constant ($8.314\ kJ/kmol.K$),

T_0 is the standard temperature (298 K).

As shown in Table 4.2, the relevant values of the chemical exergy $\varepsilon_{ch,i}$ for the syngas composition component were determined using the study's standard values.

Table 4.2. Standard chemical exergy of various gas components (La Villetta et al., 2017)

Gas component	$\boldsymbol{\varepsilon_{ch_i}}$ $\boldsymbol{(kJ/Kmol)}$
CO	275,430
CO_2	20,140
CH_4	836,510
N_2	720
H_2	238,490
H_2O (g)	11,710

4.2.3.2. Chemical exergy of biomass

Equation (4.12b) is also used to calculate the relevant chemical exergy $\varepsilon_{ch,biomass}$ of the biomass material (Mhilu, 2012; Silva et al., 2019).

$$\varepsilon_{ch,biomass} = \beta LHV_{biomass} \quad (4.12b)$$

Where:

β can be expressed using equation (4.12c) and is a factor that depends on the mass fraction of oxygen, carbon, hydrogen, and nitrogen in the feedstock (Mhilu, 2012; Silva et al., 2019).

$$\beta = \frac{1.044 + 0.016sub_h - 0.3493sub_o(\varphi) + 0.0493sub_n}{1 - 0.4124sub_o} \quad (4.12c)$$

Where:

φ denotes $(1 + 0.0531sub_h)$,

sub_h ,sub_o , and sub_n , are ratios of H/C, O/C, and N/C respectively,

H/C, O/C, and N/C represent atomic ratios of elemental components C, H, O, and N in the solid fuel.

4.2.3.3. Physical exergy of the gas

The percentage of physical exergy or sensible heat is significant in the total exergy of the final gas since the gasification process is intended to occur at higher gasification temperatures. Equation (4.12d), can be used to calculate the physical exergy of the product gas $\varepsilon_{ph,gas}$ (Mhilu, 2012; Silva et al., 2019).

$$\varepsilon_{ph,gas} = (h_1 - h_0) - T_0(s_1 - s_0) \quad (4.12d)$$

Where:

h is molar specific enthalpy,

s is molar specific entropy,

0 denotes the original state of the environment,

1 denotes the exit gas enthalpy and entropy states from the gasifier.

4.2.3.4. Irreversibility

Low amount of energy that can be used for work but is lost or referred to as irreversibility (I) is preferred for high system efficiency. Equation (4.13)**,** can be used to analyze the exergy losses that take place during the gasification process (Mhilu, 2012; Silva et al., 2019).

$$I = (1 - \eta_{exe,ch}) \quad (4.13)$$

4.3. Model implementation

The formulated model was implemented using the model flow chart shown in Figure 4.1. The biomass characteristics, gasifier operating parameters, and gasifying agent characteristics are the main inputs that have to be changed in order to run the model for different kinds of biomass feedstocks.

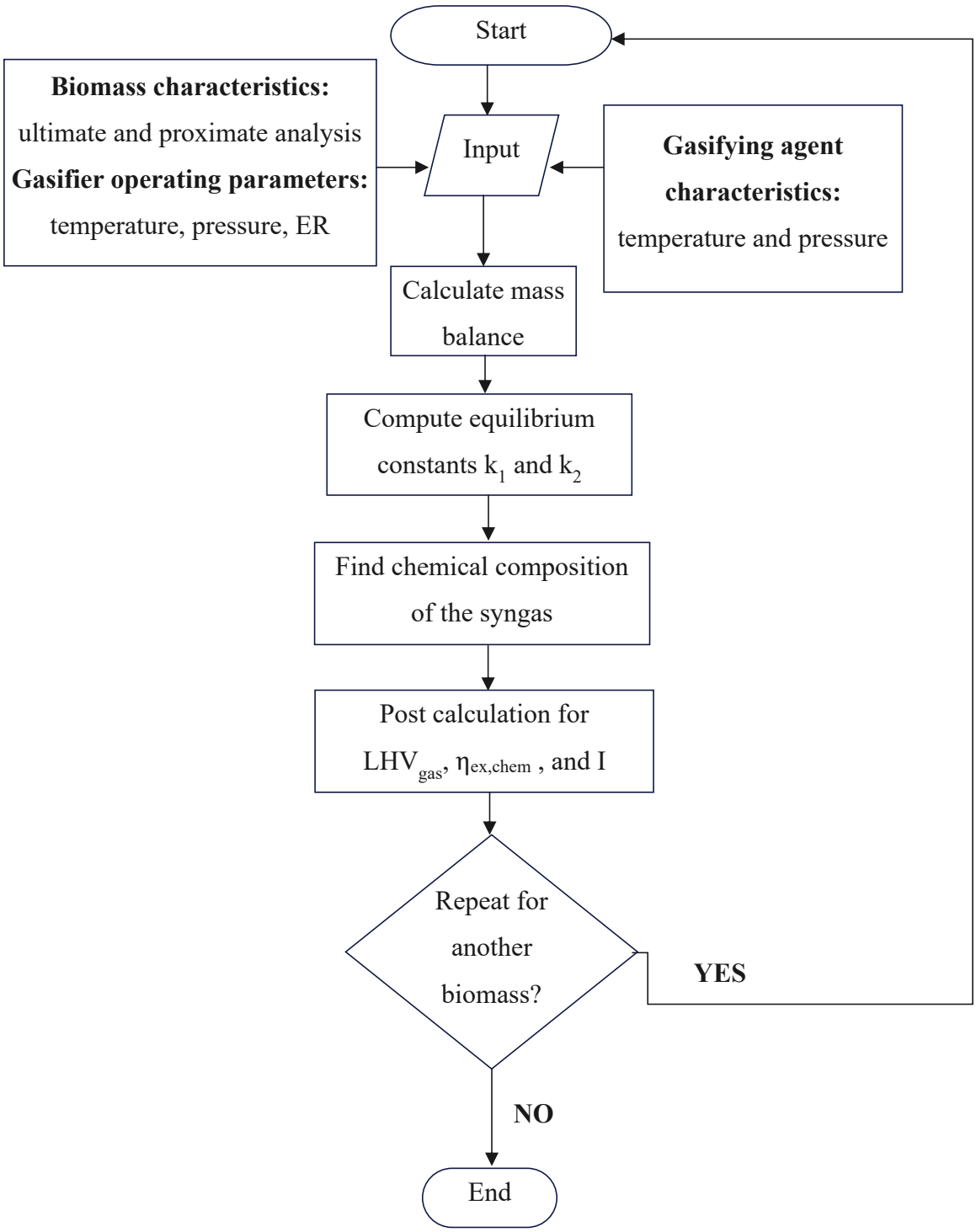

Figure 4.1. Model computation flow chart

4.3.1. Model inputs

The inputs to the model mainly include the physical, chemical, and energy parameters of the biomass samples.

4.3.1.1. Physical parameters

The MC of biomass is the primary physical factor. The total mass of a biomass sample that is made up of water is referred to as moisture. The biomass may have moisture inside of it or on its exterior surface (Perea-Moreno et al., 2016).

4.3.1.2. Chemical parameters

The chemical characteristics mostly relate to components that make up biomass. Moreover, the inorganic components, such as ash, are also frequently of importance (Perea-Moreno et al., 2018).

4.3.1.3. Energy parameters

The calorific value of a fuel is the amount of chemical energy that can be directly converted into thermal energy through a thermochemical oxidation process. Units of energy per unit of mass are typically used to express this property (Basu, 2018; La Villetta et al., 2017).

Typically, biomass feedstock sample proximate and ultimate analytical data were fed into the model. The chemical formulation of the samples is shown in Appendix A.

Proximate analysis

By weight percentages, the proximate analysis delivers information on the biomass's moisture, ash, volatile substance, and fixed carbon content. The purpose of this analysis is to pinpoint the portion of the biomass that contains the chemical energy such as fixed carbon and volatile chemicals, and also the inert portion such as ash and moisture. Volatile matter is the fraction of fuel that is released during the thermal breakdown of biomass as gases and hydrocarbon vapors. The fractions that are left after the volatile substance has been released are fixed carbon and ashes. In combustion processes, fixed carbon keeps burning slowly even after the volatiles have been released (Mata-Sánchez et al., 2013; Perea-Moreno et al., 2018). Table 4.3, which contains information from Figures B-1 and B-2 of Appendix B, displays the proximate analysis of the selected biomass samples.

Table 4.3. Proximate analysis of biomass samples (wt%)

Biomass type	% Moisture content	% Volatile matter	% Fixed carbon	% Ash	Calorific value ($Cal/gram$)
MSH	9.14	77.36	12.65	0.85	4081.94
PS	9.23	67.72	18.24	4.81	4116.04

Elemental analysis

As shown in Table 4.4, to determine the percentage by weight of the primary elements with the highest presence in the molecular structure of the organic substance, elemental analysis is utilized (Silva et al., 2019).

Table 4.4. Ultimate analysis of biomass samples (wt%) (Perea-Moreno et al., 2018; Yousef et al., 2021)

Biomass type	C %	O %	H %	N %	S%	Ash %
MSH	47.93	43.84	6.06	0.50	0.68	0.99
PS	46.42	41.77	6.61	0.50	0.54	4.26

4.4. Gasifier design inputs and outputs

As can be seen in Table 4.5, the source description is given together with the design inputs, which are the initial conditions and assumptions made. The results of this design calculation include the fuel feed rate, air flow rate, product gas flow rate, gasifier efficiency measured in terms of cold gas efficiency, throat diameter and throat inclination angle, fuel storage tube diameter, height of the reduction zone, height of the oxidation zone, and diameter, location, and arrangement of air inlets or nozzles.

Based on recommendations from (Arnaldo et al., 2019; Jayathilake & Rudra, 2017; Kashyap et al., 2019; Madadian et al., 2020; Sharma et al., 2020), and from the model ER value is taken to be 0.3 and the relative tube capacity value suggested by (Akhator et al., 2019) is taken.

Assuming that the 15-kW thermal power output and 10.5 kW electrical power output gasifier is used to provide energy for a family of 8 people, it can be assumed that the gasifier is capable of meeting the energy demand of the household. The electrical power output is the amount of power produced by the gasifier that is converted into usable electricity, and the thermal power output is the total amount of heat energy produced by the gasifier, and the ratio of them which is the electrical to thermal power output can be used to determine the efficiency of the gasifier as shown in Table 4.5 (Basu, 2018; La Villetta et al., 2017). However, the specific energy needs of the household may vary depending on factors such as the size of the home, the number and types of appliances used.

Table 4.5. Taken assumptions and initial conditions for gasifier design

Condition	Value	Source description
Gasifier type	Downdraft (Throated)	Selected with comparison
Biomass type	MSH	Selected with comparison
HHV of the feedstock	17.079 MJ/kg	Experimentally determined
Gasifier thermal power output (P_{out})	15 kW	Assumption
Gasification efficiency, $\eta_{gasifier}$	70 %	$P_{elec}/P_{thermal}$
Equivalence ratio	0.3	Assumption and model
Relative tube capacity	250 kg/m^2h	Literature
LHV of the syngas	5.719 MJ/Nm^3	From the numerical model

4.5. Design criteria

The following are the primary design requirements for a syngas gasifier:

- The gasifier should be capable of handling several fuel sizes and types.
- The gasifier ought to be able to run efficiently with a variety of fuel loads.
- The gasifier should be able to provide stable, clean gas for stove usage and an engine after further cleaning is done.
- The gasifier ought to be simple to use and maintain.
- The gasifier should be reasonably priced and made of materials that are easily accessible in the area.

4.6. Design calculations

4.6.1. Fuel feed rate

As can be seen in equation (4.14), the gasifier thermal power output (P_{out}) is divided by the fuel's LHV (LHV_{fuel}) and multiplied by gasifier efficiency to determine the fuel feed rate $\dot{m}_f$ (Basu, 2018).

$$\dot{m}_f = \frac{P_{out}}{LHV_{fuel} \times \eta_{gasifier}} \tag{4.14}$$

Where:

LHV_{fuel}, LHV_g and V_g is the lower heating value of the feed fuel, the lower heating value of the product gas, and the flow rate of the product gas respectively. LHV_{fuel} is calculated from the characterization of the fuel using equation (B.1) in Appendix B.

4.6.2. Product gas flow rate

Equation (4.15) provides the volume flow rate of the product gas, V_g, from the LHV of the gas (LHV_g) (Basu, 2010). The value of LHV_g is determined from the numerical model.

$$V_g = P_{out}/LHV_g \tag{4.15}$$

4.6.3. Air flow rate

The ultimate analysis of the biomass is necessary for calculating the flow rate of the gasifying medium which is air. Table 4.6. shows elemental compositions of the MSH.

Table 4.6. Elemental analysis (wt%) of MSH with and without ash (Yousef et al., 2021)

Biomass type	C %	O %	H %	N %	S%	%Ash
MSH	47.93	43.84	6.06	0.50	0.68	0.99
Ash free MSH	48.41	44.28	6.12	0.51	0.69	0

For all practical purposes, it is assumed that the weight of air is composed of 77 percent nitrogen and 23 percent oxygen. Air contains 79 % nitrogen and 21% oxygen, measured in terms of volume (Paraschiv et al., 2020). The amount of air required to completely burn one kilogram of fuel can be calculated once the amount of oxygen required for combustion is known. Equation (4.16) can be used to express the minimum amount of oxygen needed for 100 kg of fuel to burn completely (Akhator et al., 2019).

$$\frac{m_o}{m_f} = \frac{8}{3}C + 8\left(H - \frac{O}{8}\right) + S \tag{4.16}$$

Where:

m_o, the mass of oxygen required for complete combustion

m_f, the mass of fuel used for combustion

C, H, O, and S are the weight percent of carbon, hydrogen, oxygen, and sulfur in the fuel.

Since oxygen makes up 23% of the weight of air, 1 kilogram of oxygen is present in $\frac{100}{23} = 4.35\ kg\ of\ air$, and consequently, Equation (4.17) can be used to express the lowest amount of air necessary for the full burning of one kilogram of fuel (Basu, 2018).

$$\left(\frac{A}{F}\right)_{sto} = \left(\frac{m_a}{m_f}\right)_{sto} = 4.35 \times \frac{m_o}{m_f} \tag{4.17}$$

Where:

m_a, the mass of air required for complete combustion

$\left(\frac{A}{F}\right)_{sto}$, Stoichiometric air-fuel ratio for complete combustion

Equation (4.18) can be used to express the actual air-fuel (A/F) ratio for 1 kilogram of fuel at the anticipated equivalency ratio (Basu, 2010).

$$\left(\frac{m_a}{m_f}\right)_{act} = \left(\frac{m_a}{m_f}\right)_{sto} \times ER_{opt} \tag{4.18}$$

Equation (4.19) can be used to express the actual mass flow rate of air needed for the intended condition (Basu, 2018; La Villetta et al., 2017).

$$\dot{m}_{a_{act}} = \left(\frac{m_a}{m_f}\right)_{act} \times \dot{m}_f \tag{4.19}$$

Or in volumetric it can be expressed using equation (4.20)

$$Q_{a_{act,vol}} = \frac{\dot{m}_{a_{act}}}{\rho_{air}} \tag{4.20}$$

Where: ρ_{air}, the density of air at room temperature $(20 - 25\ ^{\circ}C)$ and 1 atm

4.6.4. Parts of the gasifier reactor

Figure 4.2, shows the configuration of different parts of the gasifier reactor that are going to be designed throughout the sections below.

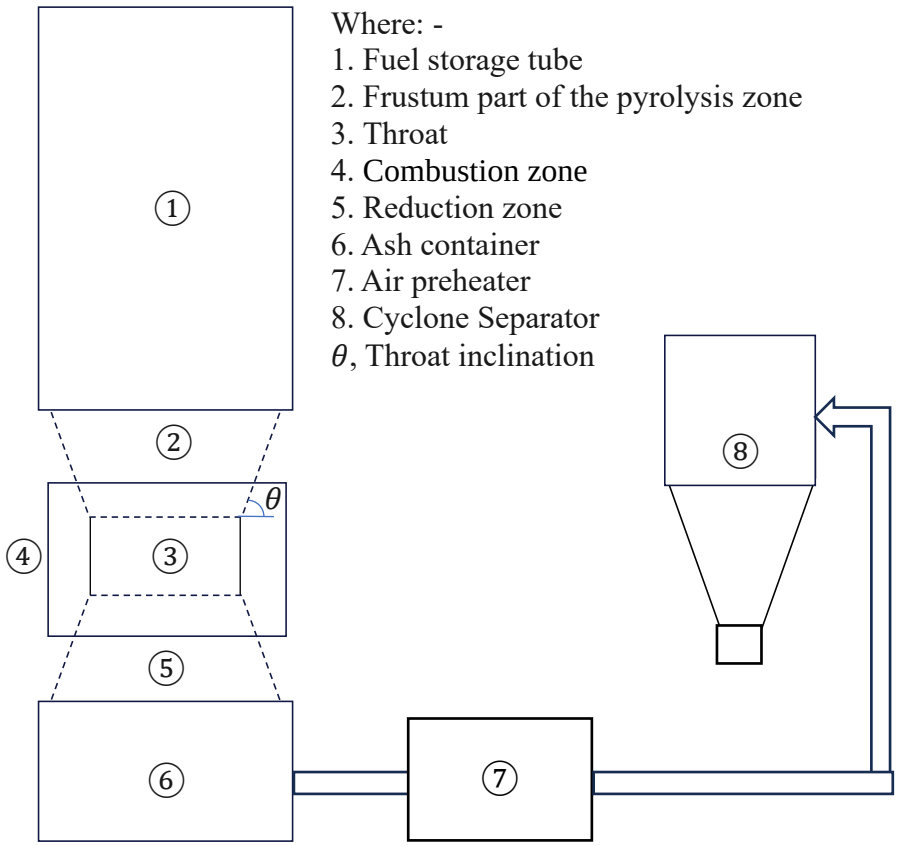

Figure 4.2. Schematic diagram of the gasifier reactor

4.6.5. Fuel storage tube diameter

Relative Tube Capacity (RTC) is used to calculate the diameter of the fuel storage tube, which includes the drying and upper pyrolysis zones, which for the downdraft gasifier is $250\ kg/m^2h$ and it can be expressed using equation (4.21) (Akhator et al., 2019).

$$RTC = \frac{\dot{m}_f}{A_{DP,tube}} \tag{4.21}$$

Where:

$A_{DP,tube}$, area of drying and upper pyrolysis zone tube for storage of biomass in m^2 and can be calculated using equation (4.21a).

$$A_{DP,tube} = \frac{\dot{m}_f}{RTC} \tag{4.21a}$$

The diameter of the tube can be determined using equation (4.22a).

$$A_{DP,tube} = \frac{\pi d_{DP,tube}^2}{4} \tag{4.22}$$

$$d_{DP,tube} = \sqrt{\frac{4 \times A_{DP,tube}}{\pi}} \tag{4.22a}$$

4.6.6. The height of fuel storage tube

The bulk density of MSH is $215.6\ kg/m^3$ (Kumar et al., 2021), nonetheless, the bulk density of biomass after palletization rises to roughly $700\ kg/m^3$ (Stelte et al., 2012; Tumuluru, 2018). Therefore, equation (4.23) can be used to calculate the volume needed to store $5.49\ kg$ of MSH when calculating storage of palletized biomass feedstock for a 1.5-hour gasifier run (Basu, 2018).

$$V_{DP,tube} = \frac{\dot{m}_f \times 1.5\ h}{\rho_{bulk,pall}} \tag{4.23}$$

To calculate the height of the fuel storage tube, equation (4.24a) can be used.

$$V_{DP,tube} = \pi \times r_{DP,tube}^2 \times h_{DP,tube} \tag{4.24}$$

$$h_{DP,tube} = \frac{V_{DP,tube}}{\pi \times r_{DP,tube}^2} \tag{4.24a}$$

Where:

$r_{DP,tube}$, the radius of drying and upper pyrolysis zone tube for storage of biomass in m.

$h_{DP,tube}$, the height of drying and upper pyrolysis zone tube for storage of biomass in m.

4.6.7. Design of the throat

The gasifier's throat area and diameter are developed using the specific gasification rate (SGR) value which can be expressed using equation (4.25). The downdraft gasifier's SGR value ranges from 1920 to 2640 Nm^3/m^2h (Akhator et al., 2019). The downdraft gasifier's SGR value for this study is assumed to be $SGR = 2000\ Nm^3/m^2h$.

$$SGR = \frac{v_g}{A_{th}} \tag{4.25}$$

Where:

A_{th}= Area of throat in m^2, which can be calculated using equation (4.25a).

$$A_{th} = \frac{v_g}{SGR} \tag{4.25a}$$

The diameter of the throat can be determined using equation (4.26a).

$$A_{th} = \frac{\pi d_{th}^2}{4} \tag{4.26}$$

$$d_{th} = \sqrt{\frac{4 \times A_{th}}{\pi}} \tag{4.26a}$$

The ratio of throat height to throat diameter is taken to be 1.5 in order to maintain the flow of biomass inside the gasifier and it can be expressed using equation (4.27) (Akhator et al., 2019).

$$h_{th} = 1.5 d_{th} \tag{4.27}$$

4.6.8. Throat inclination

After comparing the design elements of several gasifiers, it was indicated that the throat inclination should be between 45° and 60° The throat angle has an impact on the gasifier's conversion efficiency; small angles result in the highest conversion efficiency, whereas big angles have a diverging effect and have the opposite effect (Venselaar, 1982). Due to a decreased temperature for bigger neck angles as a result of the diverging effect and reaction rate, (Kumar et al., 2008) found that throat angles of approximately 45° increase cumulative conversion efficiency while larger angles of about 90° decrease cumulative conversion efficiency. Due to this an inclination angle of 45º is preferable for this work.

4.6.9. Design of combustion zone

The diameter and height of the combustion chamber can be estimated using a wide range of relations. Since the flow of biomass to be burned in the combustion zone depends on the design of the throat, relating it to the gasifier's throat diameter as given in equation (4.28) and (4.29) does seem more reasonable (Radwan et al., 2022).

$$d_{comb} = 1.5\, d_{th} \tag{4.28}$$

$$h_{comb} = 2.5\, d_{th} \tag{4.29}$$

The arrangement of the combustion zone is shown in Figure 4.3.

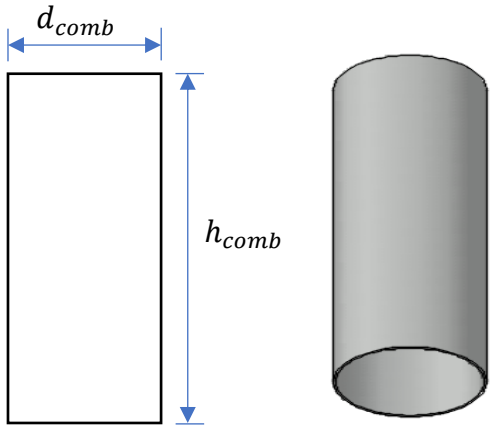

Figure 4.3. Configuration of the combustion zone

4.6.10. Area of air distributor

Air in the distributor moves at a speed of 6 to 10 m/sec (Akhator et al., 2019; Guangul et al., 2012). The area of the tuyere can be estimated with equation (4.30a) taking the average distributer air velocity 8 m/sec, which is measured from air supply unit using anemometer.

$$Q_{a_{act,vol}} = V_{air} \times A_{tu} \tag{4.30}$$

$$A_{tu} = \frac{Q_{a_{act,vol}}}{V_{air}} \tag{4.30a}$$

The diameter of the tuyere (D_{tu}) can be determined using equation (4.31).

$$D_{tu} = \sqrt{\frac{4 \times A_{tu}}{\pi}} \tag{4.31}$$

The number of tuyeres must be larger than one and odd in order to prevent nozzle-to-nozzle pressure from the straight opposite configuration of nozzles caused by having an even number of tuyeres. The magnitude of the throat diameter determines how many nozzles are needed. Furthermore, three nozzles must be used for a throat diameter of about 7 cm (Mendonça et al., 2022).

4.6.11. Height of the reduction zone

Equation (4.32), demonstrates the relationship between the throat diameter and the height of the gasifier's reduction zone (Akhator et al., 2019; Venselaar, 1982). Moreover, Figure 4.4 illustrates the reduction zone's configuration.

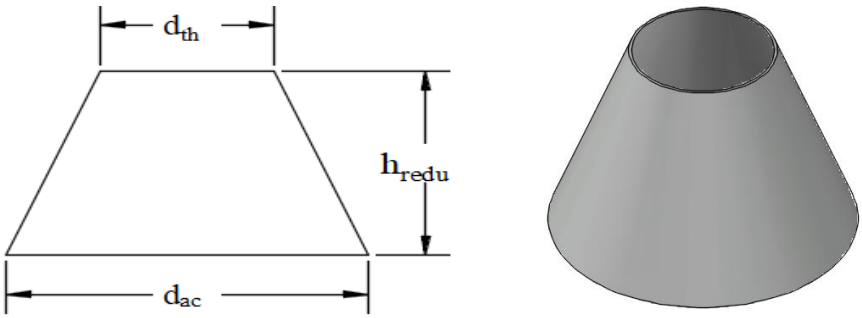

Figure 4.4. Configuration of the reduction zone

$$\frac{h_{redu}}{d_{th}} = 2 \tag{4.32}$$

4.6.12. Volume of the pyrolysis zone

The pyrolysis zone of the downdraft gasifier features a frustum part as well as a cylindrical part to its geometry (Basu, 2018; Chawdhury & Mahkamov, 2011). The configuration for the frustum part of pyrolysis zone can be seen in Figure 4.5.

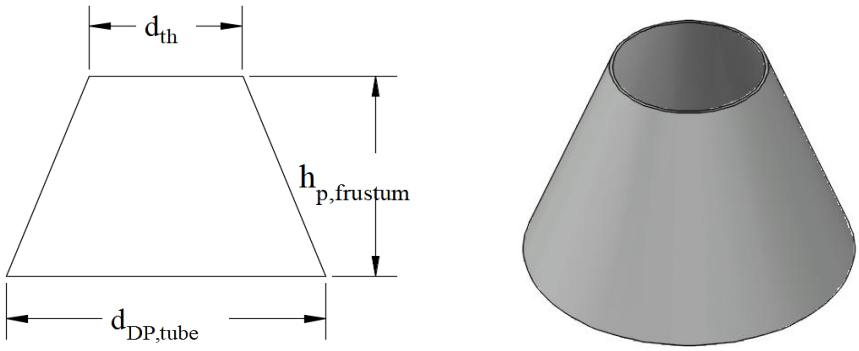

Figure 4.5. Configuration of frustum part pyrolysis zone

The height for the frustum part of the pyrolysis zone, $h_{p,furstum}$, can be determined using equation (4.34a) by making a quarter of the volume a frustum part and the remaining volume a cylindrical portion as calculated in equation (4.33).

$$V_{p,frus} = 0.25 \times V_{DP,tube} \tag{4.33}$$

$$V_{p,frus} = \frac{\pi \times h_{p,frus}}{3}\left(r_{DP,tube}^2 + r_{DP,tube} \times r_{th} + r_{th}^2\right) \tag{4.34}$$

$$h_{p,frus} = \frac{3 \times V_{p,frus}}{\pi \times \left(r_{DP,tube}^2 + r_{DP,tube} \times r_{th} + r_{th}^2\right)} \tag{4.34a}$$

Where:

$r_{DP,tube}$is the radius of drying and upper pyrolysis zone tube for storage of biomass

r_{th} is throat radius

$h_{p,frus}$, the height of frustum part of pyrolysis zone

4.6.13. Total height of the gasifier

Equation (4.35), can be used to get the reactor's overall height, which is the total of all zone heights. A support frame with a height of $h_{frame} = 40\ cm$ and an ash storage on the bed space that has a diameter that matches the reactors and a short height $h_{ash\ pit} = 20\ cm$ are also included in the total height.

$$H_{TOT} = h_{DP,tube} + h_{p,furstum} + h_{comb} + h_{redu} + h_{ash\ pit} + h_{frame} \quad (4.35)$$

4.6.14. Superficial gas velocity

The superficial gas velocity, which has a unit of velocity at reference temperature and pressure, is the hearth load, or volume flow rate of gas per unit of cross section area. Equation (4.36), can be used to calculate **t**he superficial velocity of the producer gas, V_{sup} (Basu, 2018; Chawdhury & Mahkamov, 2011; La Villetta et al., 2017).

$$V_{Sup} = \frac{V_g}{A_{th}} \quad (4.36)$$

Where:

V_g, is volumetric gas production

A_{th}, is throat cross sectional area

4.6.15. Grate diameter

Between the reduction zone and the ash pit of the gasifier, the required great will be placed. As a result, the lower portion of the reduction zone or the diameter of the ash pit is equivalent to the diameter of the great which will be 16.72 cm. The arrangement of the grate is shown in Figure 4.6.

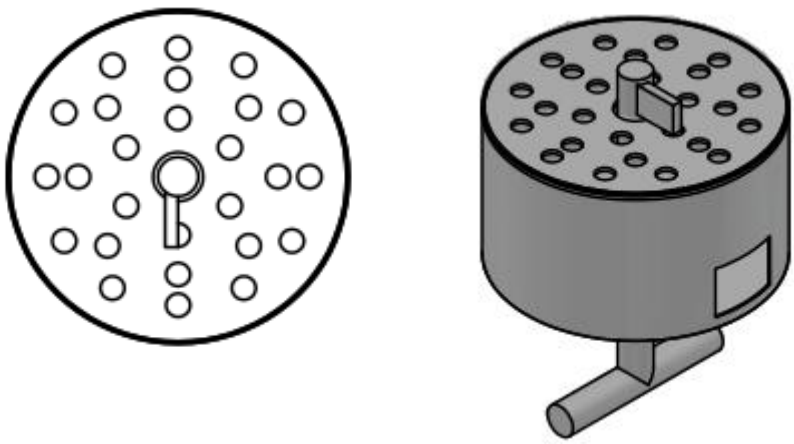

Figure 4.6. Configuration of the gasifier grate

4.6.16. Air preheater

The temperature of the gasification process is crucial since it is highly exothermic. Typically, the process runs between $800 - 1100$ ℃ with air and $1000 - 1400$ ℃ with oxygen (Basu, 2018). The heat from the producer gas leaving the gasifier, which would otherwise be considered a heat loss to the environment, can be used to heat the air entering the system around 25 ℃, since air is used as a gasifying agent in this study. This will provide relatively hotter air than the surrounding atmosphere to the combustion zone of the gasifier. A fourth of the gasification reactor can be equated to the size of the air pre heater.

4.6.17. Cold gas efficiency of the gasifier

The efficiency of gasification, which can be determined by one of two energy efficiencies: cold gas efficiency (CGE) or hot gas efficiency (HGE), is a crucial factor. The ratio of the chemical energy of the produced gas to that of the biomass used is known as CGE, as illustrated in equation (4.37). The sensible heat of the gas is however taken into account by HGE. Since heat is not the intended impact of the gasification process, most researchers choose to utilize the CGE rather than the HGE (Silva et al., 2019). Thus, CGE is chosen for this study.

$$\eta_{gasifier} = \frac{LHV_g \times V_g}{LHV_f \times \dot{m}_f} \tag{4.37}$$

4.7. Summary of gasifier design

The output data, equation number, calculated and retained values for the gasifier design are tabulated in Table 4.7.

Table 4.7. Summary of design output data, equations, calculated and retained values

Output data	Symbol	Equation no.	Calculated value	Retained value	Unit
Fuel feed rate	$\dot{m}_f$	(4.14)	5.49	5.49	$kg\ h^{-1}$
Product gas flow rate	V_g	(4.15)	9.442	9.442	Nm^3h^{-1}
Minimum amount of oxygen required for complete combustion	$\frac{m_o}{m_f}$	(4.16)	1.33133	1.33	$\frac{kg\ oxygen}{kg\ fuel}$
Minimum amount of air required for complete combustion	$\left(\frac{m_a}{m_f}\right)_{sto}$	(4.17)	5.791	5.79	$\frac{kg\ air}{kg\ fuel}$

Actual air-fuel ratio for 1 kilogram of fuel	$\left(\frac{m_a}{m_f}\right)_{act}$	(4.18)	1.737	1.74	$\frac{kg\ air}{kg\ fuel}$
Actual mass flow rate of air needed	$\dot{m}_{a_{act}}$	(4.19)	9.538	9.54	$kg\ h^{-1}$
	$Q_{a_{act,vol}}$	(4.20)	7.921	7.92	$m^3 h^{-1}$
Area of drying and upper pyrolysis zone tube for storage of biomass	$A_{DP,tube}$	(4.21a)	0.02196	0.02196	m^2
Inner diameter of drying and upper pyrolysis zone tube for storage of biomass	$d_{DP,tube}$	(4.22a)	16.72	17	cm
Storage of palletized biomass feedstock for a 1.5-hour gasifier run	$V_{DP,tube}$	(4.23)	0.01176	0.01176	m^3
Height of fuel storage tube	$h_{DP,tube}$	(4.34a)	51.8	52	cm
Area of the throat	A_{th}	(4.25a)	47.21	47.21	cm^2
Diameter of the throat	d_{th}	(4.26a)	7.75	8	cm
Height of the throat	h_{th}	(4.27)	12	12	cm
Combustion zone Inner diameter	d_{comb}	(4.28)	12	12	cm
Height of combustion zone	h_{comb}	(4.29)	20	20	cm
Area of air distributor	A_{tu}	(4.30a)	2.75	2.75	cm^2
Diameter of air distributor	d_{tu}	(4.31)	1.87	2	cm
Reduction zone height	h_{redu}	(4.32)	16	16	cm
Frustum part volume for pyrolysis zone	$V_{p,frus}$	(4.33)	2940	2940	cm^3
Frustum height volume for pyrolysis zone	$h_{p,frus}$	(4.34a)	22.965	23	cm
Total height of the gasifier	H_{TOT}	(4.35)	171	171	cm
Superficial gas velocity	V_{Sup}	(4.36)	0.5	0.5	$m\ s^{-1}$
Grate diameter	d_{gr}	-	16.72	17	cm
Calculated cold gas efficiency of the gasifier	$\eta_{gasifier}$	(4.37)	70	70	%
Gasifier thickness	G_t	-	0.3	0.3	cm

4.8. Design of cyclone separator

The total size of the cyclone is developed utilizing the relation given in Figure 4.7, regarding the value of the gasifier output diameter (P_c) which is 4 cm. Thus, $D_c = 8\ cm$, $B_c = 2\ cm$, $D_e = 4\ cm$, $L_c = 16\ cm$, $S_c = 1\ cm$, $Z_c = 16\ cm$ and $J_c = 1\ cm$ (Wiyono et al., 2020).

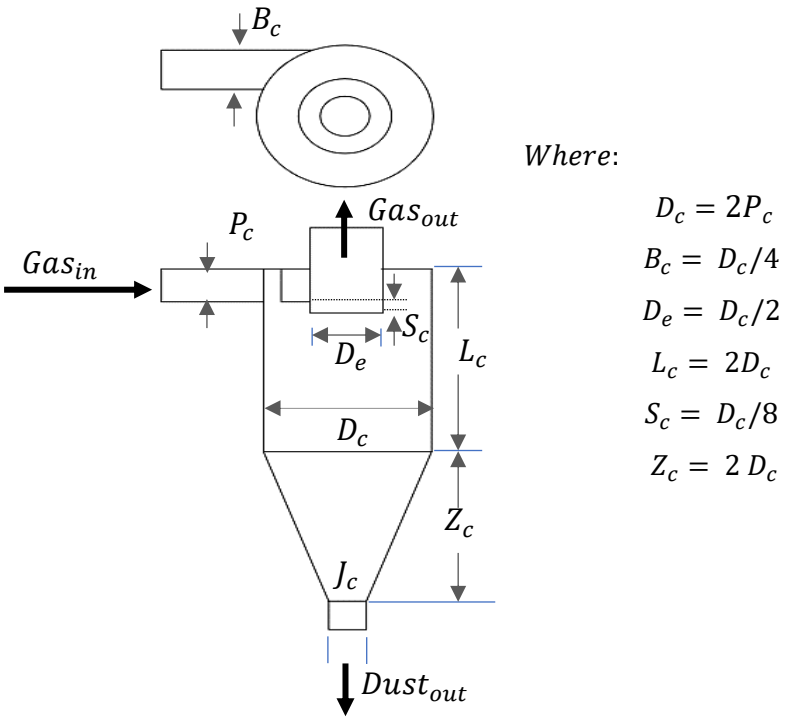

Figure 4.7. Sizing of cyclone separator

4.9. Energy balance on the gasifier

Applying the first law of thermodynamics to the gasifier's input and output provides an indirect way to calculate the amount of energy lost to the surroundings. However, an adiabatic system is considered in this study. The energy balance is governed by a general conservation of energy formula as shown in equation (4.38) (Basu, 2018).

$$\sum Energy\ in = \sum Energy\ out + Energy\ loss \tag{4.38}$$

Mass, energy, and exergy interaction in and out of the gasifier is illustrated in Figure 4.8 and in section 4.2, it is also explored in great detail. The energy flow rates of the biomass $\dot{E}_{biomass}$ entering the gasification reactor is also an input to the system (Dincer & Bicer, 2018).

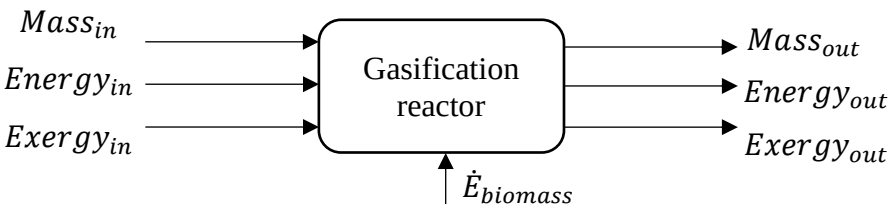

Figure 4.8. Mass, energy, and exergy interaction of the gasifier

CHAPTER FIVE

EXPERIMENTAL SETUP AND PROCEDURE

5.1. Introduction

In this chapter, the implemented experimental procedures and the comprehensive development process of the experimental setup are provided. Moreover, this section describes the fabrication of each downdraft gasifier component, the development of the final experimental setup, and the measuring equipment used.

5.2. Manufacturing processes

The downdraft gasifier system's components were built using materials that were acquired from the local market. The cost and accessibility of the materials on the local market were taken into account when choosing the materials for each part. Using Table 4.7, which is located in section 4.6 of the design analysis part, the dimensions of the components were represented in the theoretical study of the gasifier.

5.2.1. Gasifier reactor

Different zones of the gasifier were manufactured using $1\,m \times 2\,m$ mild steel sheet as depicted in Figure 5.1.

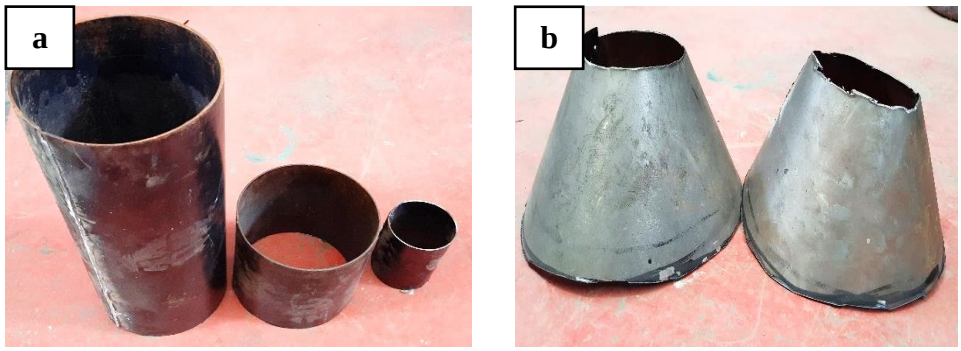

Figure 5.1. Fabricated parts of gasifier reactor (a) cylindrical parts (b) conical parts

5.2.2. Cyclone separator

As shown in Figure 5.2, the cyclone separator was also constructed using mild steel sheet.

Figure 5.2. Fabricated cyclone separator

5.2.3. Support frame

The support frame for the gasifier was constructed using a rectangular mild steel hollow bar as depicted in Figure 5.3.

Figure 5.3. Constructed gasifier support frame

5.3. Preparation for experiment

The gasifier body was filled with body filler as shown in Figure 5.3 and then painted as indicated in Figure 5.4a, in order to prevent air and gas leakage through gaps from welded portions on the body. Glass wool was employed, as shown in Figure 5.4b, to stop heat from escaping to the surroundings since it is flexible, non-flammable, highly thermally resistant, and has a low thermal conductivity. It is also inexpensive, a fire-safe material, and simple to install (Yan et al., 2021). Before beginning each experiment, a certain protocol was followed, which included testing for air and gas leaks as well as other relevant issues during a pre-run check.

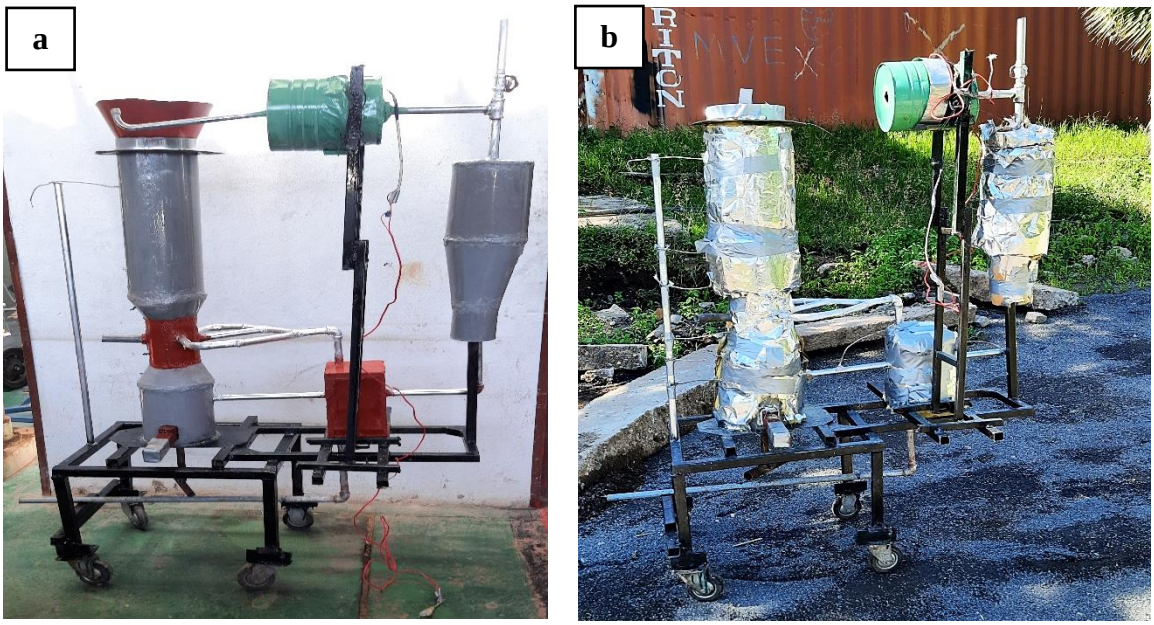

Figure 5.4. Gasifier experimental preparation (a) painted gasifier (b) insulated gasifier

5.3.1. Biomass pretreatment and preparation

As depicted in Figure 5.5, it entails preparing the biomass for use in gasification processes by treating it. To acquire the proper particle sizes, size reduction is required. To get the right amount of moisture for the process to function effectively, drying is required. The low density of biomass may also necessitate densification (Kumar et al., 2009). The selected biomass samples were handled differently based on their nature and size. Moreover, Figure C-1 and C-2 of Appendix C depicts the entire pretreatment and preparation process.

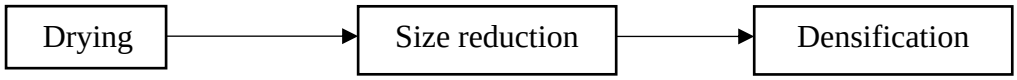

Figure 5.5. Biomass pretreatment and preparation

Densification is used to lessen or eliminate the issues with direct biomass consumption. Additionally, it would increase the structural uniformity, energy density, and heating value of raw biomass while reducing the transportation issues related to direct biomass consumption. Solid fuels are created through the process of densification, which involves applying pressure to compress particles together. Typically, traditional pressure-driven methods including screw press, hydraulic piston press, extrusion, roller press, piston type, and pallet press are used to produce marketable densification. High-pressure, medium-pressure, and low-pressure compactions are three different types of densification procedures based on compaction. Briquetting, pelletizing, bailing, and cubing are examples of common densification techniques (Ibitoye et al., 2021). As can be seen in Figure 5.6, a screw press-type pelletizer was used in this study for biomass densification.

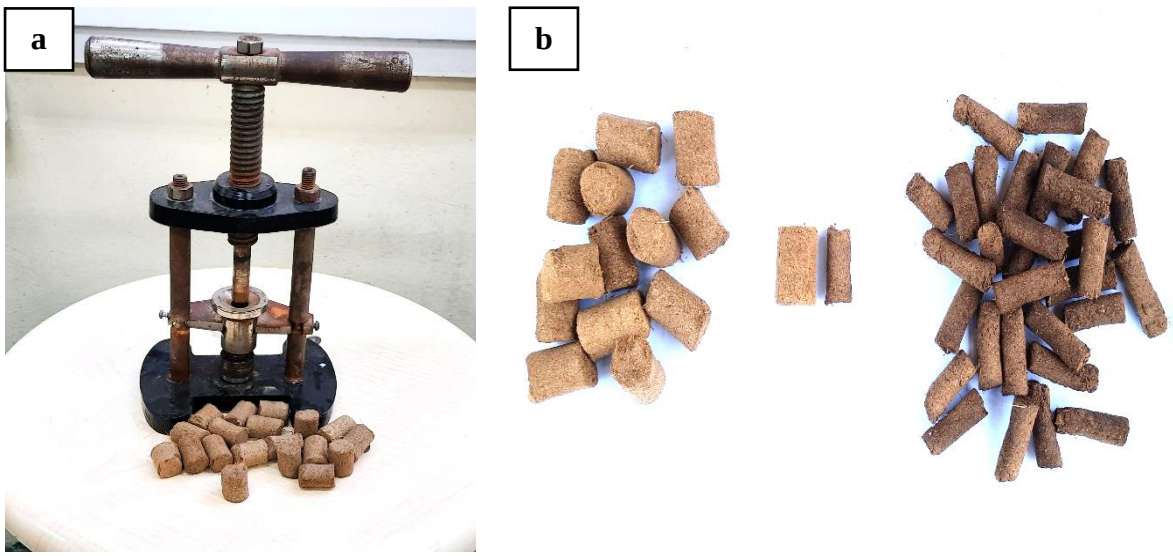

Figure 5.6. Biomass densification (a) screw type pelletizer (b) 9 mm and 15 mm diameter PS pellets

5.4. Experimental setup

Based on the thermochemical conversion of phenomena, the downdraft gasifier appears to be divided into six zones, as shown in Figure 5.7. From the top down, these zones are

1. Drying zone
2. Pre-pyrolysis zone
3. Pyrolysis zone
4. Combustion zone
5. Reaction zone
6. Ash container

The numerous downstream systems, such as the air preheater, cyclone separator, flare valve, and the suction fan are connected to the producer gas exit at the bottom which is below the reduction zone.

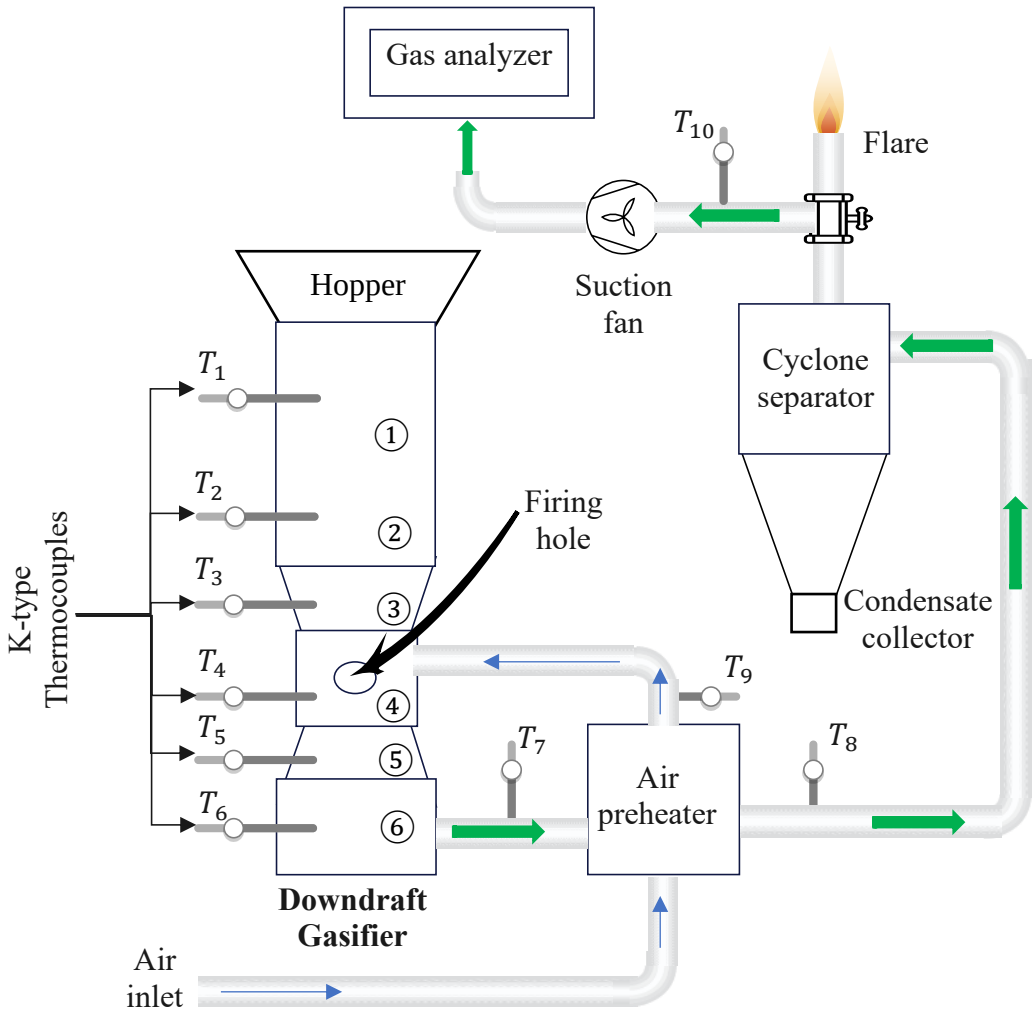

Figure 5.7. Experimental setup of downdraft gasifier

The experimental setup that was proposed to be utilized to produce syngas from a downdraft gasifier is shown in photographic detail in Figure 5.8, together with the appropriate measuring equipment. Combustion and reduction reactions drive the gasification process. In the combustion zone, heat is produced. The biomasses begin to release volatiles and transform into char, which falls down into the reduction zone as a result of the heat spreading to the pyrolysis area and drying zone. Heat that is produced in the combustion zone also spreads into the reduction zone. At the base of the reduction zone, there is a special ash handling system. Rotating the grate cleaner inside the reaction chamber removes the ash created during gasification. The configuration is offered to avoid biomass clogging at the throat. In order to further validate the experimentation, a number of variable changes and a number of instruments were taken into consideration during the experimental time.

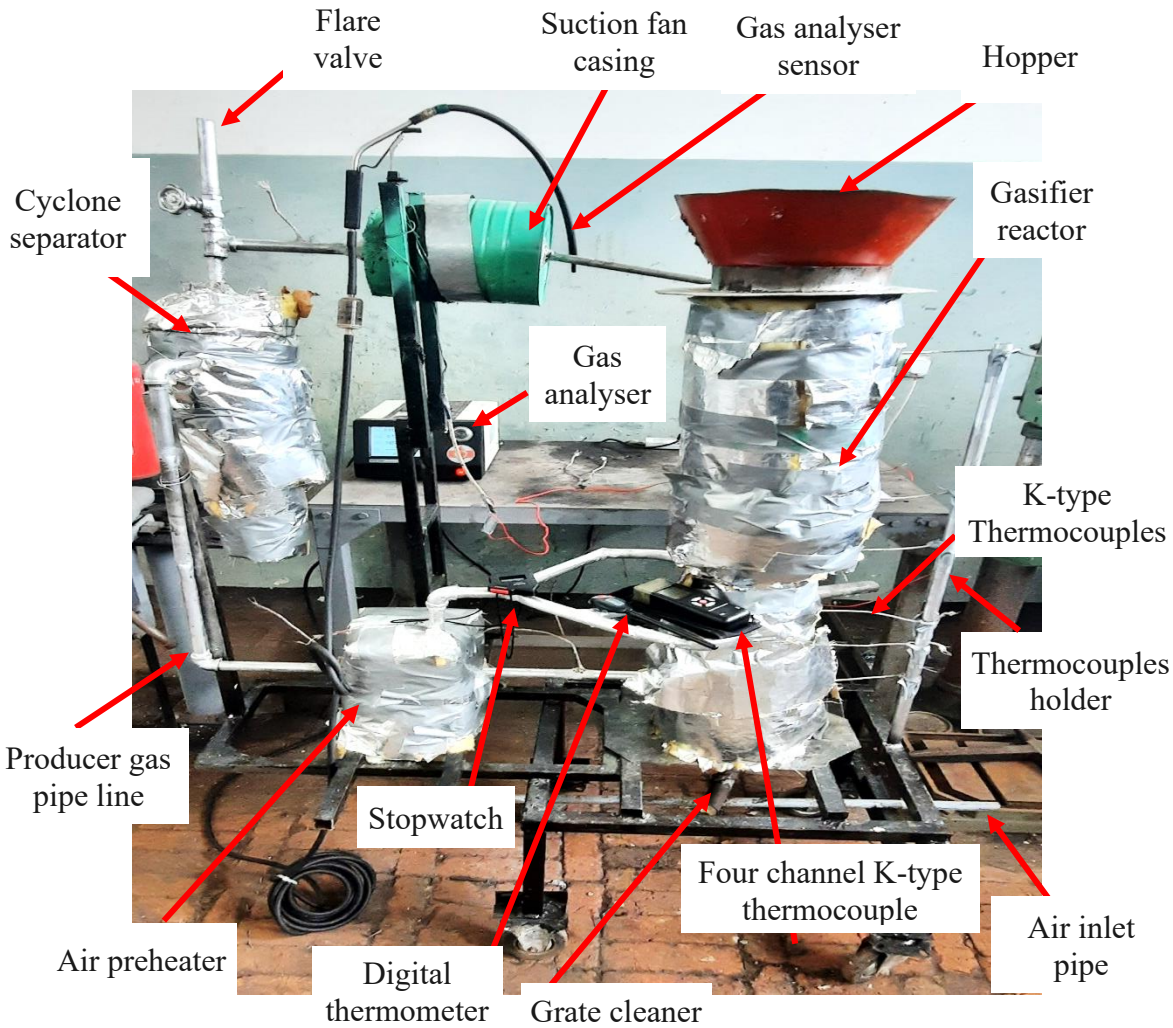

Figure 5.8. Pictorial view of downdraft gasifier experimental setup with necessary instrumentations

5.4.1. Hopper

On top of the gasifier was where the hopper is situated as shown in Figure 5.8. It facilitates the downward movement of biomass feedstock inside the gasifier, preventing feedstock clogging at the throat.

5.4.2. Cyclone separator

As shown in Figure 5.8, the hot producer gas exiting the reactor passes through a cyclone separator in order to separate condensate particles or tar. The separated tar was then gathered in a condensate collector.

5.4.3. Specification of thermocouples used

The gasifier was equipped with thermocouples to monitor the temperature distribution. K-type thermocouples have a claimed measuring range of 0 to 1350 °C and are durable (Manjhi & Kumar, 2019). K-type thermocouples were thus employed to monitor the internal operation of the gasifier. As can be seen in Figure 5.7, the thermal analysis of the gasifier involves measuring temperature using 10 thermocouples. Thermocouples were inserted into the producer gas line at various locations, including the exit of the reaction chamber, the entry and exit to the air heater, and the cyclone separator, to measure the thermal properties of the producer gas leaving the gasifier. As shown in Figure F-1 of Appendix F, a calibrated four channel K-type thermocouple sensor or digital thermometer was utilized to display the temperature that was measured utilizing the thermocouples. The thermocouples were located in various places throughout the downdraft gasifier, as indicated in Table-5.1.

Table 5.1. Location of thermocouples inside the downdraft gasifier

Zone	Number of thermocouples	Thermocouple notation	Distance from the base of the gasifier (cm)
Drying	1	T_1	75
Pre-pyrolysis	1	T_2	60
Pyrolysis	1	T_3	46
Combustion	1	T_4	34
Reduction	1	T_5	25
Ash container	1	T_6	15

The producer gas was equipped with several thermocouples at various points, as shown in Table-5.2.

Table 5.2. Location of thermocouples along producer gas line

Details of data collection	Number of thermocouples	Thermocouple notation
Measurement of the temperature of the producing gas at the exit of gasifier	1	T_7
Measurement of producer gas temperature at the exit of air preheater	1	T_8
Measurement of air temperature at exit of air preheater	1	T_9
Measurement of producer gas temperature at the exit of cyclone separator	1	T_{10}

5.5. Experimental investigation objectives

The experimental evaluation was carried out for the following main objectives:

- To characterize the producer gas at the gasifier outlet
- To characterize the producer gas throughout the gas pipeline
- To analyze the temperature variation with time throughout the gasifier
- To examine the temperature variation within different gasifier zones
- To examine the flame intensity of the producer gas for various feedstocks
- To examine the amount of condensate particle after gasification

5.6. Experimental test and procedures

After the fabrication and assembly were finished, the processed biomass materials were separated into three groups: size-reduced MSH, 9 mm, and 15 mm diameter PS pellets. The constructed gasifier was then put through several performance evaluations using the procedure below.

- The initial temperature of the system reactor was recorded with the help of pre-installed thermocouples and temperature measuring instruments.
- The reactor was supplied with the ready sample from the top for 30 minutes operation.
- After the sample was fed into the gasifier, the firing hole was opened.
- To provide the biomass with partial combustion, a fire was delivered through the firing hole into the reactor.
- To achieve noticeable temperature increases, the fan was turned on to draw air into the system and was left running for 15 minutes.
- The reactor upper lid and firing hole were both closed after 15 minutes to create an airtight chamber.

- In order to determine the temperature at which gasification will take place, the temperature at the oxidation zone was constantly monitored. Gasification is anticipated to take place between 600 and 900 ℃ (Smith et al., 2019). A thermocouple was used to measure and record the temperature.
- The composition of the produced gas was measured using a gas analyzer.
- Burning of the generated gas took place after the gasification temperature was reached and the flame characteristics from different biomass samples were evaluated.
- Following the completion of the gasification process, the ash content was gathered from the ash container and weighed in order to determine the system's efficiency. The amount of ash was measured.
- Small amounts of tar were found in the tar content that was collected at the bottom of the cyclone unit, which indicates that the biomass was gasified properly.
- It took the gasifier roughly 26 to 28 minutes to completely gasify 2.7 kilograms of biomass during testing.

For pressurized air gasification, only the fifth and the sixth procedures are omitted.

5.7. Experimental analysis and experimentation

In order to evaluate the performance of the downdraft gasifier, experiments were carried out both during the day and at night while varying various parameters.

5.7.1. Varying the biomass type

The performance evaluation for the fabricated downdraft gasifier was done using different biomass samples which are MSH and PS.

5.7.2. Varying the biomass size

The gasifier performance evaluation was investigated using biomass samples with different sizes as shown in **Figure 5.1.**

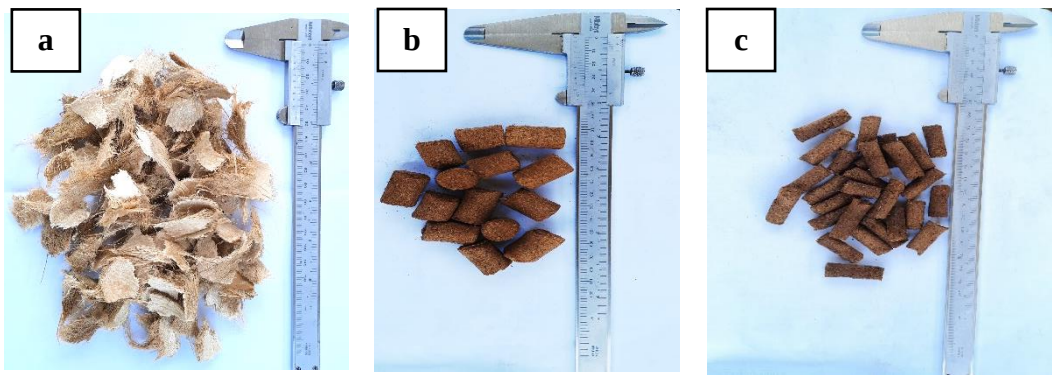

Figure 5.9. Different sizes of biomass samples used (a) MSH (b) Φ 9 mm PS pellets (c) Φ 15 mm PS pellets

5.7.3. Varying the air supply system

The analyses were conducted using two distinct types of air sources, one pressurized and the other at ambient pressure. A suction fan draws air into the reactor while simultaneously removing syngas further downstream. In contrast, pressurized air is delivered to the reactor using a compressor. The specification of the suction fan and air compressor utilized for the gasification system is illustrated in Table G-1 and G-2 of Appendix G.

5.8. Risk identified and safety precaution

Some dangers were identified during the gasifier's performance evaluation, and steps were taken to minimize any harm they might have caused.

Table 5.3. Types of risk identified and the precaution taken

Risk identified	Precaution taken
Inhaling poisonous gas	Use of face mask
High surface temperature	Insulation of hot parts
Toxic hazards	Use of hand glove
Fire hazards	Use of fire extinguisher

5.9. Experimental uncertainty analysis

The measurement technique, observation procedure, ambient factors, calibration, and measurement device error all contribute to experimental uncertainty. The measuring equipment used during the experiment is mostly responsible for external uncertainty. Experimental measurements of the ambient temperature and the temperatures at various locations within the downdraft gasifier were made. The accuracy of the measured results can be impacted by this instrument's uncertainty. Appendix F included a summary of the associated accuracy ranges, percentage errors, and ranges of instruments.

CHAPTER SIX

RESULTS AND DISCUSSIONS

6.1. Introduction

This chapter outlines the theoretical and experimental findings from the downdraft gasifier model and design. The theoretical analysis is validated by comparing the expected results with both the experimental data and the literature. Additionally, a detailed investigation is made into the effects of many parameters, including biomass type, biomass size, equivalence ratio, moisture content, and gasification temperature, on the performance of the gasification system. The summary of the experiments and the model are compiled at the end.

6.2. Model validation

Comparing the computation findings with the results from other researchers allowed the developed model in this study to be validated. The present model results for wood at 20 % MC and 800℃ gasification temperature are compared with Zainal et al. (2001) and Ayub et al. (2020b) as can be seen in Figure 6.1.

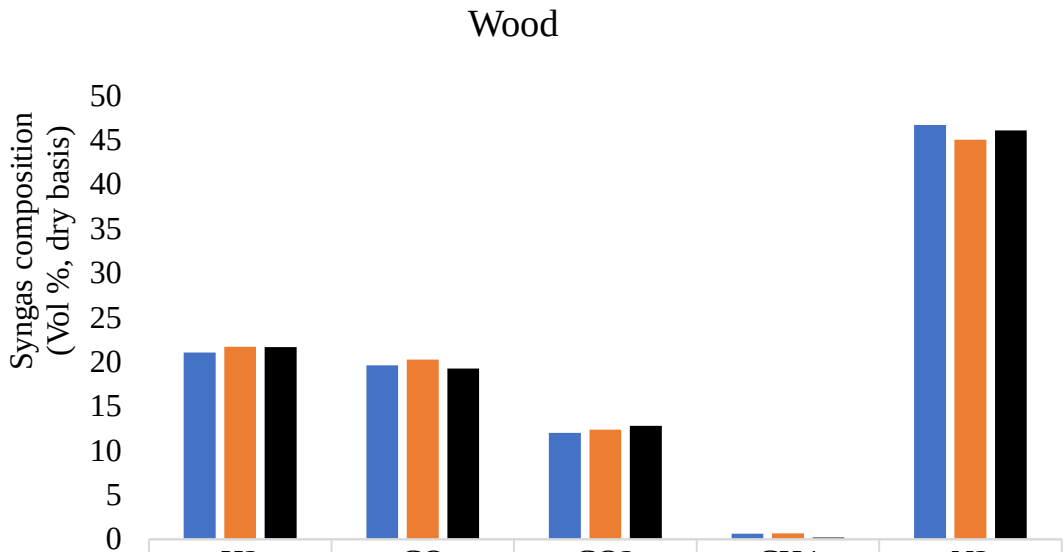

	H2	CO	CO2	CH4	N2
Zainal	21.06	19.61	12.01	0.64	46.68
Ayub	21.705	20.2402	12.3703	0.662	45.0224
Pr. Model	21.67	19.26	12.78	0.2019	46.08

Figure 6.1. Model validation.

Figure 6.1 shows that the syngas composition predicted by the current model is generally in good agreement with the literature used for validation, except for methene. This is due to the sensitivity of the model for CH_4 since methane formation reaction was used to calculate one of the equilibrium constants, to compensate for other PG constituents' values.

6.3. Model sensitivity analysis

The influence of several parameters, such as moisture content, the equivalence ratio, and gasification temperature on the producer gas composition, LHV, as well as on other process features, has been explored after the thermochemical equilibrium model has been validated. By changing the value of one parameter while keeping the values of the other parameters constant, the sensitivity analysis was estimated. For each parameter, the experiment reports the default values that were assumed. The first biomass employed in these simulations was MSH, with elemental analyses of $47.93\ \%\ C$, $6.06\ \%\ H$, $43.84\ \%\ O$, $0.5\ \%\ N$, and $0.68\ \%\ S$ and LHV $14.092\ MJ/kg$. The second biomass employed in these simulations was PS, which had elemental analyses of $46.42\ \%\ C$, $6.61\ \%\ H$, $41.77\ \%\ O$, $0.5\ \%\ N$, and $0.54\ \%\ S$, as well as LHV $14.095\ MJ/kg$. The elemental analysis results on a dry ash-free basis, served as the foundation for formulating the feedstock composition, while the moisture and ash content of the feedstock were determined using the results of the proximate analysis. Using this data, the composition of gaseous products is predicted using a stoichiometric equilibrium model.

The computation for the model was carried out using Engineering Equation Solver (EES) tool. Thermal inputs and outputs are not taken into account in the simulation described here. As a result, it is presumed that the gasifier process is adiabatic. The summary of the sensitivity analysis for this study is shown in Table 6.1; a comparison between the default values and the examined range for a given parameter range was made, and the percentage of syngas was reported.

Table 6.1.Summary of sensitivity analysis

Parameter	Unit	Default value	Observed range
Equivalence ratio (ER)	Dimensionless	0.3	$0.26 - 0.4$
Moisture content (MC)	%	20	$5 - 40$
Gasification temperature (GT)	℃	800	$800 - 1200$

6.3.1. Effect of ER

The gasification temperature of an auto thermal gasifier like this one relies on how much air was delivered into the gasifier. As a result, changing the ER or gasification temperature has the same impact on the composition and heating value of producer gas., as well as gasification efficiency.

6.3.1.1. Effect of ER on the syngas composition

In an adiabatic gasifier using MSH and PS with a 20 % moisture content, Figure 6.2 illustrates how the production gas composition varies as a function of the ER. The data for the graphs can be found in Appendix E.

The amount of air supplied into the reactor will vary depending on the air equivalence ratio. As the ratio of air to fuel rises, the gasifier receives more oxygen, which leads to greater conversion of the carbon in the fuel. However, too much oxygen oxidizes the fuel, which results in decreased syngas output.

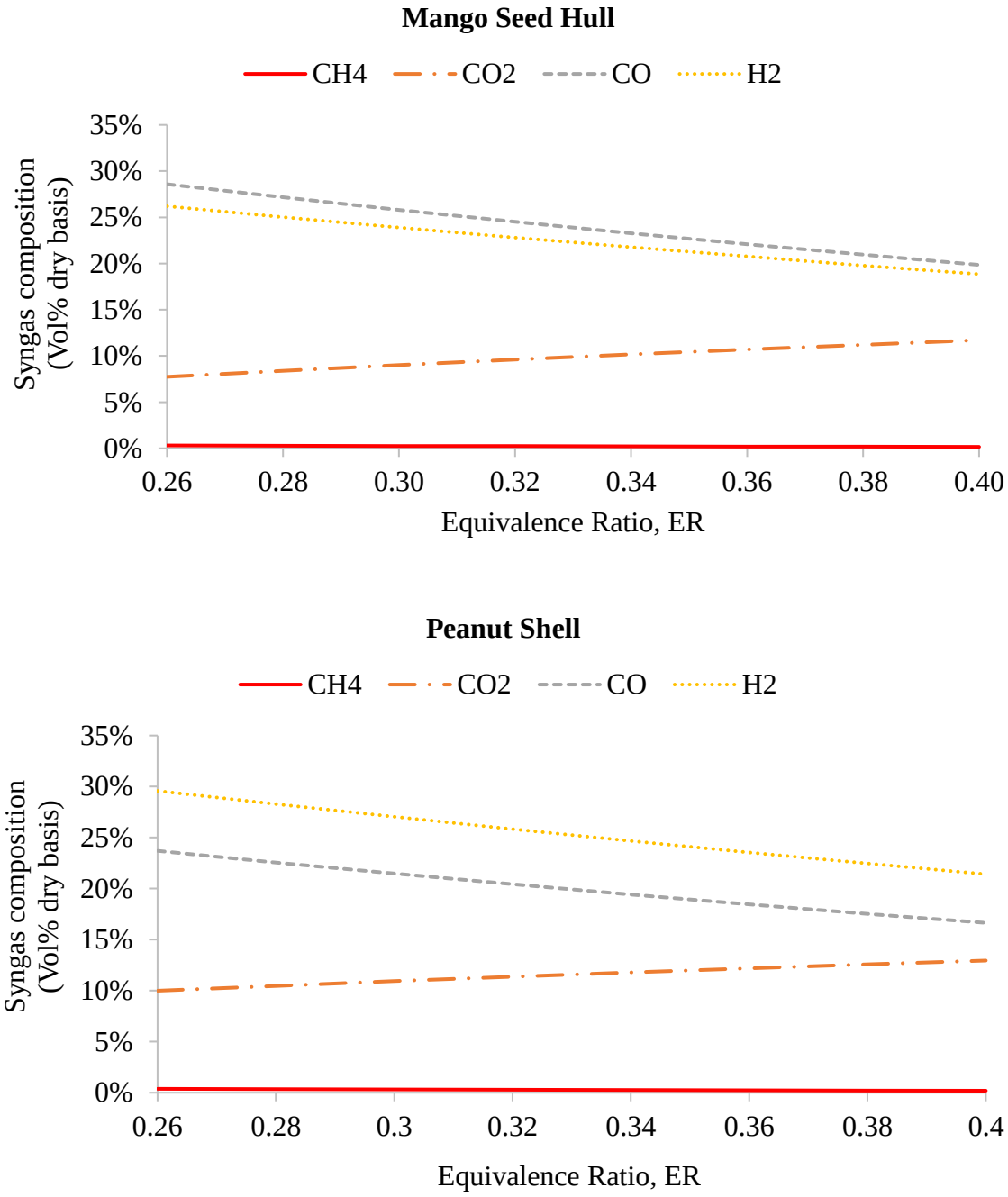

Figure 6.2. Effect of ER on the syngas composition for MSH and PS

As can be seen in Figure 6.2, for MSH the increase in ER from 0.26 to 0.4 caused the CO_2 and N_2 volume percentages to rise from 7.74 to 8.39 % and 37.17 to 49.43 % respectively. However, the value of CO, H_2, and CH_4 exhibit an opposite significant decrease from 28.58 to 19.85 %, 26.20 to 18.85 %, and 0.37 to nearly zero, respectively. Similarly, as depicted in Figure 6.2, for PS the rise in ER from 0.26 to 0.4 caused the CO_2 and N_2 volume percentage to increase from 10 to 12.95 % and 36.35 to 48.8 % respectively. However, the value of CO, H_2, and CH_4 exhibit an opposite significant decline from 23.7 to 16.64 %, 29.57 to 21.41 %, and 0.38 to nearly zero, respectively. This shows that as the air-to-fuel ratio rises, more oxygen is introduced into the carbon combustion process, leading to the generation of CO_2. Because an excessive air addition resulted in the complete burning of carbon to CO_2 over partial oxidation of carbon to CO, the fuel is totally converted to CO_2 in this situation, which reduces the production of syngas.

These results are compared to those published by Zainal et al. (2001), Dutta et al. (2014), and Ayub et al. (2020b). The three models, as well as the one presented here, exhibit the same qualitative and quantitative patterns. When the ER rises, the percentage of CH_4 stays very low and gets smaller. The H_2 percentage falls off as well when the ER rises from 0.26 to 0.4; this pattern was seen across all models. Moreover, the CO_2% slightly increases as H_2, and CO% decreases.

These tendencies could be explained by the following: (i) Endothermic processes drive the boudouard reaction equation (4.6a). Therefore, as ER and temperature increase, CO generation increases as well. (ii) Equation (4.6b)'s water-gas reaction is endothermic as well. Because of this, raising the ER and temperature causes a higher char and water consumption rate, which increases CO and H_2 production. (iii) However, it is exothermic when methane formation, equation (4.6i) occurs. As a result, the generation of CH_4 declines as ER and gasification temperature rise. This causes the gas to have more H_2. (iv) The reaction between CO and the existing O_2 results in the production of CO_2. (v) Exothermic reactions include the CO shift reaction, equation (4.6h). At higher ER and temperatures, this process yields less CO_2 and H_2. As a result, less CO and water are used. (vi) The reaction between steam and methane, equation (4.6k) reduces CH_4. The forward reaction benefits from an increase in the ER and temperature since this reaction is endothermic.

Summary of the effect of ER on the syngas composition

The impact of ER on syngas composition is summarized in Table 6.2. Reduced syngas composition resulted from an increase in ER. The highest N_2 was observed with increasing ER, while the lowest H_2 was noted with increased ER.

Table 6.2. Summary of the effect of ER on the syngas composition dry basis

Gas	Low ER $(0.26-0.3)$	Moderate ER $(0.3-0.35)$	High ER $(0.35-0.4)$	Observed results
CO	Decrease	Decrease	Decrease	High ER, caused reduced CO
CO_2	Increase	Increase	Increase	CO_2 augmented with higher ER
CH_4	Decrease	Decrease	Decrease	With larger ER, the amount of CH_4 continued to fall
N_2	Increase	Increase	Increase	Increasing ER caused a substantial and continuous rise in N_2
H_2	Decrease	Decrease	Decrease	Increased ER, caused low amount of H_2

6.3.1.2. Effect of ER on LHV of the syngas

In Figure 6.3, for a gasifier temperature of 800 ℃, the effect of the ER on the LHV of the product gas is shown. When the ER was changed to 0.4, the initial LHV value, which was 6.546 MJ/Nm^3 at an ER of 0.26, abruptly drops to 4.596 MJ/Nm^3 for MSH.

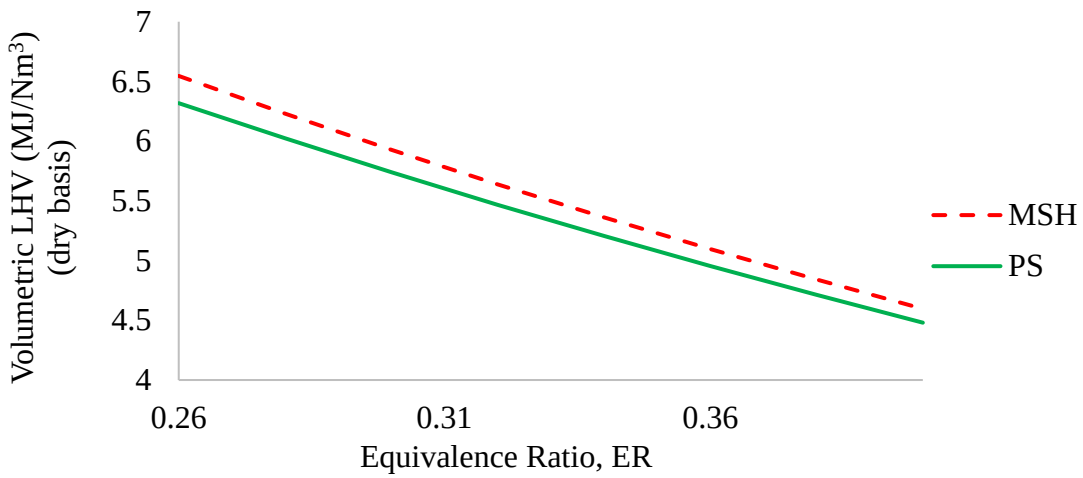

Figure 6.3. Effect of ER on LHV of the syngas for MSH and PS

Similarly for PS, as shown in Figure 6.3, when the ER was altered to 0.4, the initial LHV value, which was 6.318 MJ/Nm^3 at an ER of 0.26, abruptly decreases to 4.48 MJ/Nm^3. This is because adding more air to the process boosts the creation of CO_2 and increases the amount of N_2 in the PG. The LHV value rises if N_2 was taken out of the PG. Thus, the LHV of the gas decreases with the rise of ER. This decreasing trend can further be linked to the decline in partial combustion gas yield (CO, CH_4, and H_2) with an increase in ER, which was how LHV is defined in equation (4.11e). These results had the same tendency to those published by Zainal et al. (2001), Dutta et al. (2014), and Ayub et al. (2020b). The data of graph can be found in Table E-7 of Appendix E.

6.3.2. Effect of MC

Both the performance of the gasifier and the quality of the output gas are significantly influenced by the biomass MC. The energy needed for drying increases with increased MC in the biomass, which also decreases the pyrolysis of the biomass.

6.3.2.1. Effect of MC on the syngas composition

By changing the composition of the producing gas, the feedstock MC has a direct impact on the PG calorific value as shown in Figure 6.4 and 6.5. The results show that at an MC of 5%, the CO, and N_2 percentages were at their highest, while the CH_4, CO_2, and H_2 percentages were found to be at their lowest for both feedstocks.

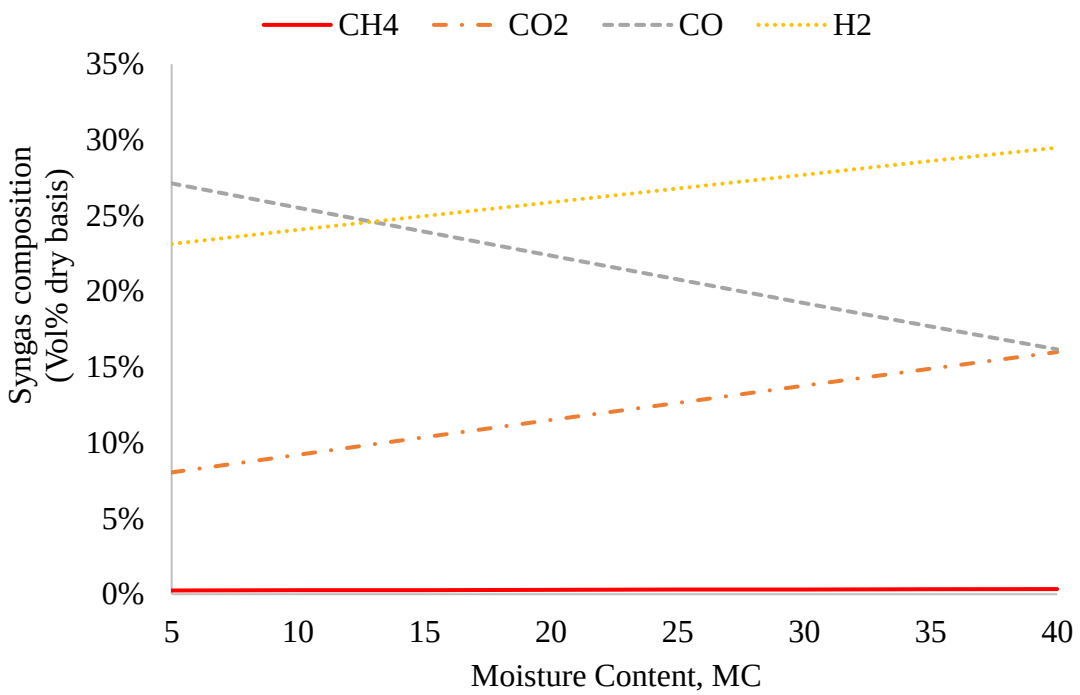

Figure 6.4. Effect of MC on the syngas composition for MSH

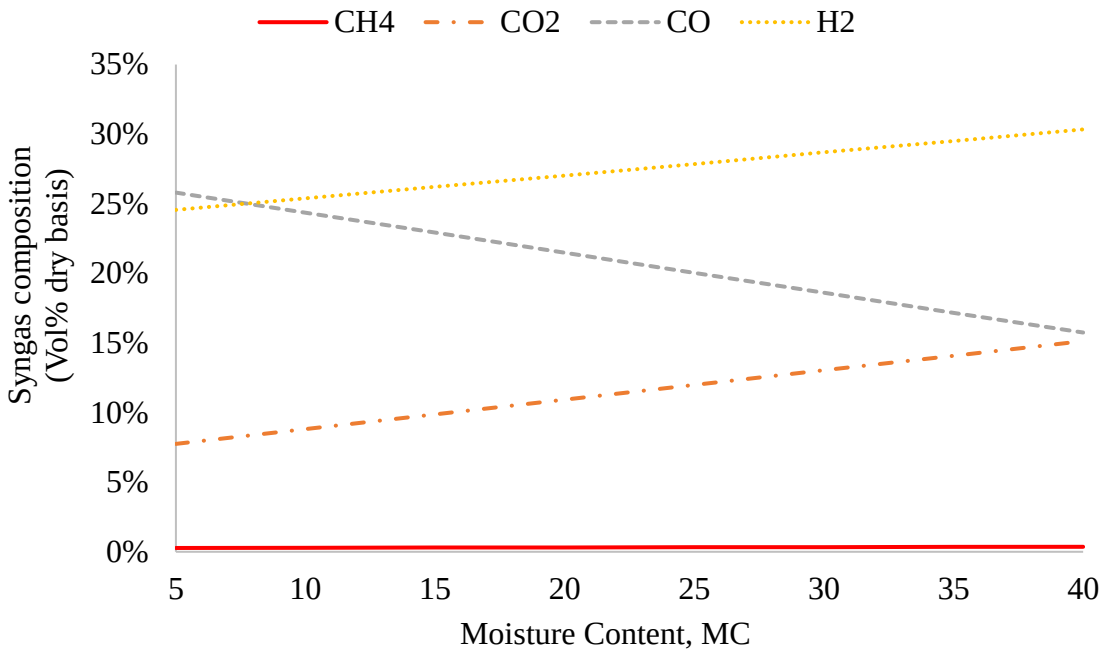

Figure 6.5. Effect of MC on the syngas composition for PS

A significant decrease in CO from 27.13 to 16.17 % and a small decrease on the side of N_2 from 41.44 to 38.02 % were seen as the MC increased from 5 to 40 in MSH as shown in Figure 6.4. Similarly, for PS a decrease in CO percentage from 25.8 to 15.75 % and a small decrease on the side of N_2 from 41.61 to 38.43 % were seen as the MC increased from 5 to 40 as depicted in Figure 6.5. With an increase in MC, H_2 production often increases. In addition, whereas CO_2 levels in both feedstocks increased significantly, CH_4 content in the product gas increased only marginally. Such behavior happens as a result of the use of moist fuels in the process, which directs some of the heat present in the reactor toward the evaporation of the water content of the raw materials in the drying zone, lowering the gasifier temperature and delaying endothermic reactions (Ayub et al., 2020b). The results presented here, show similar qualitative and quantitative trends with those published by Zainal et al. (2001), Dutta et al. (2014), and Ayub et al. (2020b).

Summary of the effect of MC on the syngas composition

When the MC is greater than 10%, there are noticeable changes, and carbon monoxide levels suddenly drop. For MSH, maximum hydrogen composition, with the gas augmented from 23.13 to 28.49 % percent, is observed at a peak value MC which is 40. The water-gas shift process, equation (4.6h) is what causes the increase in hydrogen when the MC rises. Carbon monoxide decreased from 27.13 to 16.17% when MC increased. A similar trend can be observed for the PS from Figure 6.5. The summarized trend for both feedstocks is shown in Table 6.3.

Table 6.3. Summary of effects of MC on the syngas composition dry basis

Gas	Low MC $(5-10)$	Moderate MC $(10-25)$	High MC $(25-40)$	Observed results
CO	Decrease	Decrease	Decrease	Substantial decreased amount of CO with increased MC
CO_2	Increase	Increase	Increase	CO_2 augmented with increased MC
CH_4	Increase	Considerable increase	Considerable increase	Consistent increase of CH_4 with augmented MC
N_2	Decrease	Decrease	Decrease	N_2 amount decreases with increased MC
H_2	Increase	Increase	Increase	Increased MC, led to large amount of H_2

6.3.2.2. Effect of MC on LHV of the syngas

The study from the model revealed, an increase in MC from 5 to 40 for MSH, caused a decrease in the producer gas LHV from 6.01 MJ/Nm^3 to 5.34 MJ/Nm^3. Similarly for the PS, the value of the LHV decreased from 6.004 MJ/Nm^3 to 5.387MJ/Nm^3 . The higher feedstock moisture, which decreased the thermal profile of the reactor and combustion zone, was the cause of the drop in producer gas calorific value. The effect of MC on LHV of the syngas for MSH and PS is shown in Figure 6.6. The data can be referred from Table E-7.

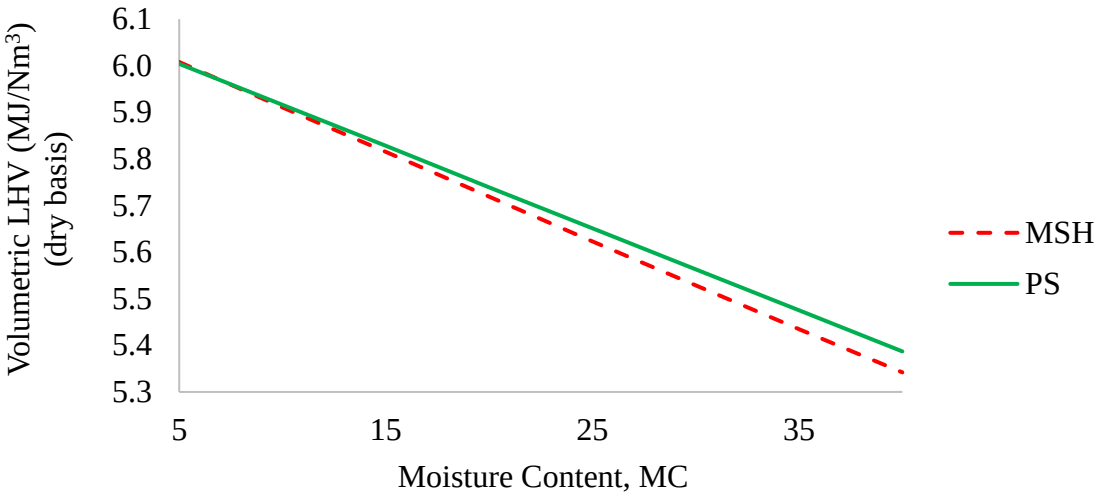

Figure 6.6. Effect of MC on LHV of the syngas for MSH and PS

6.3.3. Effect of GT

Any of the gasifier zones can experience gasification, but since the combustion zone lacks an oxidizer, gasification was more common there. A temperature range of 573 to 1473 K was used for the performance evaluation.

6.3.3.1. Effect of GT on the syngas composition

Figure 6.7, illustrates how the gasification temperature affects the syngas composition of MSH and PS. The gasification temperature was varied from 300°C to 1200°C and its effect on syngas production was studied at 1 atm operating pressure. A dry basis volume percentage was used to plot each gas component.

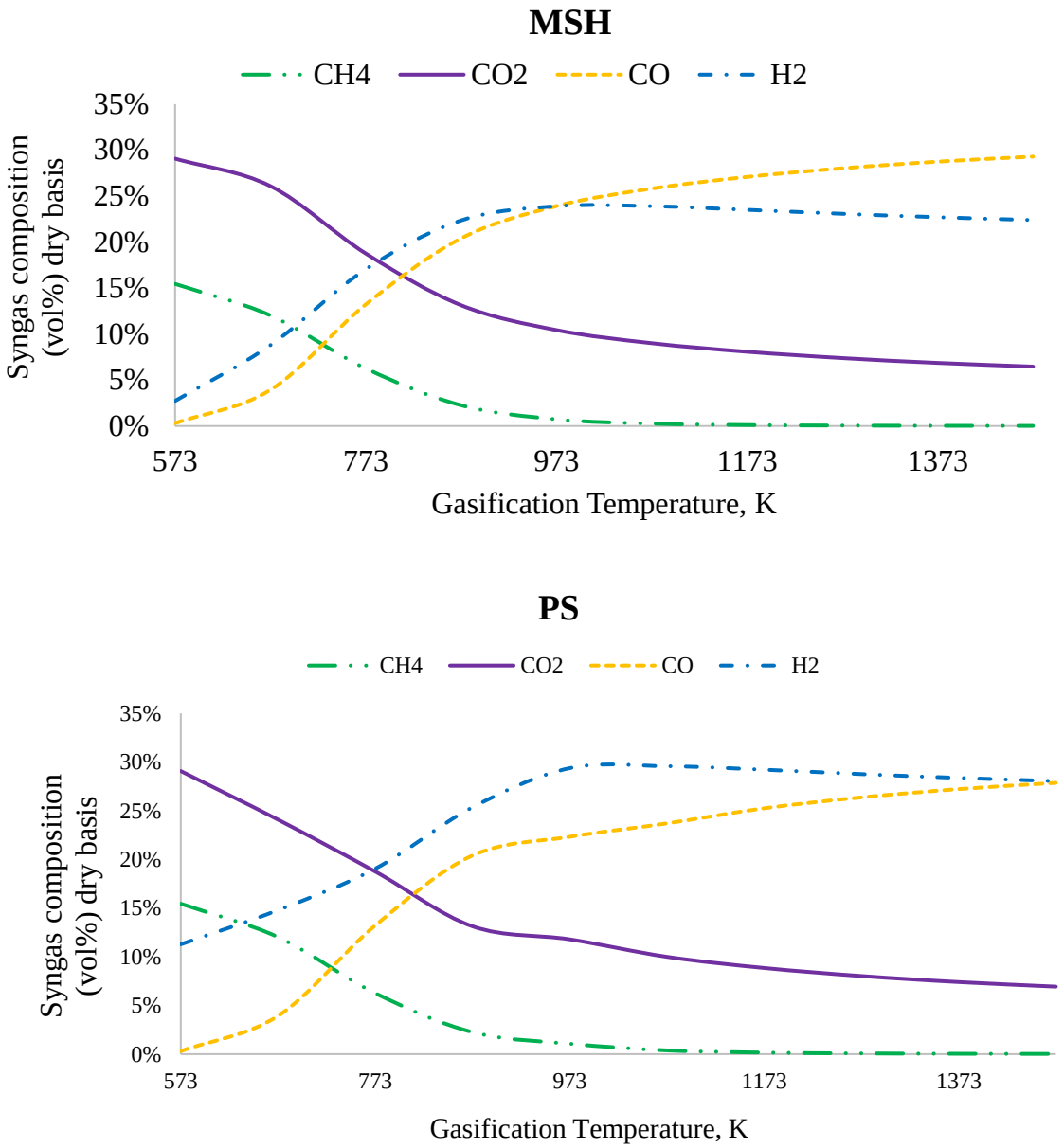

Figure 6.7. Effect of GT on the syngas composition for MSH and PS

Figure 6.7, demonstrates that for each feedstock, CO, and H_2 concentrations rise with rising GT, whereas CO_2 and CH_4 concentrations have shown the opposite pattern. This is because the carbon contained in the feedstock is not fully utilized at low temperatures (300-500°C). The syngas contains both unburned carbon and methane at this temperature, however, CO is produced by the boudouard reaction, equation (4.6a), and CH_4 was transformed to H_2 by the reverse hydrogasification reaction, equation (4.6c). However, when the temperature was augmented, the equilibrium chemical reaction will change in the opposite direction to balance the change, at those high temperatures. As a result, as the temperature rises, the chemical reaction shifts due to the equilibrium, increasing the concentration of H_2 and decreasing the concentration of CH_4. The greater temperature contributes to more favorable conditions for thermal cracking and steam reforming, according to Dutta et al. (2014) and Ayub et al. (2020b), which also validates these findings. Steam reforming, equation (4.6l) and endothermic reactions in water gas, equation (4.6b) could both be used to explain the rise in H_2 concentration as GT augmented. However, CO content would rise as a result of endothermic reactions being more prevalent than exothermic events during boudouard equation (4.6a), water gas, equation (4.6b), and steam reforming, equation (4.6k) as the equilibrium chemical reaction will move in the opposite direction at those high temperatures to counteract the change. In endothermic processes, higher GT promotes endothermic products, whereas in exothermic reactions, it favors the reactants in a positive direction.

As the gasification temperature rises, several reactions, including the hydrogasification reverse reaction, Boudouard reaction, CH_4 reforming reaction, and water gas reaction, are accelerated, which could help to explain the results. As a result, the slow conversion of CH_4 to H_2 and CO_2 to CO causes H_2 and CO contents to rise more quickly while the volume of CH_4 and CO_2 decreases more quickly.

Summary of the effect of temperature on the syngas composition

The syngas composition was affected by the temperature increase in a variety of ways. Table 6.4 displays the summary trend, which shows that changes start to become apparent about 1000 °C. For MSH, a hydrogen composition of 22.39 % and the lowest amount of CH_4, which is 0.01 % were observed at an extreme temperature of 1200 °C. A similar trend was seen when the PS was used as a feedstock.

Table 6.4. Summary of effects of GT on the syngas composition

Gas	Moderate GT ($\mathbf{800-1000}$ ℃)	High GT ($\mathbf{1000-1200}$ ℃)	Observed results
CO	Increase	Increase	CO increases with increased GT
CO_2	Decrease	Decrease	CO_2 decreases for bigger GT
CH_4	Decrease	Considerable decrease	There is notable decrease in CH_4 with increased GT
N_2	Decrease	Constant	N_2 decreases with increased GT and remains constant
H_2	Increase	Considerable decrease	Increased GT results in increased H_2 then considerably decreased H_2

6.3.3.2. Effect of GT on LHV of the syngas

Figure 6.8 shows the relationship between the GT and the LHV of syngas for the operational ER and MC. For MSH, the LHV steadily rises until it reaches its final value of 6.118 MJ/Nm^3 at the GT of 1200 ℃, up from the original value of 5.877MJ/Nm^3 at an initial GT of 300 ℃, that suddenly climbed to 5.928 MJ/Nm^3 when the GT was adjusted to 800 ℃. With the definition of the LHV equation (4.11e), this increasing trend can directly be related to the increase in the yield of partial combustion gases (CO and H_2) with temperature increment.

Similarly, for PS the LHV of the producer gas steadily rises until it reaches its final value of 6.549 MJ/Nm^3 at the GT of 1200 ℃, up from the original value of 6.241 MJ/Nm^3 at an initial GT of 700 ℃. The data can be referred from Table E-7 of Appendix E.

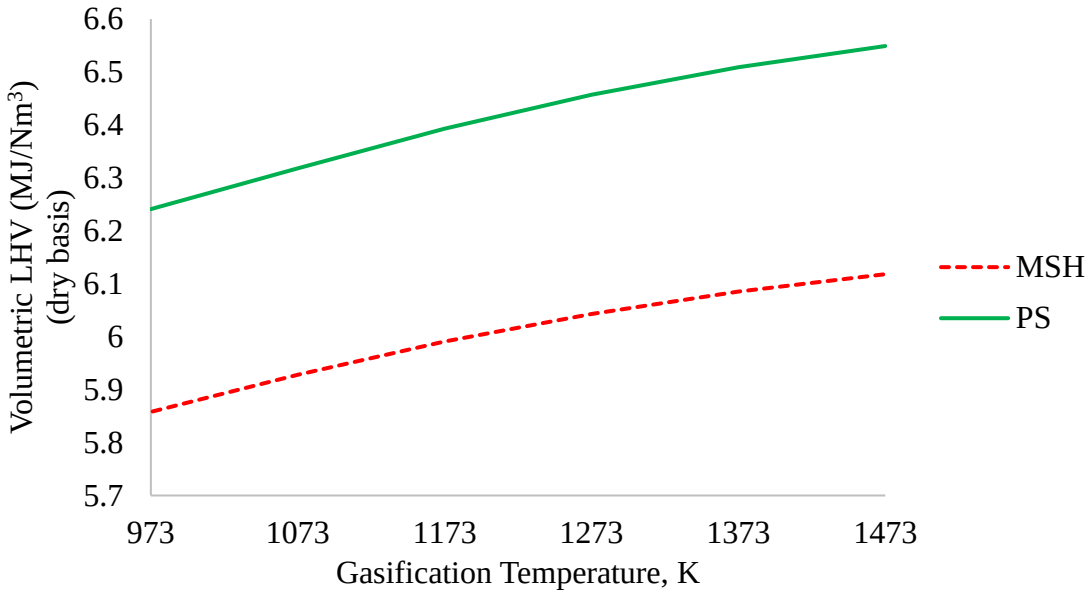

Figure 6.8. Effect of GT on LHV of the syngas for MSH and PS

6.3.4. Exergy efficiency

Figures 6.9 and 6.10 for MSH and PS, respectively, exhibit the chemical exergy efficiency of the gasification system from the model at one varying and two default values of ER, MC, and GT. Only one parameter is varied and the remaining two are set at the default values that were specified in Table 6.1. Because the temperature increase had a more significant impact on the chemical exergies of specific PG constituents than did the increases in ER and MC, the exergy efficiency owing to the GT was higher for both biomasses. Additionally, as the temperature inside the gasification system rises, the physical exergy of the PG constituents changes as well, which in turn alters the exergy efficiency shown in equation (4.12).

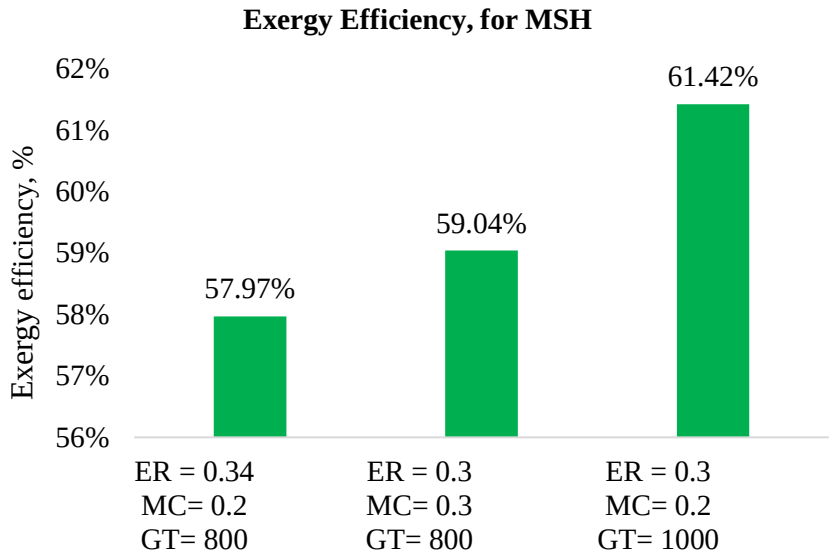

Figure 6.9. Exergy efficiency using MSH

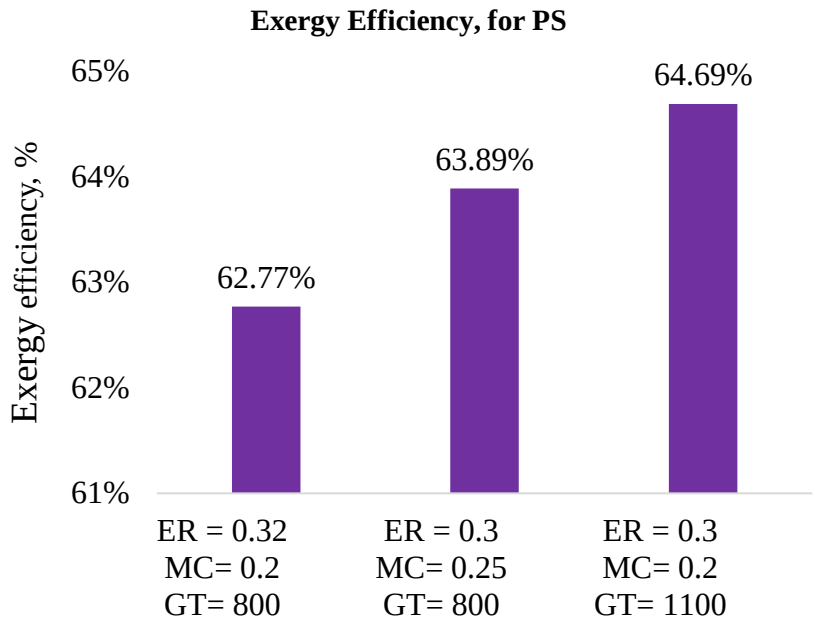

Figure 6.10. Exergy efficiency using PS

6.4. Experimental results

On the constructed biomass gasification system, experimental studies were conducted. For the current evaluations, two different kinds of biomass feedstock were used. As shown in Figure 5.7 of chapter 5 in section 5.4, the downdraft gasifier is divided into 6 zones starting from the top as drying zone, pre-pyrolysis zone, pyrolysis zone, combustion zone, reduction zone, and ash container. This division is based on preliminary studies. To evaluate the thermal characteristics of the gasifier, a thorough investigation was carried out. Additionally, estimates of the producer gas composition using various feedstocks are presented. Moreover, this section includes an assessment of the condensate particle formed during gasification as well as syngas flame characteristics.

6.4.1. Gasification with MSH as feedstock

Size-reduced 15 mm x 12 mm MSH and ER in the range of 0.3-0.35 were used for the studies. To determine the variable intake air flow rate, the ERs are calculated by detecting the input air velocity using an anemometer. MSH has a moisture content of 9.14 %. Experiments were repeated 3 times for reproducibility of results. Data that is measured is regarded as an average of these experiments. Each series of experiments takes place over the course of one hour with a 5.49 kg input feedstock.

6.4.1.1. Variation of temperature along an axial direction

Figure 6.11 shows the temperature change over time for various zones at an operating MC which is 0.0914 for MSH and 0.0923 for PS as identified from the proximate analysis of the feedstocks. For MSH, when ambient air was employed, it has been found that the temperatures in the areas of drying, pre-pyrolysis, pyrolysis, combustion zone, reduction zone, and ash container vary from 164.8 to 298.8 °C, 304.1 to 561.2 °C, 405.2 to 928.1 °C, 356.5 to 803.7 °C, and 208.4 to 435.3 °C, respectively. The data for the graphs can be found in Table E-8 and E-9 of Appendix E.

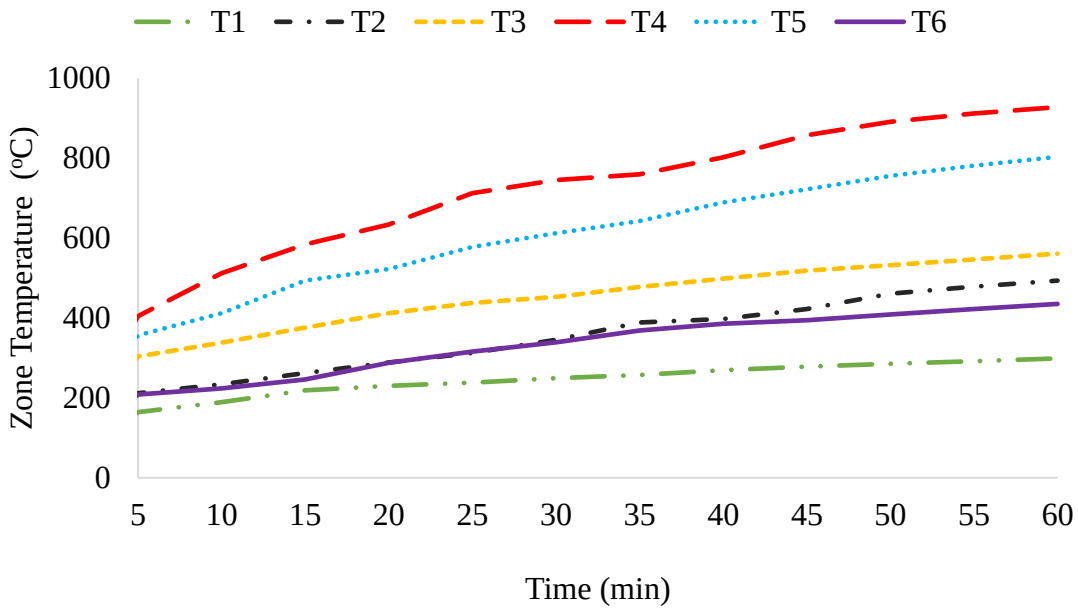

Figure 6.11. Thermal behavior of gasifier with time for MSH using atmospheric air

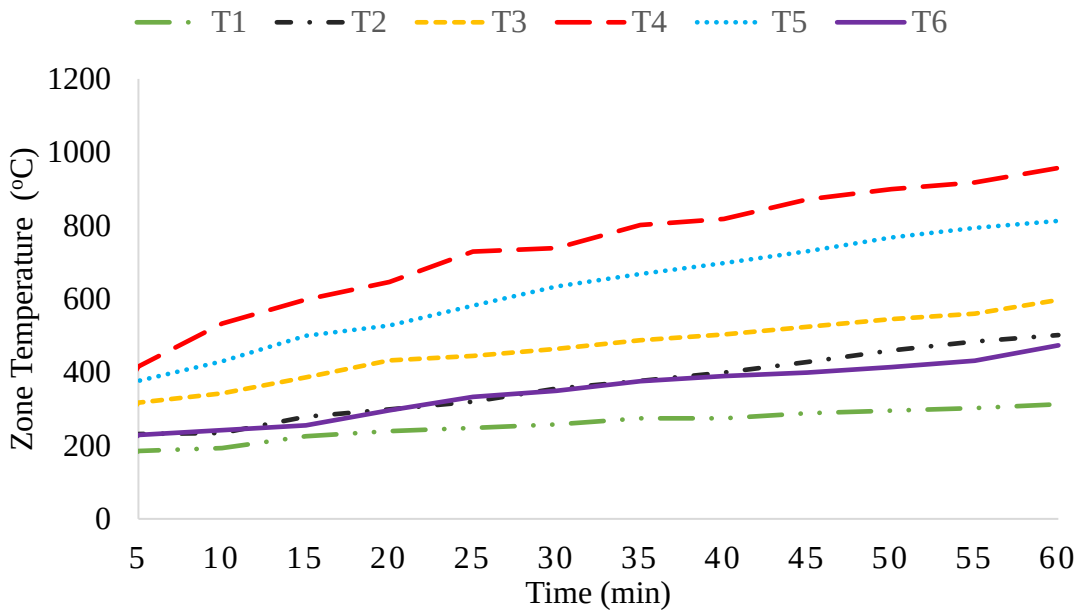

Figure 6.12. Thermal behavior of gasifier with time for MSH using compressed air

As it is depicted in Figure 6.12, for MSH when pressurized air was utilized as a gasifying agent, the temperature in drying, pre-pyrolysis, pyrolysis, combustion zone, reduction zone, and ash container were changing from 185.3 –312 °C, 231.7 – 501.3 °C, 317.2 – 597.2 °C,415.9 – 957.5 °C, 376.3 – 812.8 °C, and 228.5 – 473.9 °C respectively when the time is changed from 5 minutes to 1 hour. Furthermore, it is clear that when pressurized air is utilized, the temperature within the gasifier increased more quickly because a large amount of air was moving quickly. However, in this instance, large amount of air meant that a significant amount of biomass was being consumed (Basu, 2018). The gasification temperature of 800 $°C$ was achieved within 35 minutes when pressurized was used but this time was 40 minutes when atmospheric air is used.

6.4.1.2. Variation of temperature in a vertical direction

After one hour, the behavior of the gasifier along the vertical axis was shown in Figure 6.13. The gasification reaction is observed to be influenced by the temperature in the various zones. The combustion zone has the maximum temperature, as would be expected. Both the pressurized air and atmospheric air-supplied gasification systems exhibit the same pattern in temperature distribution. The primary distinction is that when compressed air was utilized, the greatest temperature of each zone was recorded.

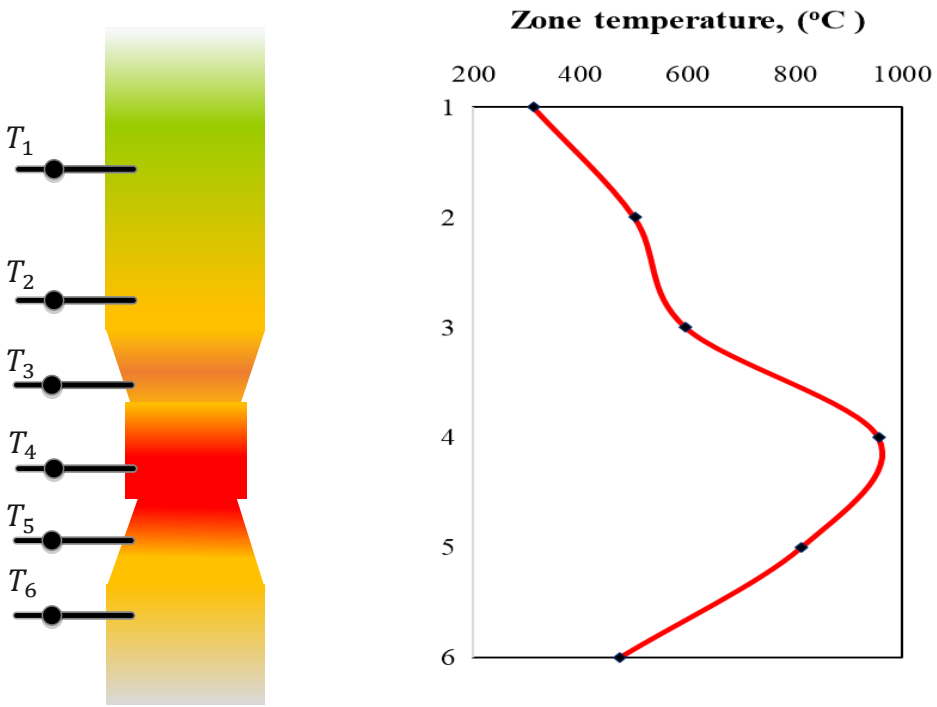

Figure 6.13. Variation of temperature in a vertical direction for MSH

6.4.1.3. Variation of temperature along the producer gas line

At several points along the producer gas line, including the gasifier gas outlet, the entrance and exit to the air heater, and the cyclone separator, temperature fluctuation was observed. There was a 23-35 °C difference between the temperature of the producer gas before and after the air was heated. A range of 55–65 °C was found to be the air temperature coming out of the air preheater. The temperature difference between the input and outlet along the cyclone separator line was up to 2-3 °C. Since the residence time of the gas in the cyclone separator depends on it and the cyclone separator is insulated, the temperature difference is very minor due to the greater producer gas flow rate.

6.4.2. Gasification with PS pellets as feedstock

For the studies, two PS pellets with respective dimensions of 9 and 15 mm in diameter and 25 and 20 mm in height as well as an ER between 0.3-0.35 were used. The ERs are computed by measuring the input air velocity with an anemometer and calculating the variable intake air flow rate. PS has a moisture content of 9.23 %. For results that can be replicated, experiments were repeated three times. The information that was measured is thought of as an average of various tests. Each set of experiments was conducted using a 5.49 kg input feedstock over the period of one hour.

6.4.2.1. Variation of temperature along axial direction

Figure 6.14 shows that for 9 mm PS pellets when atmospheric air was used as a gasifying agent, temperatures in the drying, pre-pyrolysis, pyrolysis, combustion zone, reduction zone, and ash container varied from 173.5 to 304.9 °C, 209.4 to 498.7 °C, 313.1 to 581.2 °C, 401.7 to 948.4 °C, 343.2 to 798.6 °C, and 215.4 to 432.1 °C, respectively.

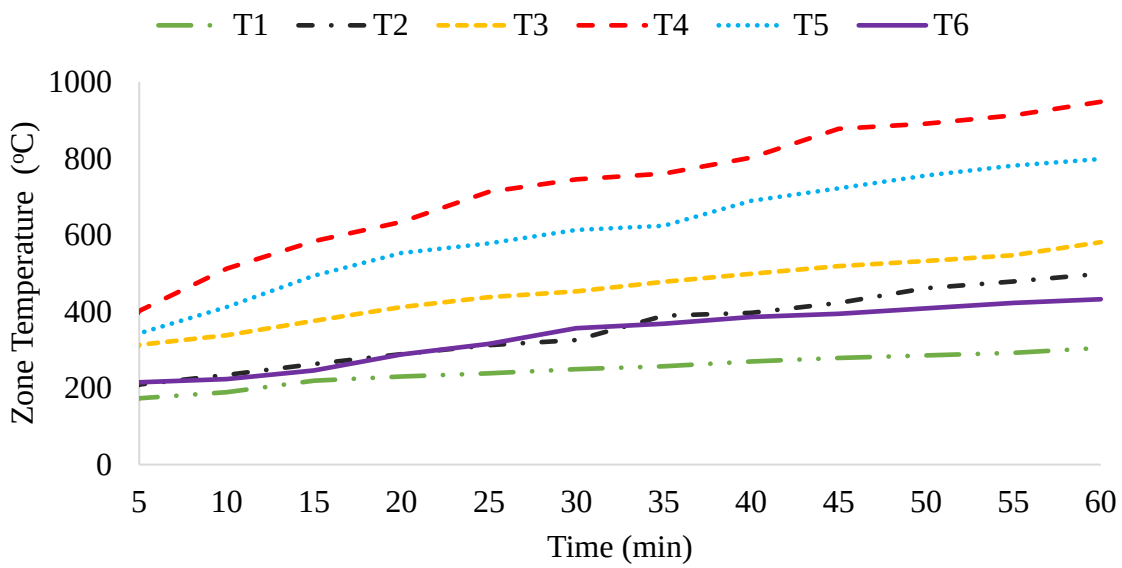

Figure 6.14. Thermal behavior of gasifier with time for 9 mm PS using atmospheric air

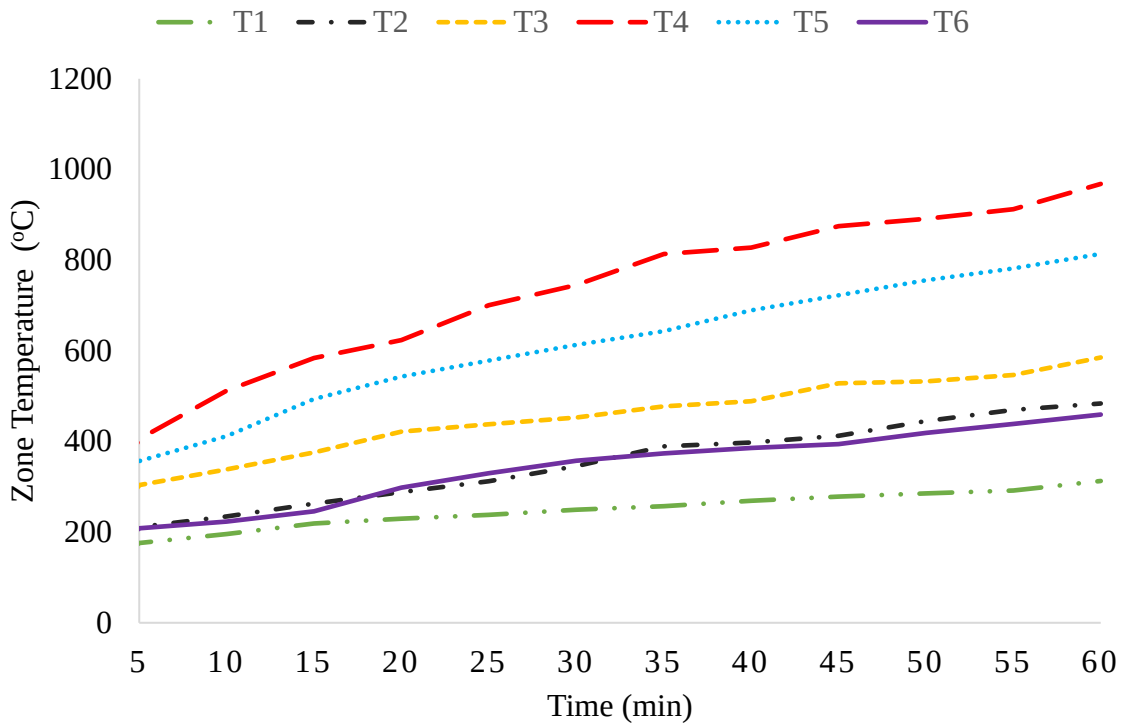

Figure 6.15. Thermal behavior of gasifier with time for 9 mm PS using compressed air

As it is depicted in Figure 6.15**,** for 9 mm PS pellets when pressurized air was utilized as a gasifying agent, the temperature in drying, pre-pyrolysis, pyrolysis, combustion zone, reduction zone, and ash container are varying from 175.8 –315.7 °C, 211.4 – 483. 7 °C, 304.1 – 585.2 °C, 408.3 – 968.7 °C, 356.5 – 813.7 °C, and 208.4 – 459.3 °C respectively when the time is changed from 5 minutes to 1 hour. At first, combustion occurred smoothly and the temperature was closer to the case when pressurized air was provided since air entered through the upper portion of the gasifier for the first case. However, as the length of residency increases, the pressurized air-supplied case starts to take control. Furthermore, it is clear that using pressurized air caused the temperature within the gasifier to rise more quickly due to the rapid movement of a lot of air. However, the presence of a lot of air in this situation meant higher biomass consumption. The gasification temperature of 800 °C was achieved within 31 minutes when pressurized was used but this time was 39 minutes when atmospheric air is used.

Figure 6.16 and 6.17 shows a similar temperature variation trend for 15 mm PS pellets, however, because of the size of the pellets, there was a clog in the gasifier's throat area, which made the temperature distribution sluggish. However, the temperature distribution was swift and appropriate once stirring was carried out using the provided grate cleaner, which is situated beneath the gasification reactor. Additionally, when pressured air was

utilized, the gasification temperature of 800 °C was reached in 45 minutes; but, when ambient air was used, it took 50 minutes.

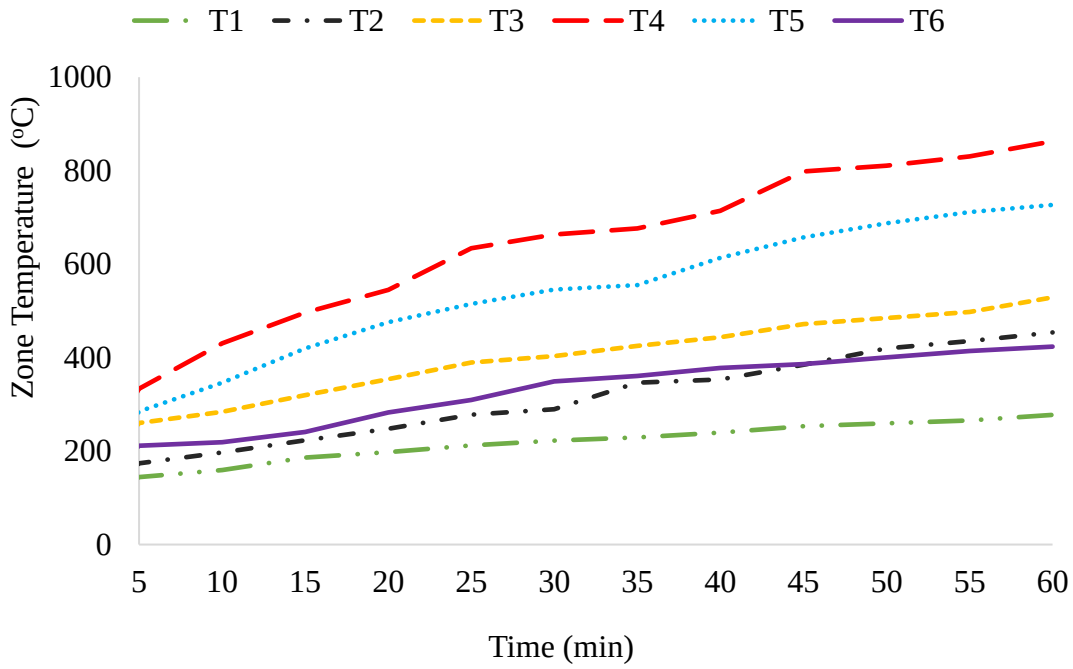

Figure 6.16. Thermal behavior of gasifier with time for 15 mm PS using atmospheric air

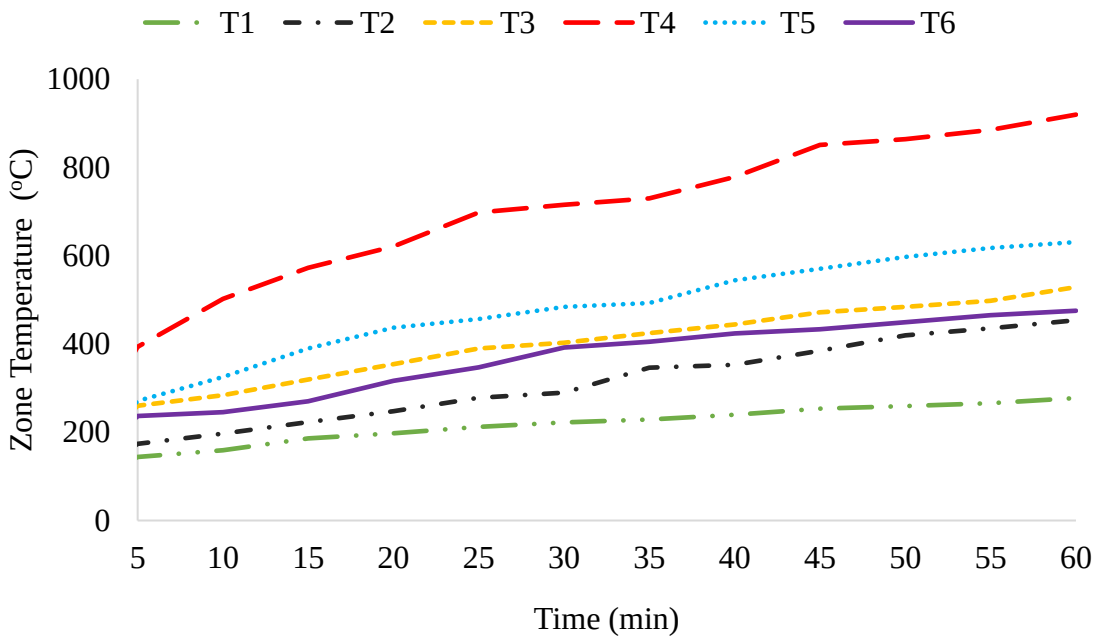

Figure 6.17. Thermal behavior of gasifier with time for 15 mm PS using compressed air

As seen in Figure 6.17, the combustion zone temperature T_4 is greater than the temperatures in the other zones as a result of the feedstock pellets obstructing the gasifier's throat, which kept heat trapped there until the stirring was done.

6.4.2.2. Variation of temperature in a vertical direction

After one hour, the gasifier's vertical axis behavior is shown in Figure 6.18 and 6.19 The temperature in the various zones is seen to have an impact on the gasification process. As might be predicted, the combustion zone exhibits the maximum temperature. The temperature distribution in the pressurized air and atmospheric air-supplied gasification systems is the same. The main difference is that each zone's highest temperature was recorded when compressed air was used. Both pellets' gasification exhibits the same pattern.

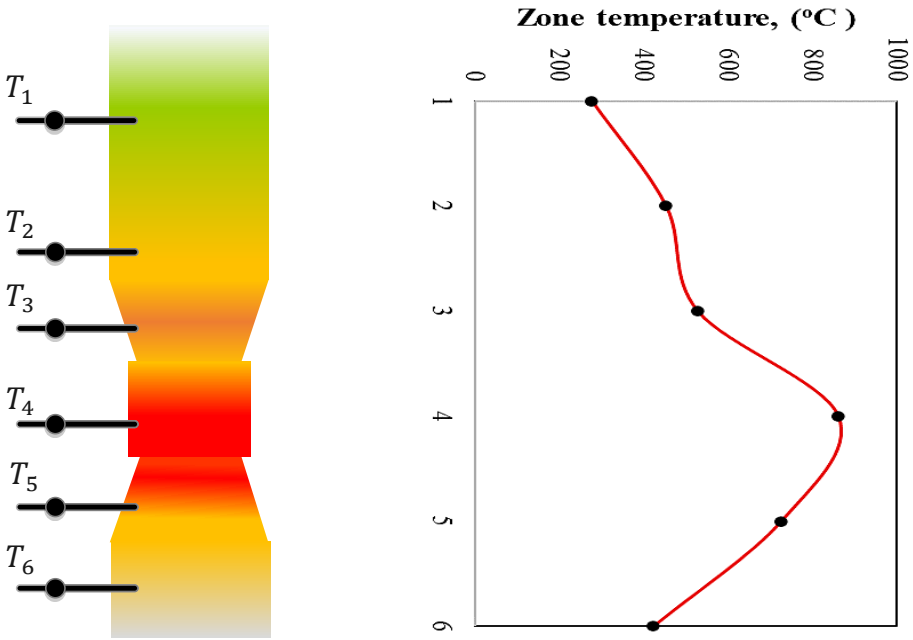

Figure 6.18. Variation of temperature in a vertical direction for 9 mm PS

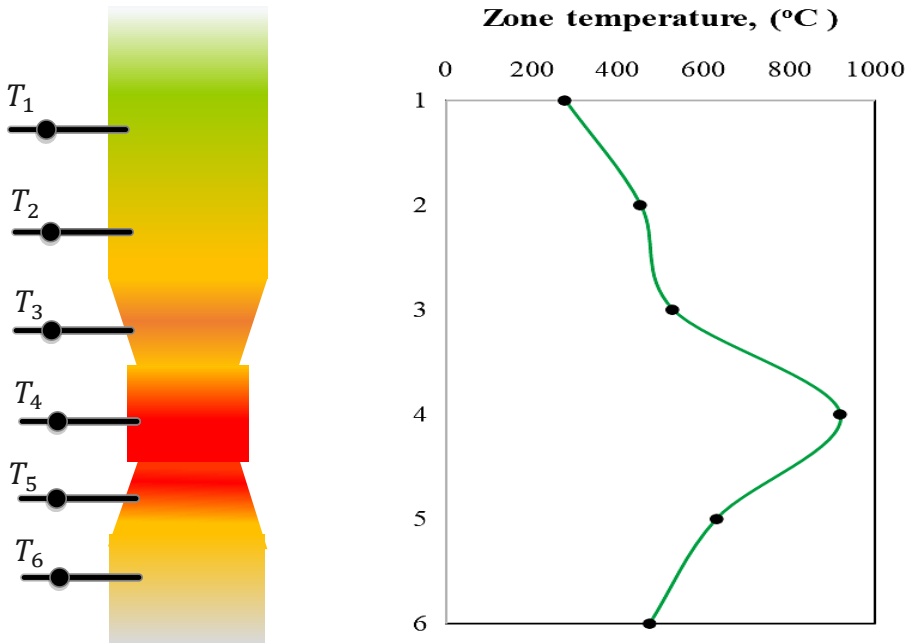

Figure 6.19. Variation of temperature in a vertical direction for 15 mm PS

6.4.2.3. Variation of temperature along the producer gas line

The temperature change was recorded at a number of locations along the producer gas line, including the gasifier gas outlet, the entrance and exit to the air heater, and the cyclone separator. The temperature of the producer gas before and after the air was heated for 9 mm and 15 mm PS pellets, respectively, varied by 28–32 °C and 20–27 °C. For 9 mm pellets, the air temperature coming out of the air preheater was determined to be between 50 and 59 °C, and for 15 mm pellets, it was between 45 and 50 °C. Up to 2-3 °C of temperature difference existed between the input and outlet along the cyclone separator line for both pellets. Due to the larger producer gas flow rate, the temperature difference is very small because the residence time of the gas in the cyclone separator depends on it and the cyclone separator is also insulated.

6.4.3. Comparison of gas composition for the feedstocks

Using an INFRALYT smart exhaust gas analyzer, the product gas produced by the gasification of MSH, 9 mm, and 15 mm pellets at 800 ^{o}C was evaluated, and the constituents are shown in Table 6.5. Only CO, CO_2, and CH_4 from the constituent of the PG can be measured with this analyzer, according to the specifications. Additionally, the analyzer only measures CO content on a scale of 10%. As a result, access to measuring equipment was limited during test runs for the measurement of H_2, H_2O, and N_2 in ASTU and other labs outside of ASTU. However, experimental data analyzing CO, CO_2, and CH_4 concentrations is quite valuable for examining the process.

Table 6.5. PG composition comparison for the feedstocks in volume percentage, wet basis

Gas Compositions	ER= 0.3		
	MSH	**9 mm**	**15 mm**
CO	6.061	6.797	5.917
CO_2	11.83	12.47	11.62
CH_4	1.272	1.286	1.253
Others	80.837	79.447	81.21

It is important to note that the CO value measured and depicted in Table 6.5 is on a scale of 10%. The additional components that are thought to be present in the PG, H_2, H_2O, and N_2, are labeled with the value "Others" as well.

6.4.4. Comparison of flame characteristics for the feedstocks

Visual inspection can be used to comparably assess the calorific value and composition of syngas from various feedstocks, and the most used one is flaming characteristics. As depicted in Figure 6.20, both MSH and the Φ 9 mm PS pellet displayed a flame of high intensity and consistency. However, for Φ15 mm PS pellets, the flame intensity somewhat decreased due to the clogging of the pellets at the throat and reduction zone, which impeded the flow of the PG. Based on this assessment, the flame from MSH, the Φ9 mm PS pellet, and the Φ15 mm PS pellet, respectively, can be rated as very good, very good, and good.

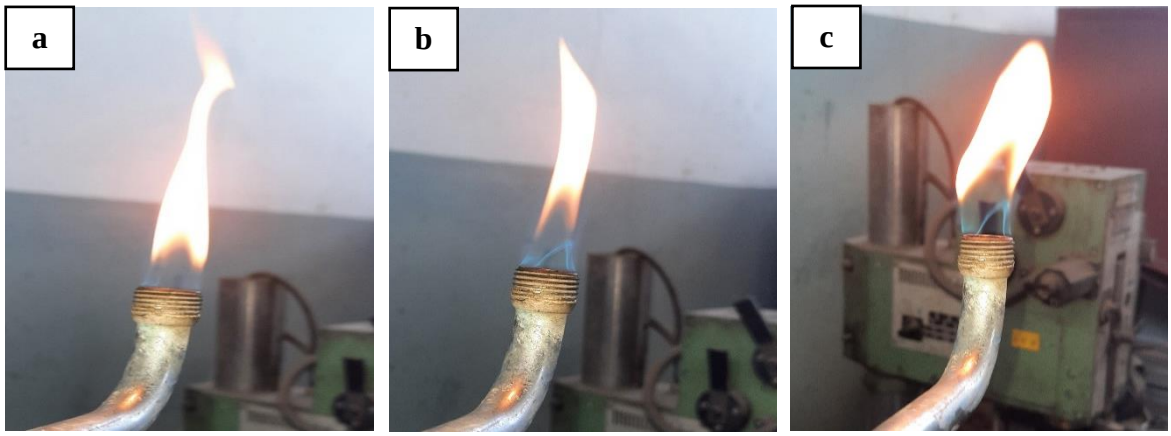

Figure 6.20. Comparison of flame quality (a) MSH (b) Φ 9 mm PS pellet (c) Φ 15 mm PS pellet

6.4.5. Comparison of char for various feedstocks

The amount of char left after gasification was collected and measured with the aid of a weighing scale. Burning one kilogram of biomass from each sample, the ash was then weighed. The measured values for MSH, 9- and 15-mm PS pellet were 38.78, 51.12, and 30.08, respectively, after deducting the value of 5-gram A4 paper as shown in Figure 6.21. The measured result demonstrates that a large portion of the biomass is transformed into gas and that the gasification process went well.

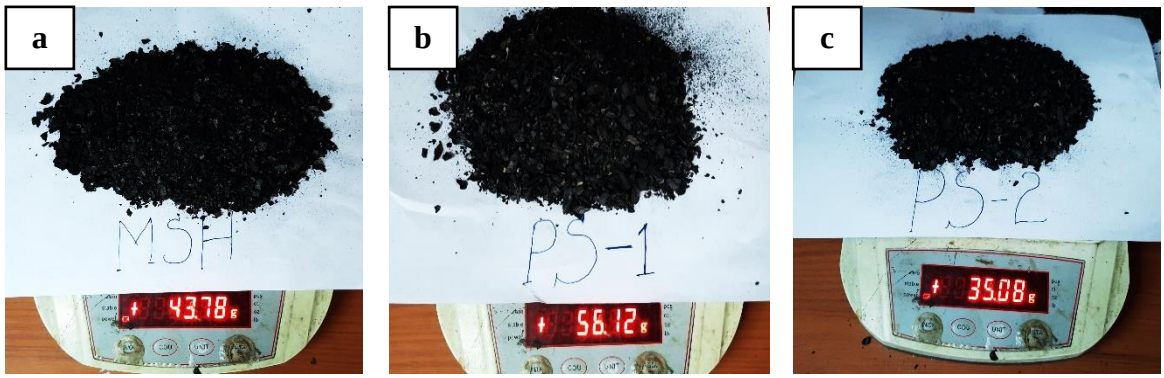

Figure 6.21. Comparison of char amount (a) MSH (b) Φ 9 mm PS pellet (c) Φ 15 mm PS pellet

6.4.6. Amount of condensate particle

The amount of tar or condensate particle was investigated in this experiment, despite the fact that it is not a major issue for a downdraft gasifier, as numerous academic publications asserted (La Villetta et al., 2017; Smith et al., 2019). Following the completion of the entire gasification process, it was collected from the lower section of the cyclone separator and measured. The amount was less than 15 milliliters as it can be seen in Figure 6.22. Thus, this result shows that the amount of tar content can be neglected as assumed in the modeling part of the gasification system.

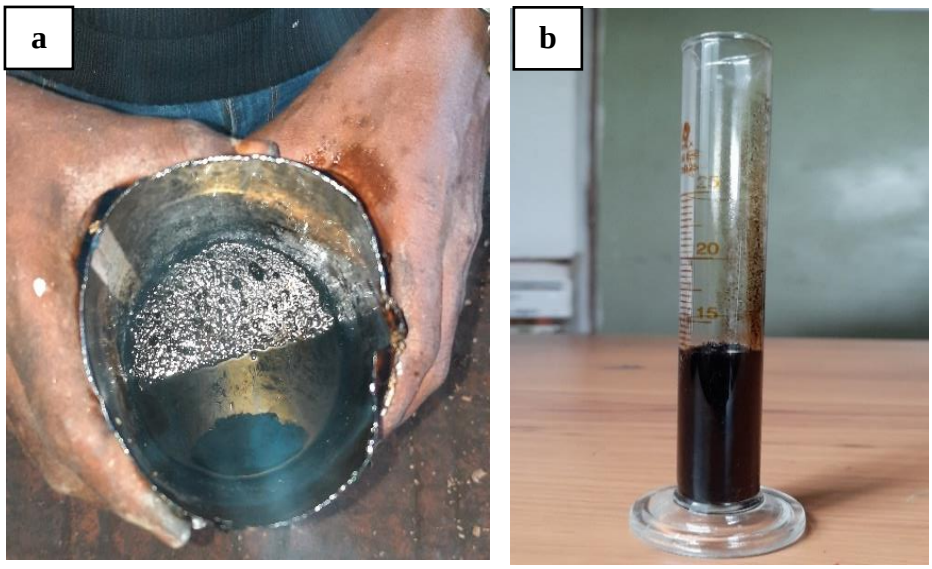

Figure 6.22. Condensate particle after the experiment (a) collected (b) measured

6.5. Comparison of model and experimental results

A comparison is made between the model and the experiment to validate the value of several parameters, such as the PG composition and LHV as illustrated in Table 6.5. Given that the volume percentage of CO in PG produced by biomass gasification is thought to be between 20 and 30 (Basu, 2018; Hamad et al., 2017; Molino et al., 2018; Safarian et al., 2019; Sittisun et al., 2019; Sivabalan et al., 2021), the experimental results can be modified by assuming that the measured value falls within a volume percentage range of 30 to account for the CO value drop due to the lower scale of the gas analyzer. Furthermore, since nitrogen is an inert gas its value in the PG is assumed to be equal with the model, to calculate the amount of H_2. The amount of the deviation of the model prediction from the experimental results was evaluated by calculating root mean square error (RMSE) as shown in Table 6.6.

Table 6.6. Error estimation of the model and the experiment

Parameter (wet basis)	Model		Experiment		Modified Exp.		RMSE $\sqrt{\frac{\sum(V_e - V_p)^2}{N}}$		RMSE,mod	
	MSH	PS	MSH	PS	MSH	PS	MSH	PS	MSH	PS
CO	24.16	22.92	6.06	6.80	18.18	20.39	18.10	16.12	5.98	2.53
CO_2	8.43	8.06	11.83	12.86	11.83	12.47	3.40	4.80	3.40	4.41
CH_4	0.24	0.20	1.27	1.28	1.28	1.29	1.03	1.08	1.04	1.09
H_2	22.38	23.55	42.42	41.00	30.29	27.41	20.04	17.45	7.91	3.86
LHV	5.55	5.53	5.80	5.89	6.02	5.47	0.25	0.36	0.47	0.06
Total							**27.23**	**24.27**	**10.54**	**6.48**

Where, V_e, V_p and N are the experimental value, predicted value, and the number of observations respectively.

Most of the error estimates of RMSE showed deviations within the acceptable limits for the modified experiment results. However, the original experimental results RMSE was larger for CO and H_2, due to the measuring scale of the gas analyzer and achieving thermodynamic equilibrium as assumed in the model was impossible when conducting an experiment.

6.6. Summary

The results obtained from both the model and the experimental evaluation are summarized as follows:

For the case of the model, for both biomass feedstocks when the value of ER increased the value of CO_2, and N_2 has shown an upward trend, nevertheless, the value of CO, CH_4, H_2, and LHV has shown, a downward trend. Moreover, with increased MC the value of CO, LHV, and N_2 have fallen, however, the value of CO_2, CH_4, and H_2 have augmented. Lastly, when the GT increased the value of CO_2, CH_4, and N_2 decreased, however, the value of CO, H_2, and LHV augmented. Additionally, the effect of GT had a higher exergy efficiency than ER and MC. For the case of the experiment, the temperature distribution for MSH, Φ 9 mm, and Φ15 mm PS pellets, has been observed to be good and the combustion zone temperature varied from $405.2 - 928.1\,°C$, $401.7 - 948.4\,°C$ and $333.41 - 862.8\,°C$ respectively when atmospheric air was used as a gasifying agent, nevertheless, this temperature value was $415.9 - 957.5\,°C$, $408.3 - 968.7\,°C$, and $393.7 - 919.6\,°C$ respectively, when pressurized air is used as a gasifying agent for an hour.

CONCLUSIONS AND RECOMMENDATIONS

Conclusions

A detailed study on the model and experimentation of pilot scale throated downdraft gasifier using MSH and PS as feedstock was conducted to see the functionality of the gasifier with different biomass. Two locally available biomasses were identified and characterized before moving on to the gasification system model and experimentation. The characterization involves elemental analysis, proximate analysis, and heating value estimation. Different gasification system parameters, such as PG composition and LHV, were predicted using a stochiometric equilibrium model integrated with the EES tool. Experimental studies on the downdraft gasifier are explained on the utilization of biomass in size-reduced and densified form. Regarding the performance evaluation of the gasifier using these biomass feedstocks, some of the key study focal areas included thermal performance, gas components, LHV, and quality. The pellets were produced using a screw-type pelletizer and have a 9 to 15 mm diameter. Thermal behavior, gas quality, and PG components from the gasification of MSH and PS pellets were compared. Finally, a study of flame characteristics was done, and the flame intensity that was observed was very good. The theoretical analysis and experimental findings were shown to be in good agreement. The following conclusions were drawn from the theoretical and experimental analysis of the downdraft gasifier.

In the case of model results

- The PG composition and LHV were found to be negatively affected by higher ER.
- It was discovered that a medium level of MC was beneficial for improved PG composition, but at the expense of LHV.
- A diminishing effect of higher GT was seen on most of the PG composition.
- Compared to the LHV of PG generated using MSH, the LHV of PG produced using PS was superior.
- Compared to a system employing PS, which had an exergy efficiency of 64.69 %, the system using MSH has a lower exergy efficiency of 61.42 %.

In the case of experimental results

- The MSH and 9 mm PS pellet were observed to have good temperature distribution inside the gasifier over time.
- The temperature distribution along the gasifier has been affected by the size of the biomass.

- When pressured air was utilized as the gasifying medium, it was found that the temperature in the combustion zone was higher. However, the biomass consumption was also higher.
- It was discovered that gasification with atmospheric air was effective and economical.
- For MSH and 9 mm PS pellets, it was found that heat from the combustion zone is effectively transferred to the pyrolysis, pre-pyrolysis, drying, and reduction zones.
- The producer gas generated with MSH has a composition of 30.29 % H_2, 18.18 % CO, and 1.28 % CH_4. The calorific value was determined to be 6.02 MJ/m^3. Similarly, the PG was produced with 9 mm PS pellets and contained 27.41% H_2, 20.39% CO, and 1.291% CH_4. The calorific value was found to be 5.47 MJ/m^3.
- When MSH and 9 mm PS pellets were utilized, gas with good flame characteristics was produced. Additionally, the gasifier's overall performance for these feedstocks was favorable.
- As a result, MSH and PS are discovered to be good biomass feedstocks for producing syngas through biomass gasification.

Recommendations

Theoretical and experimental performance evaluation of the throated downdraft gasification system was carried out in the current work, and the major findings have been thoroughly discussed. Further study could greatly enhance system performance evaluation, nevertheless. Following are some of the potential scope and recommendations for additional research:

- The gasification process entails numerous hazards, including chemical hazards, fire hazards, hazards to the environment, and potential threats from explosions. Carbon monoxide, a component of PG, is somewhat hazardous because it interacts with hemoglobin in the blood to limit oxygen absorption and cause dizziness. Thus, installing the gasifier plant outside or in well-ventilated regions is advised to prevent gas from being trapped in the room.
- The experimentally obtained data also reveals several discrepancies in the gasifier's temperature profile. The internal temperature of the gasifier, which is currently measured by thermocouples attached to its wall, might not accurately reflect the temperature of actual gasification. A better understanding of the temperature distribution inside the gasifier can be obtained by using additional temperature probes to measure the temperature in the reactor's center.

- The gasification product gas composition was measured using the INFRALYT smart exhaust gas analyzer. According to the specifications, this analyzer can only measure CO, CO_2, and CH_4 from the constituent of the PG. In ASTU and other labs outside of ASTU, access to measuring equipment was thus restricted during test runs for the measurement of H_2, H_2O, and N_2. The analyzer also only detects CO content on a scale of 10%. Therefore, it is advisable to identify the locations of the necessary measuring equipment before selecting the study area.
- Future research can be done to create a model that, depending on the setup of the gasifier, can precisely forecast the syngas composition which cannot be predicted by the equilibrium model.
- The syngas main components CO and H_2 are currently present in the producer gas that resulted from gasification. When developing the gasifier, a gas-storing mechanism might be taken into account in order to extract the syngas utilizing various techniques.

REFERENCES

Abate B., and Dechassa N. (2021). White Mango Scale, Aulacaspis tubercularis Newstead (Hemiptera: Diaspididae): a challenging mango productions in ethiopia: a review. *Bioprocess Engineering*, *5*(1), 17-22. https://doi.org/10.11648/j.be.20210501.13

Akhator P., Obanor A., et al. (2019). Design and development of a small-scale biomass downdraft gasifier. *Nigerian Journal of Technology*, *38*(4), 922-930. https://doi.org/10.4314/njt.v38i4.15

Alzate C. A. C., Toro J. C. S., et al. (2018). Fermentation, thermochemical and catalytic processes in the transformation of biomass through efficient biorefineries. *Catalysis today*, *302*, 61-72. https://doi.org/10.1016/j.cattod.2017.09.034

Anukam A., Mamphweli S., et al. (2016). Pre-processing of sugarcane bagasse for gasification in a downdraft biomass gasifier system: A comprehensive review. *Renewable and sustainable energy reviews*, *66*, 775-801. https://doi.org/10.1016/j.rser.2016.08.046

Arnaldo V.-V., Yuhan Arley L.-R., et al. (2019). Performance analysis of a commercial fixed bed downdraft gasifier using palm kernel shells. *CT&F - Ciencia, Tecnología y Futuro*, *9*, 79-88. https://doi.org/10.29047/01225383.181

Awais M., Li W., et al. (2021). Experimental investigation of downdraft biomass gasifier fed by sugarcane bagasse and coconut shells. *Biomass Conversion and Biorefinery*, *11*(2), 429-444. https://doi.org/10.1007/s13399-020-00690-5

Ayub H. M., Park S. J., et al. (2020a). Biomass to Syngas: Modified Non-Stoichiometric Thermodynamic Models for the Downdraft Biomass Gasification. *Energies*, *13*(21). https://doi.org/10.3390/en13215668

Ayub H. M., Park S. J., et al. (2020b). Biomass to Syngas: Modified Stoichiometric Thermodynamic Models for Downdraft Biomass Gasification. *Energies*, *13*(20). https://doi.org/10.3390/en13205383

Babu B. (2008). Biomass pyrolysis: a state-of-the-art review. *Biofuels, Bioproducts and Biorefining: Innovation for a sustainable economy*, *2*(5), 393-414. https://doi.org/10.1002/bbb.92

Barman N. S., Ghosh S., et al. (2012). Gasification of biomass in a fixed bed downdraft gasifier–A realistic model including tar. *Bioresource technology*, *107*, 505-511. https://doi.org/10.1016/j.biortech.2011.12.124

Baruah D., and Baruah D. C. (2014). Modeling of biomass gasification: A review. *Renewable and sustainable energy reviews*, *39*, 806-815. https://doi.org/10.1016/j.rser.2014.07.129

Baruah D., Baruah D. C., et al. (2017). Artificial neural network based modeling of biomass gasification in fixed bed downdraft gasifiers. *Biomass and Bioenergy*, *98*, 264-271. https://doi.org/10.1016/j.biombioe.2017.01.029

Basu P. (2010). *Biomass gasification and pyrolysis: practical design and theory*. Academic press.

Basu P. (2018). *Biomass gasification, pyrolysis and torrefaction: practical design and theory*. Academic press.

Begum S., Rasul M. G., et al. (2013). Performance Analysis of an Integrated Fixed Bed Gasifier Model for Different Biomass Feedstocks. *Energies*, *6*(12), 6508-6524.

Bijesh R., Arun P., et al. (2021). Modified stoichiometric equilibrium model for sewage sludge gasification and its validation based on experiments in a downdraft gasifier. *Biomass Conversion and Biorefinery*. https://doi.org/10.1007/s13399-021-01916-w

Bridgwater A. V. (1995). The technical and economic feasibility of biomass gasification for power generation. *Fuel*, *74*(5), 631-653. https://doi.org/10.1016/0016-2361(95)00001-L

Buragohain B., Mahanta P., et al. (2010). Biomass gasification for decentralized power generation: The Indian perspective. *Renewable and sustainable energy reviews*, *14*(1), 73-92. https://doi.org/10.1016/j.rser.2009.07.034

Centeno F., Mahkamov K., et al. (2012). Theoretical and experimental investigations of a downdraft biomass gasifier-spark ignition engine power system. *Renewable energy*, *37*(1), 97-108. https://doi.org/10.1016/j.renene.2011.06.008

Cervini C., Verheecke-Vaessen C., et al. (2022). Improvements within the peanut production chain to minimize aflatoxins contamination: An Ethiopian case study. *Food Control*, *136*, 108622. https://doi.org/10.1016/j.foodcont.2021.108622

Chawdhury M. A., and Mahkamov K. (2011). Development of a small downdraft biomass gasifier for developing countries. *Journal of scientific research*, *3*(1), 51-51. https://doi.org/10.3329/jsr.v3i1.5613

Chen C., Jin Y.-Q., et al. (2013). Simulation of municipal solid waste gasification in two different types of fixed bed reactors. *Fuel*, *103*, 58-63. https://doi.org/10.1016/j.fuel.2011.06.075

Chopra S., and Jain A. (2007). A review of fixed bed gasification systems for biomass. *Agricultural Engineering International: CIGR Journal*, *9*.

Ciferno J. P., and Marano J. J. (2002). Benchmarking biomass gasification technologies for fuels, chemicals and hydrogen production. *US Department of Energy. National Energy Technology Laboratory*.

Couto N., Rouboa A., et al. (2013). Influence of the Biomass Gasification Processes on the Final Composition of Syngas. *Energy Procedia*, *36*, 596-606. https://doi.org/10.1016/j.egypro.2013.07.068

Das B., and Hoque S. M. N. (2014). Assessment of the Potential of Biomass Gasification for Electricity Generation in Bangladesh. *Journal of Renewable Energy*, *2014*, 1-10. https://doi.org/10.1155/2014/429518

de Souza-Santos M. L. (2010). *Solid fuels combustion and gasification: modeling, simulation*. CRC Press.

Dincer I., and Bicer Y. (2018). 4.22 Electrochemical Energy Conversion. In I. Dincer (Ed.), *Comprehensive Energy Systems* (pp. 856-894). Elsevier. https://doi.org/10.1016/B978-0-12-809597-3.00439-9

Diyoke C., Gao N., et al. (2018). Modelling of down-draft gasification of biomass – An integrated pyrolysis, combustion and reduction process. *Applied Thermal Engineering*, *142*, 444-456. https://doi.org/10.1016/j.applthermaleng.2018.06.079

Dupuis É., Thiffault E., et al. (2021). Bioenergy Conversion Potential of Decaying Hardwoods. *Energies*, *14*(1).

Dutta P. P., Pandey V., et al. (2014). Down Draft Gasification Modelling and Experimentation of Some Indigenous Biomass for Thermal Applications. *Energy Procedia*, *54*, 21-34. https://doi.org/10.1016/j.egypro.2014.07.246

Ferreira S., Monteiro E., et al. (2019). A Holistic Review on Biomass Gasification Modified Equilibrium Models. *Energies*, *12*(1).

Field C. B., Campbell J. E., et al. (2008). Biomass energy: the scale of the potential resource. *Trends in ecology & evolution*, *23*(2), 65-72. https://doi.org/10.1016/j.tree.2007.12.001

Gambarotta A., Morini M., et al. (2018). A non-stoichiometric equilibrium model for the simulation of the biomass gasification process. *Applied Energy*, *227*, 119-127. https://doi.org/10.1016/j.apenergy.2017.07.135

Gollakota A. R. K., Kishore N., et al. (2018). A review on hydrothermal liquefaction of biomass. *Renewable and sustainable energy reviews*, *81*, 1378-1392. https://doi.org/10.1016/j.rser.2017.05.178

Gómez-Barea A., and Leckner B. (2010). Modeling of biomass gasification in fluidized bed. *Progress in Energy and Combustion Science*, *36*(4), 444-509. https://doi.org/10.1016/j.pecs.2009.12.002

González-Vázquez M. P., García R., et al. (2018). Comparison of the gasification performance of multiple biomass types in a bubbling fluidized bed. *Energy Conversion and Management*, *176*, 309-323. https://doi.org/10.1016/j.enconman.2018.09.020

Guangul F. M., Sulaiman S. A., et al. (2012). Gasifier selection, design and gasification of oil palm fronds with preheated and unheated gasifying air. *Bioresource technology*, *126*, 224-232.

Hamad M. A. F., Radwan A. M., et al. (2017). Review of Biomass Thermal Gasification. https://doi.org/10.5772/66362

Havilah P. R., Sharma A. K., et al. (2022). Biomass Gasification in Downdraft Gasifiers: A Technical Review on Production, Up-Gradation and Application of Synthesis Gas. *Energies*, *15*(11).

Hernández J. J., Aranda-Almansa G., et al. (2010). Gasification of biomass wastes in an entrained flow gasifier: Effect of the particle size and the residence time. *Fuel Processing Technology*, *91*(6), 681-692. https://doi.org/10.1016/j.fuproc.2010.01.018

Higman C. (2008). Gasification. In *Combustion engineering issues for solid fuel systems* (pp. 423-468). Elsevier. https://doi.org/10.1016/B978-0-12-373611-6.00011-2

Himmel M. E., Ding S.-Y., et al. (2007). Biomass recalcitrance: engineering plants and enzymes for biofuels production. *science*, *315*(5813), 804-807. https://doi.org/10.1126/science.1137016

Hsi C.-L., Wang T.-Y., et al. (2008). Characteristics of an air-blown fixed-bed downdraft biomass gasifier. *Energy & Fuels*, *22*(6), 4196-4205.

Ibitoye S. E., Jen T. C., et al. (2021). Densification of agro-residues for sustainable energy generation: an overview. *Bioresour Bioprocess*, *8*(1), 75. https://doi.org/10.1186/s40643-021-00427-w

IEA. (2019). *Africa Energy Outlook 2019*. IEA. https://www.iea.org/reports/africa-energy-outlook-2019

Inayat M., Sulaiman S. A., et al. (2016). Effect of blending ratio on co-gasification performance of tropical plant-based biomass. https://doi.org/10.1049/cp.2016.1331

Jarungthammachote S., and Dutta A. (2007). Thermodynamic equilibrium model and second law analysis of a downdraft waste gasifier. *Energy*, *32*(9), 1660-1669. https://doi.org/10.1016/j.energy.2007.01.010

Jayathilake R., and Rudra S. (2017). Numerical and Experimental Investigation of Equivalence Ratio (ER) and Feedstock Particle Size on Birchwood Gasification. *Energies*, *10*(8).

Jha S., Nanda S., et al. (2022). A Review of Thermochemical Conversion of Waste Biomass to Biofuels. *Energies*, *15*(17).

Jia J., Xu L., et al. (2018). Effects of operating parameters on performance of a downdraft gasifier in steady and transient state. *Energy Conversion and Management*, *155*, 138-146. https://doi.org/10.1016/j.enconman.2017.10.072

Karamarkovic R., and Karamarkovic V. (2010). Energy and exergy analysis of biomass gasification at different temperatures. *Energy*, *35*(2), 537-549. https://doi.org/10.1016/j.energy.2009.10.022

Kashyap P. V., Pulla R. H., et al. (2019). Development of a non-stoichiometric equilibrium model of downdraft gasifier. *Energy Sources, Part A: Recovery, Utilization, and Environmental Effects*, 1-19. https://doi.org/10.1080/15567036.2019.1689316

Kathi S. (2016). Chapter 6 - Bioenergy from Phytoremediated Phytomass of Aquatic Plants via Gasification. In M. N. V. Prasad (Ed.), *Bioremediation and Bioeconomy* (pp. 111-128). Elsevier. https://doi.org/10.1016/B978-0-12-802830-8.00006-X

Kaushal P., Abedi J., et al. (2010). A comprehensive mathematical model for biomass gasification in a bubbling fluidized bed reactor. *Fuel*, *89*(12), 3650-3661. https://doi.org/10.1016/j.fuel.2010.07.036

Khonde R., Hedaoo S., et al. (2021). Prediction of product gas composition from biomass gasification by the method of Gibbs free energy minimization. *Energy Sources, Part A: Recovery, Utilization, and Environmental Effects*, *43*(3), 371-380. https://doi.org/10.1080/15567036.2019.1624890

Kumar A., Jones D. D., et al. (2009). Thermochemical biomass gasification: a review of the current status of the technology. *Energies*, *2*(3), 556-581. https://doi.org/10.3390/en20300556

Kumar S. S., Pitchandi K., et al. (2008). Modeling and simulation of down draft wood gasifier. *Journal of Applied Sciences*. https://doi.org/10.3923/jas.2008.271.279

Kumar T., Aradwad P. P., et al. (2021). Briquetting of mango seed shell: Effect of temperature, pressure and binder. *Agricultural Engineering Today*, *45*(4), 23-28. https://doi.org/10.52151/aet2021454.1544

Kushwah A., Reina T. R., et al. (2022). Modelling approaches for biomass gasifiers: A comprehensive overview. *Science of The Total Environment*, *834*, 155243. https://doi.org/10.1016/j.scitotenv.2022.155243

La Villetta M., Costa M., et al. (2017). Modelling approaches to biomass gasification: A review with emphasis on the stoichiometric method. *Renewable and sustainable energy reviews*, *74*, 71-88. https://doi.org/10.1016/j.rser.2017.02.027

Loha C., Gu S., et al. (2014). Advances in mathematical modeling of fluidized bed gasification. *Renewable and sustainable energy reviews*, *40*, 688-715. https://doi.org/10.1016/j.rser.2014.07.199

Luo H., Lin W., et al. (2019). Three dimensional full-loop CFD simulation of hydrodynamics in a pilot-scale dual fluidized bed system for biomass gasification. *Fuel Processing Technology*, *195*, 106146. https://doi.org/10.1016/j.fuproc.2019.106146

Madadian E., Amiri L., et al. (2020). Thermodynamic Analysis of Wood Pellet Gasification in a Downdraft Reactor for Advanced Biofuel Production. *Waste and Biomass Valorization*, *11*(7), 3665-3676. https://doi.org/10.1007/s12649-019-00663-4

Maitlo G., Ali I., et al. (2022). Thermochemical Conversion of Biomass for Syngas Production: Current Status and Future Trends. *Sustainability*, *14*(5).

Manjhi S. K., and Kumar R. (2019). Performance assessment of K-type, E-type and J-type coaxial thermocouples on the solar light beam for short duration transient measurements. *Measurement*, *146*, 343-355. https://doi.org/10.1016/j.measurement.2019.06.035

Marcantonio V., Bocci E., et al. (2020). Development of a Chemical Quasi-Equilibrium Model of Biomass Waste Gasification in a Fluidized-Bed Reactor by Using Aspen Plus. *Energies*, *13*(1).

Martínez J. D., Mahkamov K., et al. (2012). Syngas production in downdraft biomass gasifiers and its application using internal combustion engines. *Renewable energy*, *38*(1), 1-9. https://doi.org/10.1016/j.renene.2011.07.035

Massoudi Farid M., Jeong H. J., et al. (2016). Kinetic study on coal–biomass mixed char co-gasification with H_2O in the presence of H_2. *Fuel*, *181*, 1066-1073. https://doi.org/10.1016/j.fuel.2016.04.130

Mata-Sánchez J., Pérez-Jiménez J., et al. (2013). Statistical evaluation of quality parameters of olive stone to predict its heating value. *Fuel*, *113*, 750-756. https://doi.org/https://doi.org/10.1016/j.fuel.2013.06.019

McKendry P. (2002a). Energy production from biomass (part 2): conversion technologies. *Bioresource technology*, *83*(1), 47-54. https://doi.org/10.1016/S0960-8524(01)00119-5

McKendry P. (2002b). Energy production from biomass (part 3): gasification technologies. *Bioresource technology*, *83*(1), 55-63. https://doi.org/10.1016/S0960-8524(01)00120-1

Mendonça M., Mantilla V., et al. (2022). Design and experimental tests of an Imbert type downdraft gasifier prototype and clean-up system for small-scale biomass-based power generation. *Renew. Energy Environ. Sustain.*, *7*. https://doi.org/10.1051/rees/2021057

Mhilu C. (2012). Modeling performance of high-temperature biomass gasification process. *International Scholarly Research Notices*, *2012*.

Mikulandrić R., Lončar D., et al. (2014). Artificial neural network modelling approach for a biomass gasification process in fixed bed gasifiers. *Energy Conversion and Management*, *87*, 1210-1223. https://doi.org/10.1016/j.enconman.2014.03.036

Mishra S., and Upadhyay R. K. (2021). Review on biomass gasification: Gasifiers, gasifying mediums, and operational parameters. *Materials Science for Energy Technologies*, *4*, 329-340. https://doi.org/10.1016/j.mset.2021.08.009

Molino A. J., Larocca V., et al. (2018). Biofuels Production by Biomass Gasification: A Review. *Energies*, *11*, 811. https://doi.org/10.3390/EN11040811

Musse D., Bogale W., et al. (2020). Modeling of gasification of refuse derived fuel: optimizations and experimental investigations. Advances of Science and Technology: 7th EAI International Conference, ICAST 2019, Bahir Dar, Ethiopia, August 2–4, 2019, Proceedings 7,

Ngamsidhiphongsa N., Ponpesh P., et al. (2020). Analysis of the Imbert downdraft gasifier using a species-transport CFD model including tar-cracking reactions. *Energy Conversion and Management*, *213*, 112808. https://doi.org/10.1016/j.enconman.2020.112808

Obernberger I., and Thek G. (2004). Physical characterisation and chemical composition of densified biomass fuels with regard to their combustion behaviour. *Biomass and Bioenergy*, *27*(6), 653-669. https://doi.org/10.1016/j.biombioe.2003.07.006

Ong H. C., Chen W.-H., et al. (2019). Catalytic thermochemical conversion of biomass for biofuel production: A comprehensive review. *Renewable and sustainable energy reviews*, *113*, 109266. https://doi.org/10.1016/j.rser.2019.109266

Osman A. I., Mehta N., et al. (2021). Conversion of biomass to biofuels and life cycle assessment: a review. *Environmental Chemistry Letters*, *19*(6), 4075-4118. https://doi.org/10.1007/s10311-021-01273-0

Ozturk M., and Dincer I. (2018). 4.10 Integrated Gasification Combined Cycles. In I. Dincer (Ed.), *Comprehensive Energy Systems* (pp. 364-473). Elsevier. https://doi.org/10.1016/B978-0-12-809597-3.00412-0

Paiva M. V. d., Vieira A. L., et al. (2021). Simulation of a Downdraft Gasifier for Production of Syngas from Different Biomass Feedstocks. https://doi.org/10.3390/CHEMENGINEERING5020020

Pandey B., Prajapati Y. K., et al. (2021). CFD analysis of biomass gasification using downdraft gasifier. *Materials Today: Proceedings*, *44*, 4107-4111. https://doi.org/10.1016/j.matpr.2020.10.451

Panwar N. L., Kothari R., et al. (2012). Thermo chemical conversion of biomass – Eco friendly energy routes. *Renewable and sustainable energy reviews*, *16*(4), 1801-1816. https://doi.org/10.1016/j.rser.2012.01.024

Paraschiv L. S., Serban A., et al. (2020). Calculation of combustion air required for burning solid fuels (coal / biomass / solid waste) and analysis of flue gas composition. *Energy Reports*, *6*, 36-45. https://doi.org/10.1016/j.egyr.2019.10.016

Patra T. K., and Sheth P. N. (2015). Biomass gasification models for downdraft gasifier: A state-of-the-art review. *Renewable and sustainable energy reviews*, *50*, 583-593. https://doi.org/10.1016/j.rser.2015.05.012

Perea-Moreno A.-J., Aguilera-Ureña M.-J., et al. (2016). Fuel properties of avocado stone. *Fuel*, *186*, 358-364. https://doi.org/10.1016/j.fuel.2016.08.101

Perea-Moreno M.-A., Manzano-Agugliaro F., et al. (2018). Peanut Shell for Energy: Properties and Its Potential to Respect the Environment. *Sustainability*, *10*(9).

Prasertcharoensuk P., Hernandez D. A., et al. (2018). Optimisation of a throat downdraft gasifier for hydrogen production. *Biomass and Bioenergy*, *116*, 216-226. https://doi.org/10.1016/j.biombioe.2018.06.019

Puig-Arnavat M., Bruno J. C., et al. (2010). Review and analysis of biomass gasification models. *Renewable and sustainable energy reviews*, *14*(9), 2841-2851. https://doi.org/10.1016/j.rser.2010.07.030

Rabea K., Bakry A. I., et al. (2021). Real-time performance investigation of a downdraft gasifier fueled by cotton stalks in a batch-mode operation. *Fuel*, *300*, 120976. https://doi.org/10.1016/j.fuel.2021.120976

Radwan A., Abd Ethamid A., et al. (2022). C++ Software Program for Downdraft Gasifier Design and Development. *Journal of Technology Innovations and Energy*, *1*(2), 1-7. https://doi.org/10.56556/jtie.v1i2.152

Rajvanshi A. (1986). Biomass gasification, alternative energy in agriculture. *Energy Sources*, *2*, 83-104.

Ren J., Cao J.-P., et al. (2019). Recent advances in syngas production from biomass catalytic gasification: A critical review on reactors, catalysts, catalytic mechanisms and mathematical models. *Renewable and sustainable energy reviews*, *116*, 109426. https://doi.org/10.1016/j.rser.2019.109426

Roy P., Datta A., et al. (2013). An assessment of different biomass feedstocks in a downdraft gasifier for engine application. *Fuel*, *106*, 864-868. https://doi.org/10.1016/j.fuel.2012.12.053

Ruiz J. A., Juárez M. C., et al. (2013). Biomass gasification for electricity generation: Review of current technology barriers. *Renewable and sustainable energy reviews*, *18*, 174-183. https://doi.org/10.1016/j.rser.2012.10.021

Safarian S., Ebrahimi Saryazdi S. M., et al. (2020). Artificial neural network integrated with thermodynamic equilibrium modeling of downdraft biomass gasification-power production plant. *Energy*, *213*, 118800. https://doi.org/10.1016/j.energy.2020.118800

Safarian S., Unnþórsson R., et al. (2019). A review of biomass gasification modelling. *Renewable and sustainable energy reviews*, *110*, 378-391. https://doi.org/10.1016/j.rser.2019.05.003

Shahbeig H., Shafizadeh A., et al. (2022). Exergy sustainability analysis of biomass gasification: a critical review. *Biofuel Research Journal*, *9*(1), 1592. https://doi.org/10.18331/BRJ2022.9.1.5

Shaikh M. H., and Sinhal S. N. (2018). Numerical Study of Downdraft Gasifier. *International Journal of Innovative Research in Technology*, *5*(2).

Sharma P. K., Sharma A. K., et al. (2020). Performance analysis of a medium-scale downdraft gasifier using Lantana camera biomass as feeding material. *Energy Sources, Part A: Recovery, Utilization, and Environmental Effects*, 1-15. https://doi.org/10.1080/15567036.2020.1809565

Sheth P. N., and Babu B. (2009). Experimental studies on producer gas generation from wood waste in a downdraft biomass gasifier. *Bioresource technology*, *100*(12), 3127-3133. https://doi.org/10.1016/j.biortech.2009.01.024

Shin D., Francis A., et al. (2022). Numerical Evaluation of Biochar Production Performance of Downdraft Gasifier by Thermodynamic Model. *Energies*, *15*(20). https://doi.org/10.3390/en15207650

Sikarwar V. S., and Zhao M. (2017). Biomass Gasification. In M. A. Abraham (Ed.), *Encyclopedia of Sustainable Technologies* (pp. 205-216). Elsevier. https://doi.org/10.1016/B978-0-12-409548-9.10533-0

Sikarwar V. S., Zhao M., et al. (2016). An overview of advances in biomass gasification. *Energy & Environmental Science*. https://doi.org/10.1039/C6EE00935B

Silva I. P., Lima R. M. A., et al. (2019). Thermodynamic equilibrium model based on stoichiometric method for biomass gasification: A review of model modifications. *Renewable and sustainable energy reviews*, *114*, 109305. https://doi.org/10.1016/j.rser.2019.109305

Singh V. C. J., Sekhar S. J., et al. (2014). Performance studies on downdraft gasifier with biomass energy sources available in remote villages. *American Journal of Applied Sciences*, *11*(4), 611. https://doi.org/10.3844/ajassp.2014.611.622

Singla M., Singh M., et al. (2020). Experimental investigation of imbert downdraft gasifier using rice straw briquettes. *Energy Sources, Part A: Recovery, Utilization, and Environmental Effects*, 1-11. https://doi.org/10.1080/15567036.2020.1771478

Sittisun P., Tippayawong N., et al. (2019). Biomass gasification in a fixed bed downdraft reactor with oxygen enriched air: a modified equilibrium modeling study. *Energy Procedia*, *160*, 317-323. https://doi.org/10.1016/j.egypro.2019.02.163

Sivabalan K., Hassan S., et al. (2021). A review on the characteristic of biomass and classification of bioenergy through direct combustion and gasification as an alternative power supply. *Journal of Physics: Conference Series*, *1831*(1), 012033. https://doi.org/10.1088/1742-6596/1831/1/012033

Smith J. D., Alembath A., et al. (2019). Validation and Application of a Kinetic Model for Downdraft Biomass Gasification Simulation. *Chemical Engineering & Technology*, *42*(12), 2505-2519. https://doi.org/10.1002/ceat.201900304

Stelte W., Sanadi A. R., et al. (2012). Recent developments in biomass pelletization – A review. *BioResources*. https://doi.org/10.15376/BIORES.7.3.4451-4490

Susastriawan A. A. P., Saptoadi H., et al. (2019). Comparison of the gasification performance in the downdraft fixed-bed gasifier fed by different feedstocks: Rice husk, sawdust, and their mixture. *Sustainable Energy Technologies and Assessments*, *34*, 27-34. https://doi.org/10.1016/j.seta.2019.04.008

Tiruye G. A., Besha A. T., et al. (2021). Opportunities and challenges of renewable energy production in Ethiopia. *Sustainability*, *13*(18), 10381. https://doi.org/10.3390/su131810381

Tumuluru J. S. (2018). Effect of pellet die diameter on density and durability of pellets made from high moisture woody and herbaceous biomass. *Carbon Resources Conversion*, *1*(1), 44-54. https://doi.org/10.1016/j.crcon.2018.06.002

Upadhyay D. S., Sakhiya A. K., et al. (2019). Effect of equivalence ratio on the performance of the downdraft gasifier – An experimental and modelling approach. *Energy*, *168*, 833-846. https://doi.org/10.1016/j.energy.2018.11.133

Van der Drift A., Boerrigter H., et al. (2004). *Entrained flow gasification of biomass. Ash behaviour, feeding issues, system analyses*.

Venselaar J. (1982). 'Design rules for downdraft wood gasifiers: A short review. *Joint Technical Assistance Project, JTA-9A-Research Development1 at the Institut Teknologi Bandung, Indonesia*, 1-24.

Waldheim L., and Nilsson T. (2001). Heating value of gases from biomass gasification. *Report prepared for: IEA bioenergy agreement, Task*, *20*.

Wilhelm D. J., Simbeck D. R., et al. (2001). Syngas production for gas-to-liquids applications: technologies, issues and outlook. *Fuel Processing Technology*, *71*(1), 139-148. https://doi.org/10.1016/S0378-3820(01)00140-0

Wiyono A., Gandidi I. M., et al. (2020). Design, development and testing of integrated downdraft gasifier and multi IGCS system of MSW for remote areas. *Case Studies in Thermal Engineering*, *20*, 100612. https://doi.org/10.1016/j.csite.2020.100612

Yan Q., Meng Z., et al. (2021). Experimental study on improving the properties of rock wool and glass wool by silica aerogel. *Energy and Buildings*, *247*, 111146. https://doi.org/10.1016/j.enbuild.2021.111146

Yousef S., Eimontas J., et al. (2021). Pyrolysis and gasification kinetic behavior of mango seed shells using TG-FTIR-GC–MS system under N_2 and CO_2 atmospheres. *Renewable energy*, *173*, 733-749. https://doi.org/10.1016/j.renene.2021.04.034

Zaimes G. G., Soratana K., et al. (2015). Biofuels via Fast Pyrolysis of Perennial Grasses: A Life Cycle Evaluation of Energy Consumption and Greenhouse Gas Emissions. *Environmental Science & Technology*, *49*(16), 10007-10018. https://doi.org/10.1021/acs.est.5b00129

Zainal Z. A., Ali R., et al. (2001). Prediction of performance of a downdraft gasifier using equilibrium modeling for different biomass materials. *Energy Conversion and Management*, *42*(12), 1499-1515. https://doi.org/10.1016/S0196-8904(00)00078-9

Zhang L., Xu C., et al. (2010). Overview of recent advances in thermo-chemical conversion of biomass. *Energy Conversion and Management*, *51*(5), 969-982. https://doi.org/10.1016/j.enconman.2009.11.038

APPENDICES

Appendix A: Empirical formula of MSH and PS

The empirical formula for MSH and the PS was first computed based on their ultimate analysis from Table 4.4. The empirical formula for the MSH and PS can be calculated as follows, as shown in Tables A-1 and A-2. Utilizing mass percentages obtained through elemental analysis, the molar composition was computed by dividing each mass percentage by the component's atomic weight. To make stoichiometric calculation more convenient, it is crucial to normalize the result with regard to carbon.

Table A-1. Empirical formula calculation of MSH

Element	$\boldsymbol{Wt}\%$	$\frac{\boldsymbol{Wt}\%}{\boldsymbol{molecular\ weight}}$	**Normalized to C**	**Subscript (a,b,c)**
C	47.93	$47.93/12$	$3.994167/3.994167$	1
H	6.06	$6.06/1$	$6.06/3.994167$	1.517
O	43.84	$43.84/16$	$2.74/3.994167$	0.686
N	0.50	$0.50/14$	$0.0357/3.994167$	0.0089

Table A-2. Empirical formula calculation of PS

Element	$\boldsymbol{Wt}\%$	$\frac{\boldsymbol{Wt}\%}{\boldsymbol{molecular\ weight}}$	**Normalized to C**	**Subscript (a,b,c)**
C	46.42	$46.42/12$	$3.8683/3.8683$	1
H	6.61	$6.61/1$	$6.06/3.8683$	1.566
O	41.77	$41.77/16$	$2.6106/3.8683$	0.675
N	0.50	$0.50/14$	$0.0357/3.8683$	0.0092

The general chemical formula for the MSH and PS used was $CH_aO_bN_c$ and substituting the calculated values from Table A-1 and Table A-2, yields $CH_{\mathbf{1.517}}O_{\mathbf{0.686}}N_{\mathbf{0.0089}}$ and $CH_{\mathbf{1.566}}O_{\mathbf{0.675}}N_{\mathbf{0.0092}}$ respectively.

Appendix B: Proximate analysis of MSH and PS

The proximate analysis of both biomass samples choosen for the study was conducted in geochemical laboratory desk of Geological Institute of Ethiopia as depicted in Figure B-1 and Figure B-2.

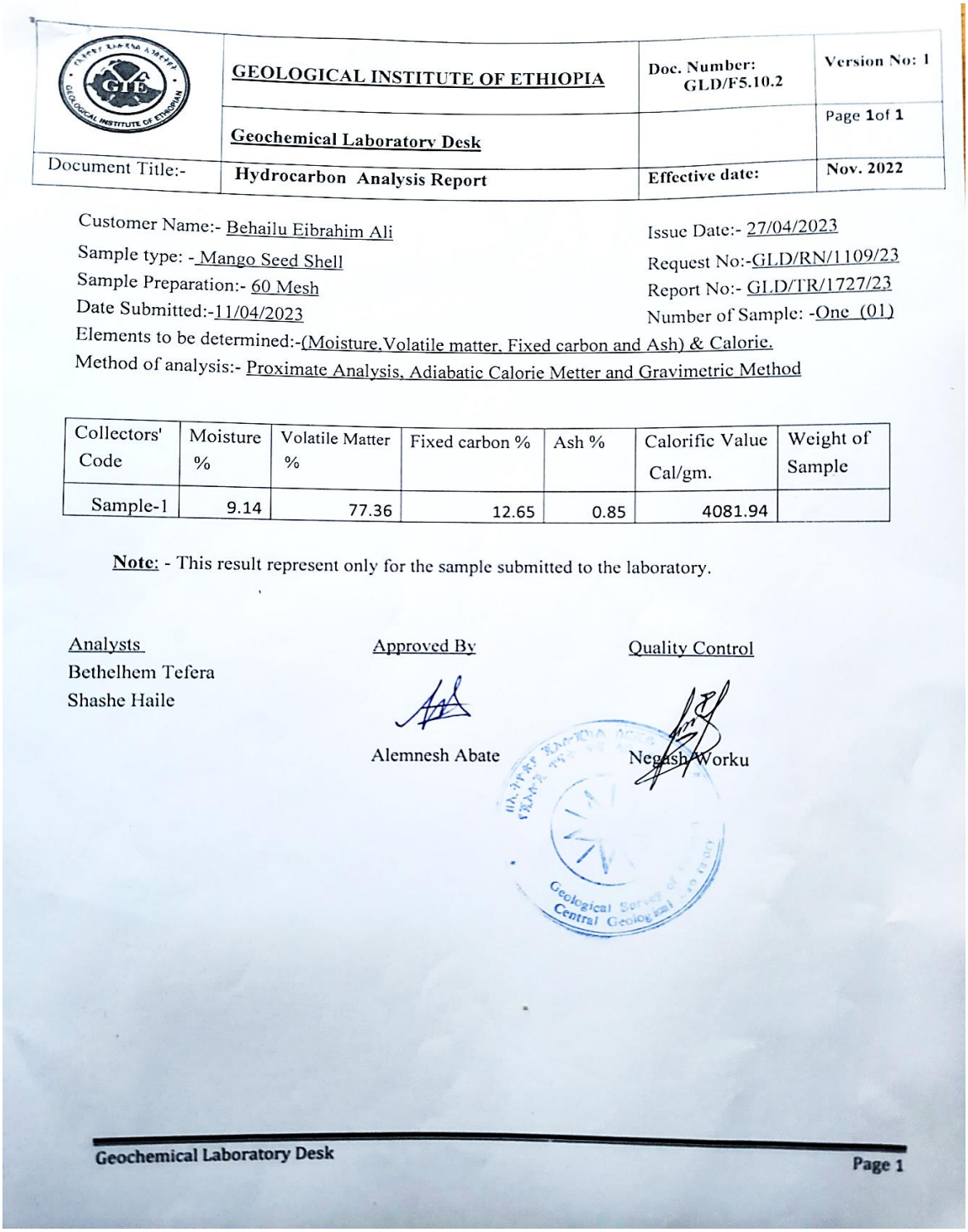

GEOLOGICAL INSTITUTE OF ETHIOPIA	Doc. Number: GLD/F5.10.2	Version No: 1
Geochemical Laboratory Desk		Page 1of 1
Document Title:- Hydrocarbon Analysis Report	Effective date:	Nov. 2022

Customer Name:- Behailu Eibrahim Ali
Issue Date:- 27/04/2023
Sample type: - Mango Seed Shell
Request No:-GLD/RN/1109/23
Sample Preparation:- 60 Mesh
Report No:- GLD/TR/1727/23
Date Submitted:-11/04/2023
Number of Sample: -One (01)
Elements to be determined:-(Moisture,Volatile matter, Fixed carbon and Ash) & Calorie.
Method of analysis:- Proximate Analysis, Adiabatic Calorie Metter and Gravimetric Method

Collectors' Code	Moisture %	Volatile Matter %	Fixed carbon %	Ash %	Calorific Value Cal/gm.	Weight of Sample
Sample-1	9.14	77.36	12.65	0.85	4081.94	

Note: - This result represent only for the sample submitted to the laboratory.

Analysts
Bethelhem Tefera
Shashe Haile

Approved By
Alemnesh Abate

Quality Control
Negash Worku

Geochemical Laboratory Desk Page 1

Figure B-1. Proximate analysis of MSH

	GEOLOGICAL INSTITUTE OF ETHIOPIA	Doc. Number: GLD/F5.10.2	Version No: 1
	Geochemical Laboratory Desk		Page 1of 1
Document Title:-	Hydrocarbon Analysis Report	Effective date:	Nov. 2022

Customer Name:- Behailu Eibrahim Ali
Issue Date:- 27/04/2023
Sample type: - Peanut Shell (Graund nut)
Request No:-GLD/RN/1110/23
Sample Preparation:- 60 Mesh
Report No:- GLD/TR/1728/23
Date Submitted:-11/04/2023
Number of Sample: -One (01)
Elements to be determined:-(Moisture,Volatile matter, Fixed carbon and Ash) & Calorie .
Method of analysis:- Proximate Analysis, Adiabatic Calorie Metter and Gravimetric Method

Collectors' Code	Moisture %	Volatile Matter %	Fixed carbon %	Ash %	Calorific Value Cal/gm.	Weight of Sample
Sample-2	9.23	67.72	18.24	4.81	4116.04	

Note: - This result represent only for the sample submitted to the laboratory.

Analysts
Bethelhem Tefera
Shashe Haile

Approved By
Alemnesh Abate

Quality Control
Negash Worku

Geological Survey of Ethiopia Central Geological Lab

Figure B-2. Proximate analysis of PS

NCV of the fuel or LHV_{fuel} can be calculated using equation (B.1) by taking the data of MC, hydrogen content and also HHV or GCV from the characterization of the fuel (Obernberger & Thek, 2004; Ozturk & Dincer, 2018)

$$NCV = GCV(1 - MC) - 2.444MC - 21.839H(1 - MC) \quad \text{(B.1)}$$

Where:

NCV is net calorific value MJ/Kg (w.b)

GCV is net calorific value MJ/Kg (d.b)

MC , the water content in wt% (w.b)

H , the hydrogen content in wt% (d.b)

Appendix C: Biomass preparation and pretreatment

The biomasses selected for the study were handled differently based their nature and size.

I. Mango seed hull or Mango seed shell

The mango seeds for the current study were gathered from a local fresh fruit juice shop in Adama city. Due to the enormous amounts of mango waste created, the drying process which is frequently performed in laboratory studies utilizing ovens, is challenging to do and also consumes a huge amount of energy. As a result, drying in the sun is thought to be one of the most effective and energy-efficient drying techniques. Furthermore, the biomass type used for the study is devoid of dangerous elements that can escape into the atmosphere during drying. The MSH preparation procedure is depicted in Figure C-1.

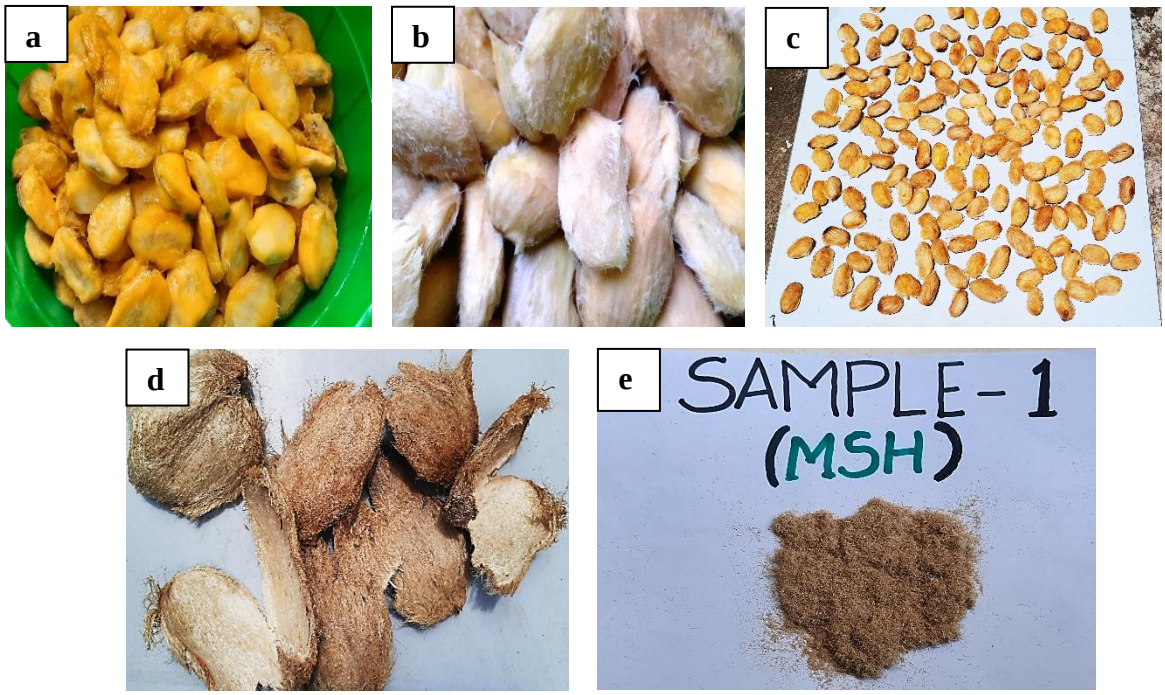

Figure C-1. MSH preparation, (a) mango stones to be washed, (b) washed mango stones (c) sun drying the mango stones, (d) liberated MSH, (e) milled MSH

The seeds were removed from extra mango skin, gently rinsed in water, and then allowed to dry in the sun for 48 hours. After the drying was done, using the proper mechanical equipment, the seed shells and kernel were separated (Yousef et al., 2021). Moreover, the liberated shells were ground using a coffee bean grinder and sieved into small particles in order to reduce the size of the liberated shells and reduce heat transfer resistance during sample testing. However, for the experiment only size reduction was done because it was difficult to change the MSH into powdered form due to its fiber like structure.

II. Peanut shell

The peanut shells were procured from the neighborhood market in Adama city and, it was cleaned of any contaminants. After sun drying, a feed grinder was used to pulverize the shells into small particles, which was then be sieved. Then, the sample was made into tiny pallets using screw press pelletizer. The PS preparation procedure is shown in Figure C-2.

Figure C-2. PS preparation (a) sun drying (b) dried and cleaned PS (c) sieving (d) milled PS (e) PS palettes

Appendix D: Measuring instruments used to measure different parameters

Weighting scale

Glass and digital thermometer

Four channel K-type thermocouple sensor

Anemometer

Exhaust gas analyser

Figure D-1. Measuring instruments

Appendix E: Data tables for different calculations and graphs

These tables serve as samples; additional data is available but requires more pages.

Table E-1. The value of h_f° and coefficients of the empirical equation for $\Delta g_{f,T,i}^\circ$ (Jarungthammachote & Dutta, 2007)

Gas	h_f° (kJ/mol)	a (10^{-3})	b (10^{-6})	c (10^{-9})	d (10^{-12})	e (10^{2})	f	g (10^{-2})
CO	-110.53	5.619	-11.9	6.383	-1.846	-4.891	0.8684	-6.131
CO_2	-393.52	-19.49	31.122	-24.48	6.946	-4.891	5.270	-12.07
H_2	-241.82	-8.95	-3.672	5.209	-1.478	0	2.868	-1.722
CH_4	-74.85	-4.62	11.3	13.19	-6.647	-4.891	14.11	-22.34

Table E-2. Constant pressure specific heat ideal gas temperature relations (Karamarkovic & Karamarkovic, 2010)

Gas	$C_{p,i}\left(\frac{kJ}{kmol}\right), \phi = \frac{T}{100}$	Range (K)	Max. Error (%)
CO	$69.145 - 0.70463(\phi)^{0.75} - 200.77(\phi)^{-0.5} + 176.76(\phi)^{-0.75}$	300-3500	0.42
CO_2	$-3.7359 - 30.529(\phi)^{0.5} - 4.1034(\phi)^{1} + 0.024198(\phi)^{2}$	300-3500	0.19
CH_4	$-672.87 + 439.74(\phi)^{0.25} - 24.875(\phi)^{0.75} + 323.88(\phi)^{-0.5}$	300-2000	0.15
N_2	$39.06 - 512.79(\phi)^{-1.5} + 1072.7(\phi)^{-2} - 820.4(\phi)^{-3}$	300-3500	0.43
H_2	$56.505 - 702.74(\phi)^{-0.75} + 1165(\phi)^{-1} - 560.70(\phi)^{-1.5}$	300-3500	0.60
O_2	$37.432 + 0.020102(\phi)^{1.5} - 178.57(\phi)^{-1.5} + 236.88(\phi)^{-2}$	300-3500	0.30
H_2O	$143.05 - 183.54(\phi)^{0.25} + 82.751(\phi)^{0.5} - 3.6989(\phi)^{1}$	300-3500	0.43

Table E-3. PG composition in volume fraction and LHV for MSH, dry basis, against ER

ER	CH_4	CO_2	CO	H_2	N_2	LHV (MJ/Nm^3)
0.26	0.003117	0.0774	0.2858	0.262	0.3717	6.546
0.28	0.00283	0.08387	0.2716	0.2502	0.3914	6.23
0.30	0.002569	0.09005	0.2581	0.239	0.4103	5.928
0.32	0.002331	0.09594	0.2451	0.2281	0.4285	5.639
0.34	0.002113	0.1016	0.2327	0.2177	0.4459	5.362
0.36	0.001914	0.107	0.2208	0.2076	0.4627	5.096
0.38	0.001732	0.1121	0.2095	0.1979	0.4788	4.841
0.40	0.001565	0.1171	0.1985	0.1885	0.4943	4.596

Table E-4. PG composition in volume fraction and LHV for PS, dry basis, against ER

ER	CH_4	CO_2	CO	H_2	N_2	LHV (MJ/Nm^3)
0.26	0.00381	0.09995	0.237	0.2957	0.3635	6.318
0.28	0.00347	0.1047	0.2256	0.2828	0.3834	6.023
0.3	0.00316	0.1093	0.2147	0.2703	0.4025	5.739
0.32	0.00287	0.1137	0.2043	0.2583	0.4209	5.467
0.34	0.00261	0.1179	0.1942	0.2467	0.4386	5.206
0.36	0.00236	0.1219	0.1846	0.2355	0.4557	4.955
0.38	0.00214	0.1258	0.1753	0.2246	0.4721	4.713
0.4	0.00194	0.1295	0.1664	0.2141	0.488	4.48

Table E-5. PG composition in volume fraction and LHV for MSH, dry basis, against MC

MC	CH_4	CO_2	CO	H_2	N_2	LHV (MJ/Nm^3)
5	0.0024	0.0804	0.2713	0.2313	0.4144	6.008
10	0.0026	0.0920	0.2553	0.2406	0.4095	5.911
15	0.0028	0.1036	0.2394	0.2497	0.4045	5.815
20	0.0029	0.1151	0.2236	0.2589	0.3996	5.719
25	0.0030	0.1264	0.2079	0.2680	0.3947	5.623
30	0.0032	0.1377	0.1923	0.2770	0.3898	5.529
35	0.0033	0.1489	0.1769	0.2860	0.3850	5.435
40	0.0034	0.1599	0.1617	0.2949	0.3802	5.342

Table E-6. PG composition in volume fraction and LHV for PS, dry basis, against MC

MC	CH_4	CO_2	CO	H_2	N_2	LHV (MJ/Nm^3)
5	0.0027	0.0775	0.2580	0.2456	0.4161	6.004
10	0.0029	0.0881	0.2436	0.2538	0.4116	5.916
15	0.0030	0.0987	0.2292	0.2621	0.4070	5.828
20	0.0032	0.1093	0.2147	0.2703	0.4025	5.739
25	0.0033	0.1199	0.2003	0.2786	0.3979	5.651
30	0.0034	0.1304	0.1860	0.2869	0.3934	5.563
35	0.0035	0.1409	0.1717	0.2951	0.3888	5.475
40	0.0036	0.1513	0.1575	0.3034	0.3843	5.387

Table E-7. The value of syngas LHV for MSH and PS at various ER, MC an GT

ER	LHV (MJ/Nm^3)		MC	LHV(MJ/Nm^3)		GT (K)	LHV(MJ/Nm^3)	
	MSH	**PS**		**MSH**	**PS**		**MSH**	**PS**
0.26	6.546	6.318	5	6.01	6.004	973	5.858	6.241
0.28	6.23	6.023	10	5.91	5.916	1073	5.928	6.318
0.30	5.928	5.739	15	5.82	5.828	1173	5.991	6.393
0.32	5.639	5.467	20	5.72	5.739	1273	6.043	6.457
0.34	5.362	5.206	25	5.62	5.651	1373	6.085	6.509
0.36	5.096	4.955	30	5.53	5.563	1473	6.118	6.549
0.38	4.841	4.713	35	5.44	5.475			
0.40	4.596	4.48	40	5.34	5.387			

Table E-8. Variation of temperature with time for MSH using atmospheric

		Zone temperature (℃)					
		T_1	**T_2**	**T_3**	**T_4**	**T_5**	**T_6**
	0	28.4	28.8	27.5	31.6	29.3	33.1
	5	164.8	211.4	304.1	405.2	356.5	208.4
	10	189.5	234.3	338.2	512.3	411.9	223.4
	15	219.1	262.5	375.9	584.1	493.8	245.9
	20	229.8	288.3	411.7	633.9	522.9	288.1
	25	238.4	312.5	437.8	712.5	578.3	315.8
Time (min)	**30**	249.7	345.6	452.9	745.3	612.8	339.4
	35	257.3	389.2	477.5	760.2	643	368.4
	40	269.1	397.8	498.7	802.3	689.1	385.4
	45	278.4	422.5	518.4	857.8	722.3	394.2
	50	285.2	461.3	532.3	891.1	755.7	408.6
	55	291.7	478.4	546.9	912.3	781.6	422.7
	60	298.8	493.7	561.2	928.1	803.7	435.3

Table E-9. Variation of temperature with time for MSH using pressurized air

		Zone temperature (℃)					
		T_1	**T_2**	**T_3**	**T_4**	**T_5**	**T_6**
	0	27.3	27.3	27.7	29.9	29.5	28.2
	5	185.3	231.7	317.2	415.9	376.3	228.5
	10	192.7	234.3	342.2	532.3	429.5	242.4
	15	225.8	278.5	385.9	597.9	499.3	254.7
	20	239.7	298.3	432.6	645.9	527.4	296.1
	25	248.3	319.7	444.3	728.9	581.6	332.8
Time (min)	**30**	257.3	355.6	463.7	738.3	633.9	349.5
	35	274.5	376.2	487.1	801.2	667.8	375.3
	40	274.5	399.5	502.8	818.4	697.3	389.4
	45	288.2	427.8	523.5	871.3	729.5	398.7
	50	295.2	458.9	545.3	899.2	767.4	413.5
	55	302.6	483.7	559.4	917.8	793.5	431.7
	60	312.6	501.3	597.2	957.5	812.8	473.9

Appendix F: Calibration of thermocouple

Thermocouples must be calibrated with a standard thermocouple in order to ensure the accuracy of the temperature measurement. As shown in Figure F-1, with standard thermocouples found in a thermal engineering laboratory of ASTU, a calibration test for a four-channel K-type digital thermocouple was carried out using a 15-minute boiling test of one kilogram of water.

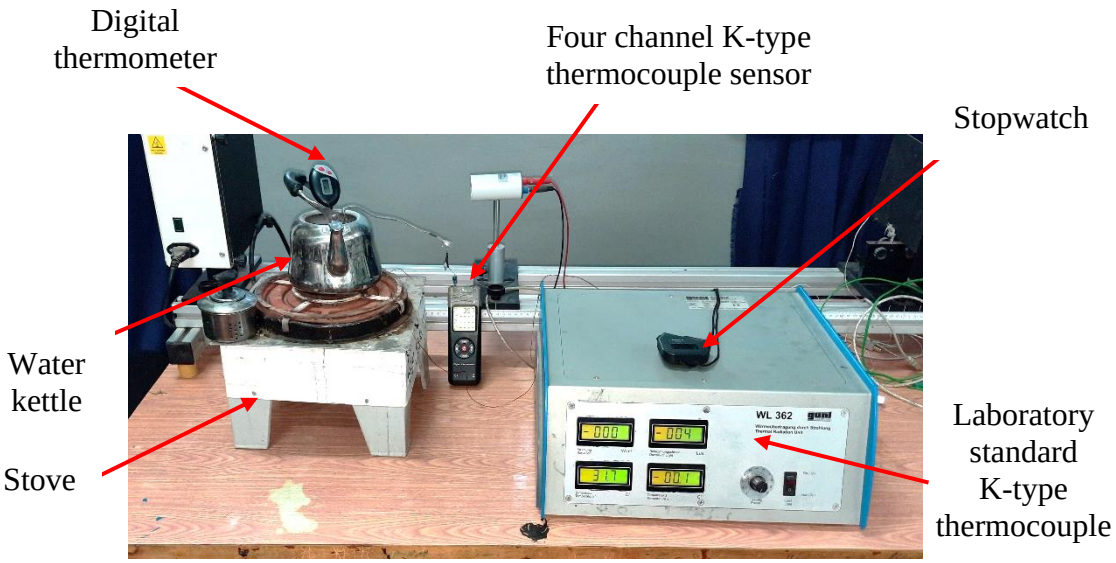

Figure F-1. Calibration setup with standard and K-type thermocouples

In Table F-1, the data collected during calibration with the aid of a standard thermocouple and a K-type thermocouple are shown together with the degree of measurement uncertainty.

Table F-1. Water temperature measuring test by using K-type thermocouples

Time (min)	T_{wt_1} **(Standard thermocouple)**	T_{wt_2} **(Four channel K-type thermocouple)**	**Uncertainty (%)** $[\frac{T_{wt_1} - T_{wt_2}}{T_{wt_1}}] x\ 100$
1	33.3	33.1	0.60
3	44.6	44.3	0.67
5	52.6	52.2	0.76
7	59.5	59.3	0.34
9	68	67.7	0.44
11	76.8	76.4	0.52
13	86.9	86.7	0.23
15	96.3	95.9	0.42

Where:

T_{wt}, water temperature

In Figure F-2, the measured temperature is drawn against the line of the corrected temperature linear equation which was obtained by curve fitting technique from the data Table F-1. To show the strength of data correlation R^2 was calculated.

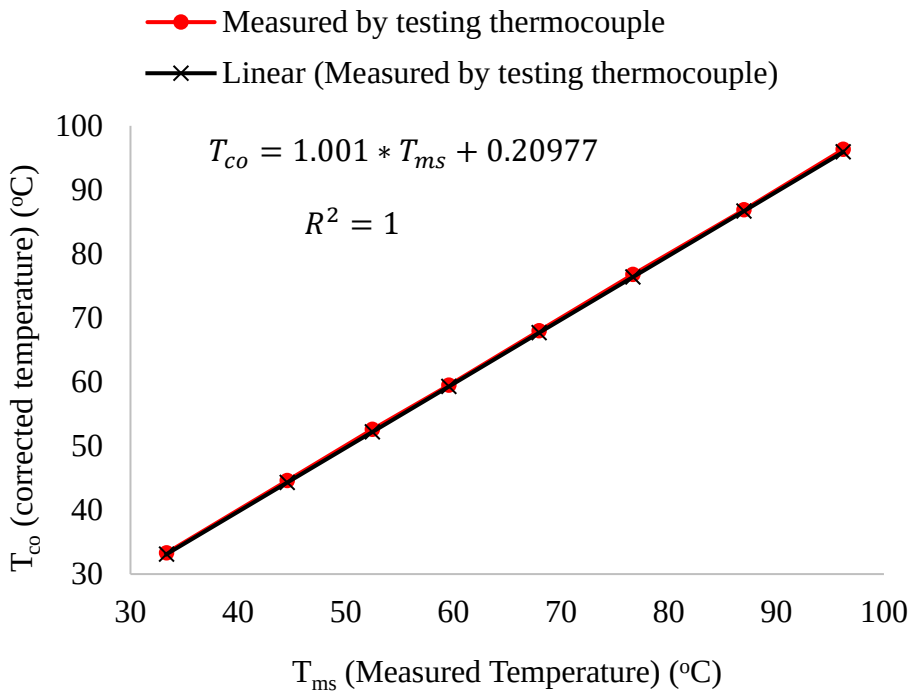

Figure F-2. Measured temperature versus corrected temperature

K-type thermocouples were used to measure the temperatures in the different zones of the gasifier and the producer gas line. According to it specification, the accuracy of the Four channel K-type digital or thermometer is $\pm$ 0.1 °C. The experimentally determined lowest temperature is 27 $°C$. The ratio between the least count and minimum temperature measured indicates the degree to which the temperature measurement was inaccurate. Therefore, the maximum possible error is $0.1/27 = 0.0037$. Thus, the percentage error can be identified as

$$\% \, error = 0.0037 \times 100 = 0.37\%$$

A digital thermometer was also used to measure both the ambient temperature and the char temperature that resulted from the gasification process. With a $\pm$ 0.1 °C accuracy, the temperature measurement range is from -50 to + 300 $°C$. The experimentally determined lowest temperature is 27 $°C$. Therefore, the maximum possible error is $0.1/27 = 0.0037$. and $\% \, error = 0.0037 \times 100 = 0.37\%$.

Appendix G: Specification of the fan and compressor used

The specification of the fan and compressor utilized for the gasification system is illustrated in Table G-1 and G-2 with their corresponding picture in Figure G-1 and G-2 respectively.

Table G-1. Specification of the fan utilized for the gasifier

Model No.	Frequency (Hz)	Air (cfm)	Volume (m^3/min)	Current (A)	Power (W)	Speed (rpm)
FP-108EX (S-1)	50	190	5.40	0.2	38	2800

Figure G-1. Suction fan utilized for the gasifier

Table G-2. Specification of the air compressor utilized for the gasifier

Model No.	Pressure (Mpa)	Motor (kW)	Capacity (l/min)	Tank cap. (l)
MY 2065/8	0.8	2.2	250	100

Figure G-2. Air compressor utilized for the gasifier

Appendix H: Gasifier manufacturing cost

Table H-1, displays the total cost of the materials needed to manufacture the various components of the throated downdraft gasifier system.

Table H-1. Manufacturing cost of the gasification system

No	Item	Unit	Quantity	Unit price (ETB)	Total price (ETB)
1	Mild steel sheet	Meter	$1x2$	2500.00	2500.00
2	Mild steel hollow rectangular bar	Meter	2.5	500.00	1250.00
3	Galvanized pipe	Meter	3	700.00	2100.00
4	Suction fan	Quantity	1	6000.00	6000.00
5	Welding	Days	10	300.00	3000.00
	Subtotal (ETB)				**14850.00**
6	Operating and maintenance cost (10 % of investment cost)				1485.00
			Total (ETB)		**16335.00**

Appendix I: Code for the stoichiometric equilibrium model

```
"This code is developed for the performance evaluation of gasification system under various process parameters"
"GENERAL PARAMETERS"
R= 8.314472e-3 [kJ/mol-K] " Universal gas constant"
h_fg=44.011[MJ/kmol] " Enthalpy of vaporization of water"
V_m=22.414 [Nm^3/kmol] "Molar volume of an ideal gas at normal conditions of pressure and temperature (101.325 kPa, 273.15K)"
T_amb=298.15 [K] "25 degree Celsius"
T_gas=1073 [K] "Gasification temperature 800-degree Celsius"
P_atm=0.101[MPa] "1 atm pressure"
H_vap = 2260 [kJ/kg] " Heat of vaporization of water"
"INPUT PARAMETERS"
"Fuel formulation: C-H_a-O_b-N_c "
"General fuel properties"
```

```
Qm_fuel=0.001255 "Feed rate, kg daf/s ,  daf= dry ash free"
Q_fuel= Qm_fuel/M_fuel"Feed rate, kmol/s"
M_fuel=MolarMass('C')+(sub_h) * MolarMass('H') +(sub_o) *
MolarMass('O')
"Insert the data of ultimate analysis, proximate analysis,
and heating value of the biomass fuel"
C = 47.93 " wt% dry basis, NO daf"
H = 6.06 " wt% dry basis, NO daf"
O = 43.84  " wt% dry basis, NO daf"
N = 0.50  " wt% dry basis, NO daf"
Other = 0.54  " wt% dry basis, NO daf"
Ash = 0.69  " Ash, wt% dry basis"
GCV = 17.079 [MJ/kg]"Gross Calorific Value"
MC= 0.2 "Moisture content, wt% wet"
sum= C+H+O+N+Other+Ash
C_1= C*(100/(C+H+O+N)) " wt% dry basis,daf"
H_1= H*(100/(C+H+O+N)) "wt% dry basis,daf"
O_1= O*(100/(C+H+O+N)) " wt% dry basis,daf"
N_1= N*(100/(C+H+O+N))" wt% dry basis,daf"
sum_1=C_1+H_1+O_1+ N_1
sub_h=(H_1/MolarMass('H'))/(C_1/MolarMass('C')) "Number of
atoms of H per a single atom of C"
sub_o=(O_1/MolarMass('O'))/(C_1/MolarMass('C')) "Number of
atoms of O per a single atom of C"
sub_n=(N_1/MolarMass('N'))/(C_1/MolarMass('C')) "Number of
atoms of N per a single atom of C"
"MASS BALANCE
<<<<Gasification reaction>>>>>
CH[a]O[b]N[c] + mH[2]O + nO_2 + 3.76n*N_2 = (1-alpha) C+
x_a*H_2+ x_b*CO + x_c*CO_2 + x_d*H[2]O + x_e*CH_4 + 3.76nN_2
where
x_a ,x_b ,x_c ,x_d ,x_e and (1-alpha) are moles of the
components in the reaction
w, molar quantity of water
```

```
n, oxygen per mole of feedstock"
ER= 0.3 "Ranges for the study 0.26-0.4"
alpha= 1
"alpha= 0.32+0.84*(1-exp((-ER/0.229)))" "Carbon conversion
factor"
n_AO= ER*(1+sub_h/4-sub_o/2) "From the gasification reaction
a=sub_h , b=sub_o "
m = (MC*(12+sub_h+16*sub_o))/(18*(1-MC)) "m, molar quantity
of water"
w =(M_fuel*MC)/(MolarMass('water')*(1-MC)) "w, molar
quantity of water"
"The balanced equation of the components in the reaction are
determined:"
"For carbon"
 x_b+x_c+x_e= alpha
"For Hydrogen"
2*m+sub_h=2*x_a+2*x_d+4*x_e
"For Oxygen"
 m+sub_o+2*n_AO=x_b+2*x_c+x_d
"For Nitrogen"
x_N_g=sub_n/2 + 3.76*n_AO
"where"
x_t=x_a+x_b+x_c+x_d+x_e
x_t_dry=x_a+x_b+x_c+x_e
x_gas= x_t+ x_N_g
x_gas_dry = x_t_dry + x_N_G
"EXIT STREAM"
Q_gas=x_gas*Q_fuel "Exit rate, kmol/s"
"Mole fraction in the product gas"
X_h2 = x_a/x_gas
X_co = x_b/x_gas
X_co2 = x_c/x_gas
X_h2o = x_d/x_gas
X_ch4 = x_e/x_gas
```

```
X_n2 = x_N_g/x_gas
"In the dry form"
X_h2_dry = x_a/x_gas_dry
X_co_dry = x_b/x_gas_dry
X_co2_dry = x_c/x_gas_dry
X_ch4_dry = x_e/x_gas_dry
X_n2_dry = x_N_g/x_gas_dry
"Volumic"
Qv_gas=Q_gas*V_m
V_h2 = x_a*V_m "Nm^3/kmol of fuel"
V_co = x_b*V_m
V_co2 = x_c*V_m
V_h2o = x_d*V_m
V_ch4 = x_e*V_m
V_n2 = x_N_g*V_m
V_gas=V_h2+ V_co+V_co2+V_h2o+V_ch4+V_n2 "Nm^3/kmol of fuel"
V_gas_dry= V_co+V_co2+V_ch4+V_h2+V_n2
VF_h2=V_h2/V_gas
VF_co=V_co/V_gas
VF_co2=V_co2/V_gas
VF_h2o=V_h2o/V_gas
VF_ch4=V_ch4/V_gas
VF_n2=V_n2/V_gas
"In the dry form"
VF_co_dry=V_co/V_gas_dry
VF_co2_dry=V_co2/V_gas_dry
VF_ch4_dry=V_ch4/V_gas_dry
VF_h2_dry=V_h2/V_gas_dry
VF_n2_dry=V_n2/V_gas_dry
"Lower and higher heating value of the biomass"
NCV = GCV *(1-MC)-2.44*MC-21.839*H*(1-MC)/100 [MJ/kg] "If
heating value and ultimate analysis data is available"
```

```
LHV_biomass =
(0.0041868+0.00062801*O*(7837.667*C+33888.889*H-
0.125*O))/1000 "In MJ/Nm^3"
HHV= 0.3491*C+1.1783*H+0.1005*Other-0.1034*O-0.0151*N-
0.0211*Ash
LHV = HHV -9*((H_1/sum_1)*(h_fg/(MolarMass('water')))) "h_fg
should be in MJ/kmol for the same unit"
"THERMODYNAMIC EQUILIBRIUM"
"Equilibrium reaction with equilibrium constants k[1] and
k[2]"
"Methane formation, endothermic reaction, C+2H[2]= CH[4]"
DELTAG_T_1=DELTAg_f_T_ch4
K[1]=exp(-DELTAG_T_1/(R*T_gas))
K[1]=( x_ch4)/(x_h2)^2
"K[1]=(x_b*x_a^3)/(x_e*x_d)"
"Water gas shift, exothermic reaction, CO+H[2]O=CO[2]+H[2]"
DELTAG_T_2=DELTAg_f_T_co2-DELTAg_f_T_co-DELTAg_f_T_h2o
K[2]=exp(-DELTAG_T_2/(R*T_gas))
K[2]=(x_co2*x_h2)/(x_h2o*X_co)
"Standard Gibbs function of formation at temperature T[gas]
,kJ/mol"
"For CO"
h_f_co= -110.5   [kJ/mol]
a_co=5.619e-3
b_co=-1.19e-5
c_co=6.383e-9
d_co=-1.846e-12
e_co=-4.891e2
f_co=8.684e-1
g_co=-6.131e-2
DELTAg_f_T_co=h_f_co-a_co*T_gas*ln(T_gas)-b_co*T_gas^2-
c_co/2*T_gas^3-d_co/3*T_gas^4+e_co/(2*T_gas)+f_co+g_co*T_gas
"For CO[2]"
h_f_co2= -393.5   [kJ/mol]
```

```
a_co2=-1.942e-2
b_co2=3.122e-5
c_co2=-2.248e-8
d_co2=6.946e-12
e_co2=-4.891e2
f_co2=5.27
g_co2=-1.207e-1
DELTAg_f_T_co2=h_f_co2-a_co2*T_gas*ln(T_gas)-b_co2*T_gas^2-
c_co2/2*T_gas^3-
d_co2/3*T_gas^4+e_co2/(2*T_gas)+f_co2+g_co2*T_gas
"For H[2]O"
h_f_h2o= -241.8   [kJ/mol]
a_h2o=-8.95e-3
b_h2o=-3.672e-6
c_h2o=5.209e-9
d_h2o=-1.478e-12
e_h2o=0
f_h2o=2.868
g_h2o=-1.722e-2
DELTAg_f_T_h2o=h_f_h2o-a_h2o*T_gas*ln(T_gas)-b_h2o*T_gas^2-
c_h2o/2*T_gas^3-d_h2o/3*T_gas^4
+e_h2o/(2*T_gas)+f_h2o+g_h2o*T_gas
"For CH[4]"
h_f_ch4= -74.8   [kJ/mol]
a_ch4=-4.62e-2
b_ch4=1.13e-5
c_ch4=1.319e-8
d_ch4=-6.647e-12
e_ch4=-4.891e2
f_ch4=14.11
g_ch4=-2.234e-1
DELTAg_f_T_ch4=h_f_ch4-a_ch4*T_gas*ln(T_gas)-b_ch4*T_gas^2-
c_ch4/2*T_gas^3-
d_ch4/3*T_gas^4+e_ch4/(2*T_gas)+f_ch4+g_ch4*T_gas
```

"THERMODYNAMICS DATA"

"Let, CO=1, CO[2]=2, CH[4]=3, H[2]=4, N[2]=5, H[2]O(g)=6, O[2]=7, H[2]O(l)=8"

"Specific heat at constant pressure for ideal gas [300-3500 K], CH[4] [300-2000k] and heat capacity of solid carbon, kJ/(kmol.K)"

```
Cp[1]=69.145-0.70463*(T/100)^0.75-200.77*(T/100)^(-0.5)
+176.76*(T/100)^(-0.75)
Cp[2]= -3.7357+30.529*(T/100)^0.5-
4.1034*(T/100)+0.024198*(T/100)^2
Cp[3]= -672.87+439.74*(T/100)^0.25-
24.875*(T/100)^0.75+323.88*(T/100)^(-0.5)
Cp[4]= 56.505-702.74*(T/100)^(-0.75)+1165*(T/100)^(-1)-
560.7*(T/100)^(-1.5)
Cp[5]= 39.06- 512.79*(T/100)^(-1.5)+1072.7*(T/100)^(-2)-
820.4*(T/100)^(-3)
Cp[6]=143.05-183.54*(T/100)^0.25+82.751*(T/100)^0.5-
3.6989*(T/100)
Cp[7]= 37.432+0.020102*(T/100)^1.5-178.57*(T/100)^(-
1.5)+236.88*(T/100)^(-2)
Cp[8]= 143.05-183.54*(T/100)^0.25+82.751*(T/100)^0.5-
3.6989*(T/100)
```

"Enthalpy difference between T_amb and T_gas kJ/kmol"

```
DELTAh_T_1=integral(Cp[1],T,T_amb,T_gas)
DELTAh_T_2=integral(Cp[2],T,T_amb,T_gas)
DELTAh_T_3=integral(Cp[3],T,T_amb,T_gas)
DELTAh_T_4=integral(Cp[4],T,T_amb,T_gas)
DELTAh_T_5=integral(Cp[5],T,T_amb,T_gas)
DELTAh_T_6=integral(Cp[6],T,T_amb,T_gas)
DELTAh_T_7=integral(Cp[7],T,T_amb,T_gas)
DELTAh_Tp_8=integral(Cp[8],T,T_amb,T_gas)
```

"Molar specific enthalpy of formation , kJ/kmol, (T[amb=298] K, P[atm=0.1] MPa)"

```
h_0_1=-110.53e3   [kJ/kmol]
```

```
h_0_2=-393.52e3    [kJ/kmol]
h_0_3=-74.85e3     [kJ/kmol]
h_0_4=0            [kJ/kmol]
h_0_5=0            [kJ/kmol]
h_0_6=-241.82e3    [kJ/kmol]
h_0_7= 0           [kJ/kmol]
h_0_8= -285.83e3   [kJ/kmol]
"Enthalpy at T_gas and P_atm, kJ/kmol"
h_T_1=DELTAh_T_1+h_0_1
h_T_2=DELTAh_T_2+h_0_2
h_T_3=DELTAh_T_3+h_0_3
h_T_4=DELTAh_T_4+h_0_4
h_T_5=DELTAh_T_5+h_0_5
h_T_6=DELTAh_T_6+h_0_6
h_T_7=DELTAh_T_7+h_0_7
"Molar specific absolute , kJ/(kmol.K), (T[amb=298] K,
P[atm=0.1] MPa)"
S_0_1=197.65    [kJ/kmol-K]
S_0_2=213.8     [kJ/kmol-K]
S_0_3=186.16    [kJ/kmol-K]
S_0_4=130.68    [kJ/kmol-K]
S_0_5=191.61    [kJ/kmol-K]
S_0_6=188.83    [kJ/kmol-K]
S_0_7= 205.04   [kJ/kmol-K]
S_0_8= 69.92    [kJ/kmol-K]
"Entropy at T_gas and P_atm, kJ/(kmol.K)"
S_T_1=S_0_1+integral(Cp[1]/T,T,T_amb,T_gas)-R*10^3*ln(X_co)
S_T_2=S_0_2+integral(Cp[2]/T,T,T_amb,T_gas)-R*10^3*ln(X_co2)
S_T_3=S_0_3+integral(Cp[3]/T,T,T_amb,T_gas)-R*10^3*ln(X_ch4)
S_T_4=S_0_4+integral(Cp[4]/T,T,T_amb,T_gas)-R*10^3*ln(X_h2)
S_T_5=S_0_5+integral(Cp[5]/T,T,T_amb,T_gas)-R*10^3*ln(X_n2)
S_T_6=S_0_6+integral(Cp[6]/T,T,T_amb,T_gas)-R*10^3*ln(X_h2o)
"LOWER HEATING VALUE (LHV) ANALYSIS "
"Volumic LHV"
```

```
LHV_vol_h2 = 10.78 [MJ/Nm^3]
LHV_vol_ch4 = 35.88 [MJ/Nm^3]
LHV_vol_co = 12.63 [MJ/Nm^3]
LHV_vol_gas = VF_h2 * LHV_vol_h2 + VF_ch4 * LHV_vol_ch4 +
VF_co * LHV_vol_co
LHV_vol_gas_dry = VF_h2_dry * LHV_vol_h2 + VF_ch4_dry *
LHV_vol_ch4 + VF_co_dry * LHV_vol_co
"Molar LHV"
LHV_h2 = 241827 [kJ/kmol]
LHV_ch4 = 802303 [kJ/kmol]
LHV_co = 282993 [kJ/kmol]
LHV_gas = X_h2 * LHV_h2 + X_ch4 * LHV_ch4 + X_co * LHV_co
LHV_gas_dry = X_h2_dry * LHV_h2 + X_ch4_dry * LHV_ch4 +
X_co_dry * LHV_co
"EXERGY ANALYSIS"
"Producer gas exergy"
"Standard chemical exergy of syngas compounds, kJ/kmol,
(T[amb], P[atm]) "
e_0_ch_h2 = 238490 [kJ/kmol]
e_0_ch_co = 275430 [kJ/kmol]
e_0_ch_co2 = 20140 [kJ/kmol]
e_0_ch_h2o = 11710 [kJ/kmol]
e_0_ch_ch4 = 836510 [kJ/kmol]
e_0_ch_n2 = 720 [kJ/kmol]
"Chemical exergy, kJ/kmol"
exe_ch_h2 = (e_0_ch_h2 + R*T_amb * ln(x_h2)*10^3)*x_h2
exe_ch_co = (e_0_ch_co + R*T_amb * ln(x_co)*10^3)*x_co
exe_ch_co2 = (e_0_ch_co2 + R*T_amb * ln(x_co2)*10^3)*x_co2
exe_ch_h2o = (e_0_ch_h2o + R*T_amb * ln(x_h2o)*10^3)*x_h2o
exe_ch_ch4 = (e_0_ch_ch4 + R*T_amb * ln(x_ch4)*10^3)*x_ch4
exe_ch_n2 = (e_0_ch_n2 + R*T_amb * ln(x_n2)*10^3)*x_n2
"Total mixture chemical exergy, kJ/kmol"
exe_ch_gas = exe_ch_h2 + exe_ch_co + exe_ch_co2 + exe_ch_h2o
+ exe_ch_ch4 + exe_ch_n2
```

```
"Physical exergy, kJ/kmol"
exe_ph_co = (h_T_1-h_0_1-T_amb*(S_T_1-S_0_1))* x_co
exe_ph_co2 = (h_T_2-h_0_2-T_amb*(S_T_2-S_0_2))* x_co2
exe_ph_ch4 = (h_T_3-h_0_3-T_amb*(S_T_3-S_0_3))* x_ch4
exe_ph_h2 = (h_T_4-h_0_4-T_amb*(S_T_4-S_0_4))* x_h2
exe_ph_n2 = (h_T_5-h_0_5-T_amb*(S_T_5-S_0_5))* x_n2
exe_ph_h2o = (h_T_6-h_0_6-T_amb*(S_T_6-S_0_6))* x_co
"Total mixture physical exergy, kJ/kmol"
exe_ph_gas = exe_ph_h2 + exe_ph_co + exe_ph_co2 + exe_ph_h2o
+ exe_ph_ch4 + exe_ph_n2
"Total gas exergy"
exe_gas = exe_ch_gas + exe_ph_gas
"Chemical exergy for fuel per mass, kJ/kg"
exe_ch_fuelmass = xi * LHV_biomass * 10^3
"Chemical exergy for fuel per mole, kJ/kmol"
exe_ch_fuel = exe_ch_fuelmass * M_fuel
factor_xi = O_1/C_1
xi = (1.044+0.016*sub_h-
0.3493*sub_o*(1+0.0531*sub_h)+0.0493*sub_n)/(1-0.4124*sub_o)
"Exergy efficiency"
Eta_exe_ch = x_t*(exe_ch_gas + exe_ph_gas) /exe_ch_fuel
"Irreversibility, I "
I = 1-Eta_exe_ch
```

Appendix J: Drawing of different parts of the gasifier

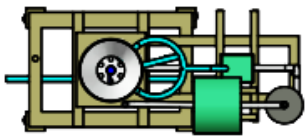

TOP VIEW

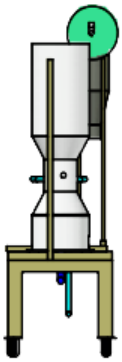

LEFT SIDE VIEW

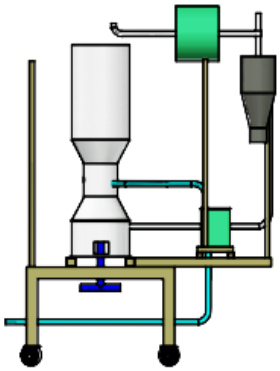

FRONT VIEW

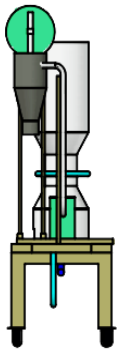

RIGHT SIDE VIEW

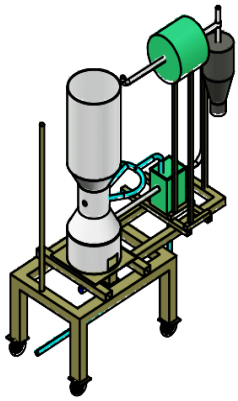

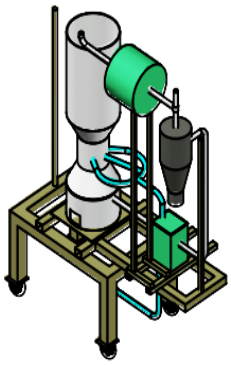

DRAWN BY BEHAILU I.	DATE 10/5/2023	**ADAMA SCIENCE AND TECHNOLOGY UNIVERSITY**		
CHECKED BY Dr. DAWIT G.	DATE 20/5/2023	SIZE A4	DRAWING NUMBER 01	
APPROVED BY Dr. DAWIT G.		SCALE 1:10	WEIGHT	SHEET 1/1